1-1-2018

MULTIPLE STIMULI RESPONSIVE DRUG DELIVERY SYSTEM BASED ON MAGNETIC NANOPARTICLE EMBEDDED CHITOSAN MICROBEADS

Ankita Mohapatra

MULTIPLE STIMULI RESPONSIVE DRUG DELIVERY SYSTEM BASED ON MAGNETIC NANOPARTICLE EMBEDDED CHITOSAN MICROBEADS

by

Ankita Mohapatra

A Dissertation

Submitted in Partial Fulfillment of the

Requirements for the Degree of

Doctor of Philosophy

Major: Electrical and Computer Engineering

The University of Memphis

May 2018

DEDICATION

This dissertation is dedicated to my parents, who gave me wings to fly and the strength to soar high.

ACKNOWLEDGEMENTS

I want to extend my sincere gratitude to Dr. Bashir I. Morshed for his endless patience, insight, mentorship and support throughout my work; and for always having my back. I want to thank the members of my committee: Dr. Warren Haggard, Dr. Madhusudhanan Balasubramanian, Dr. Eddie Jacobs, and Dr. Sanjay Mishra for their invaluable advice and feedback on this research. I would also like to thank Dr. Tomoko Fujiwara, Dr. Amber Jennings, and Dr. Joel Bumgardner who were always willing to guide me in this multi-disciplinary research and have vastly enriched my knowledge in this domain.

I also want to express my heartfelt gratitude to my lab-mates who were always happy to help and made the workplace a delight to work in. A special thanks to all my friends, family, and well-wishers whose encouragement and support helped me in sustaining this far.

ABSTRACT

Mohapatra, Ankita. Ph.D. The University of Memphis. April, 2018. Multiple Stimuli Responsive Drug Delivery System Based on Magnetic Nanoparticle Embedded Chitosan Microbeads. Major Professor: Dr Bashir I. Morshed

Direct drug administration has several shortcomings such as low circulation concentration due to rapid flushing by the immune system, non-specificity to target tissue and inefficient delivery to avascular sites. A widely adopted solution to these limitations is to sterically shield the drug from a harsh *in vivo* environment by encapsulation in a biocompatible, bio-degradable substrate. These Drug Delivery System (DDS) can be localized at the site and release drug gradually until the drug reserve is exhausted. However, the efficiency of this DDS can be further enhanced by designing them to elute drug in response to an external stimulus. This enhancement would enable a healthcare provider to customize therapeutic profiles from the same DDS according to the clinical needs of the patient, without repeated invasive procedures or stronger dosages to maintain potent drug concentration.

Our work explored a chitosan based DDS in the form of microbeads which was successfully shown to be responsive to both magnetic and electric stimuli. Chitosan was chosen because it is biodegradable, biocompatible, non-cytotoxic, and has high drug loadability. Magnetic Nanoaparticles (MNP) were added in the chitosan matrix to facilitate stimulus response. Over the course of this research, several cross-linkers like poly-ethylene glycol dimethacrylate (PEGDMA) and glyoxal were tested, and the microbeads loaded with different antibiotics like tetracycline, vancomycin, etc. The current formulation is chitosan/MNP cross-linked with PEGDMA and carrying vancomycin as the drug molecule of interest. The average size

distribution of microbeads with this composition was measured at 288.4 ± 62.2 μm, with the embedded MNP sized at 10.89 ± 2.67 nm.

A MagneTherm (nanoTherics, UK) was used to provide magnetic stimuli of 25mT at 109.9 kHz to the DDS for 30 mins. Tests conducted *in vitro* suggested that the DDS was capable of burst-releasing higher amount of drugs on multiple instances of stimuli, separated from each other by several hours (short term study) or even several days (long term study). In a long term study spanning 16 days, magnetic hyperthermia was able to boost vancomycin elution above minimum inhibitory concentration even after 15 days of continuous elution *in vitro*. It was also observed to be non-responsive to normal temperature elevation (general hyperthermia), indicating that drug elution will not be impacted by *in vivo* fluctuations in temperature.

Our preliminary study using electric stimuli to cause drug delivery was performed with electrodes inside Surface Acoustic Wave (SAW) resonators. The statistically significant drug release compared to non-stimulated samples established DDS sensitivity to electric stimuli and laid the groundwork for designing our custom Inter-Digitated Electrodes (IDEs) with a larger scale on a flexible substrate. We printed IDEs with an Inkjet Materials Printer (DMP 2831, Fujifilm, USA) to apply short bursts of electric pulses of 100 Hz for several seconds to the DDS, and caused a subsequent higher release of vancomycin. These IDEs have an overall dimension of 18.7 mm x 35 mm. The printed electrodes were < 2 μm in height, and were printed by depositing Silver nanoparticle ink (40% loading) on a Polyimide substrate (1 mil thickness). Results demonstrated statistically significant drug release for 3 mins of stimulation.

The results showed that both electric and magnetic stimuli can be used to control drug discharge from the chitosan DDS. The platform can be easily customized according to the site of implant and desired dosage profile. The DDS allows multiple stimuli, which can be used

independently or in conjunction. The health-provider can choose suitable stimulus to repeatedly administer drug dosage non-invasively when required, leading to enhanced patient recovery and compliance.

PREFACE

This dissertation is in presented in three journal articles format. I am the first author of all of them.

Article 1 is titled “Stealth Engineering for *In Vivo* Drug Delivery Systems” is listed as Chapter 2 and has been published in Critical Reviews in Biomedical Engineering and available online with the citation: A. Mohapatra, B. I. Moshed, W. O. Haggard., R. A. Smith, “Stealth Engineering for *In Vivo* Drug Delivery Systems”, *Crit. Rev. Biomed. Eng.,* 43(5-6), 2015

Article 2 is titled “Magnetic stimulus responsive vancomycin drug delivery system based on chitosan microbeads embedded with magnetic nanoparticles” is listed as Chapter 3 and has been published in Journal of Biomedical Materials Research Part B: Applied Biomaterials and is available online with the citation: A. Mohapatra, M. A. Harris, D. Levine, M. Ghimire, J. A. Jennings, B. I. Morshed, W. O. Haggard, J. D. Bumgardner, S. R. Mishra, T. Fujiwara, “Magnetic stimulus responsive vancomycin drug delivery system based on chitosan microbeads embedded with magnetic nanoparticles”, *J. Biomed. Mater. Res. B Appl. Biomater.,* 2017

Article 3 is titled “Electric Stimulus Responsive Chitosan/MNP Microbeads for a Smart Drug Delivery System”, and is ready for submission to IEEE Transactions on Biomedical Engineering in April 2018.

TABLE OF CONTENTS

LIST OF TABLES

LIST OF FIGURES

Chapter 1

INTRODUCTION

1.1 OVERVIEW

Systemic drug administration faces several deterrent factors like rapid opsonisation and flushing out of circulation [1]. They also tend to have very low target specificity, thus requiring dosages to be repeated at high concentrations to maintain therapeutic levels needed for treatment. A Drug Delivery System (DDS) can be described as a vehicle to carry the drug to the target site, while protecting it from opsonization by the immune system. The DDS is biocompatible, biodegradable and enhances the lifetime of the drug, thereby ensuring longer bioavailability with potent concentration at the intended tissue site [2-4].

Although these DDS prolong the drug efficiency, they are characterized by a first-order release profile until the drug is exhausted [5]. To further allow control and flexibility over the treatment method, some of these DDS have been modified to be sensitive to a stimulus and release a higher drug amount as a response when stimulated (Fig. 1.1). The stimulus type may be external (e.g. magnetic field, electric field, ultrasound) or internal (e.g. pH, temperature).

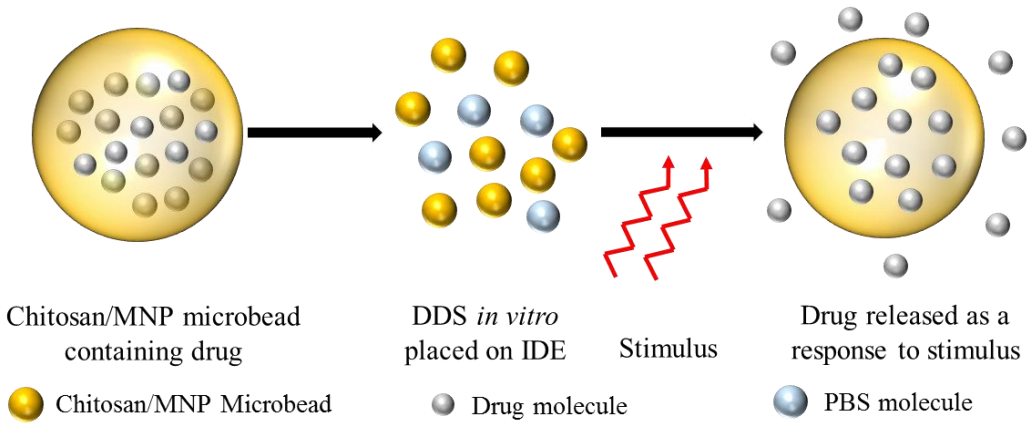

Fig. 1.1: Conceptualized framework for a DDS responsive to external stimuli

This work describes a chitosan based DDS in the form of microbeads that was formulated and tested with both magnetic and electric stimuli. A MagneTherm (Nanotherics, UK) was used to provide magnetic stimulation, whereas electric stimulus was initially applied by using a Surface Acoustic Wave (SAW) resonator chip, and later with an inkjet printed interdigitated electrodes (IDE). Stimuli were applied in multiple spans and in all instances, and drug release was observed to be significantly higher when compared to the elution profile in non-stimulated groups at the time of stimulation. This novel DDS will allow health-providers to choose one of either modes or both in conjunction to administer drug dosages non-invasively and without discomfort to the patient, allowing better regulation over dosage amount and timings and overall therapeutic effectiveness.

1.2 RELATED WORKS

1.2(a) Drug Release by Magnetic Field Stimulus:

Gilchrist et *al* demonstrated magnetic hyperthermia in tissues with Ferric Oxide nanoparticles in 1957 [6]. This breakthrough was followed by new therapeutic uses of hyperthermia like cancer treatment and drug delivery.

Drug release by hyperthermia was first demonstrated in 1987 [11] when polymeric matrices were designed with embedded magnets. They were loaded with insulin and implanted in diabetic rats. After stimulation by a magnetic field, the glucose level dropped by 30% more than the glucose drop observed in the rats that did not receive the stimulation. A similar insulin release from alginate/chitosan microbeads was observed by Finotelli *et al* when they applied an external magnetic field of 1800 G, 33 Hz [12]. Koppolu et al designed MNP cores with outer multilayered shells of the temperature-responsive polymer poly(N-isopropylacrylamaide) (PNIPAAm) and poly(D,L-lactideco-glycolide) (PLGA) as carriers of both curcumin and bovine

serum albumin (BSA); while curcumin showed a sustained release profile over 13 days, BSA could be burst-released from PNIPAAm layer by elevating temperature [13]. Katagiri and his group designed polyelectrolyte hollow multilayered shells containing dye, coated with Fe_3O_4 MNP and an amphiphilic bilayer. They magnetically irradiated at 236 Oersted, 360 kHz for 60 min and measured dye release, which was associated with a heat-induced change in phase of amphiphile membrane, rather than any structural fissure [14].

Drug delivery by magnetic hyperthermia can be broadly classified into two mechanisms: through bond breaking and through enhanced permeability [15]. The proposition in the first type is that MNP forms bonds with the drug molecule which is damaged due to heat or vibrational energy generated by MNP in a magnetic field. As an extension of this hypothesis, it is also possible that the drug molecules form chemical bonds with the polymer or cross-linker which are broken down due to heat generated by MNP. To demonstrate this mechanism, fluorescent DNA was tethered to MNP and implanted in mice. After stimulation, fluorescence was detected in surrounding tissues [16]. In the second proposed mechanism, intense localized heating by magnetic hyperthermia causes fissures in the polymer matrix, thus releasing the drug. This technique was used to deliver drugs in an on-off pattern, from a PNIPAm/cellulose based polymer embedded with MNP, by thermally modulating the polymer permeability via a magnetic field [17]. Hu *et al* formulated Fe_3O_4/poly(allylamine) polyelectrolyte microcapsules encapsulating doxorubicin hydrochloride, which formed micro-cavities releasing high drug quantities, under a magnetic stimulation [18].

1.2(b) Drug release by Electric Field Stimulus:

The applications of drug release by electric stimulation have not been as vastly researched on as magnetic hyperthermia. In one of the earliest works, Miller *et al* showed that applying a low

voltage of 1 V to a polypyrrole films could induce higher glutamate release from the films compared to glutamate release from non-stimulated films [19]. Some researchers implanted polypyrrole nanoparticles loaded with fluorescent molecules in mice and detected release upon applying 1.5 V/cm electric field for 40s [20]. Kwon *et al.* formulated a PMMA based polymer system which had the capability to dissolve rapidly when an electric current was passed through it. They used this property to cause insulin discharge from such hydrogel "patches" [21]. Fantozzi *et al.* covered electrodes with guar gum hydrogel carrying bleomycin solution. The electrodes were then brought in contact with cancer cells and on applying an electric field, bleomycin was directly delivered to them [22]. Polyaniline based hydrogel had similar electro-responsive properties that were proportionately dependent on the intensity of voltage applied across the substrate [23]. Alginate films have also been used for electrochemically controlled release of bovine serum albumin (BSA) or lysozyme [20]. Liu *et al.* developed a miniature drug delivery device that was designed as an array of metallic contacts on a silicon base. They used electro-responsive Polymethacrylic acid hydrogel as the Drug Delivery System (DDS) for various drugs. This hydrogel reservoir could shrink or swell in response to the applied electric field, thus releasing drugs [24]. There were no previous reports describing an electrically stimulated drug delivery mechanism based on chitosan and magnetic nanoparticles.

1.3 RESEARCH OBJECTIVES, APPROACH AND SCOPE

The DDS tested in this study was a chitosan framework structured as microbeads and containing magnetic nanoparticles (MNP). Over the course of this work, several cross-linkers like PEGDMA and glyoxal were tested, and the microbeads loaded with different antibiotics like tetracycline, vancomycin, etc. The current formulation is chitosan/MNP cross-linked with PEGDMA and carry vancomycin as the drug molecule of interest. The objective was to trigger a

drug release controllably, repeatedly and non-invasively by an external stimulus, as conceptualized in the sketch drawn in Fig. 1.1. In an ideal scenario, the drug would have been restrained inside the DDS, until an external stimulus is applied to release it. In practical settings, however, the DDS passively discharges drug and the stimulus is expected to elevate the drug release at a later time-point when higher therapeutic levels of drug are desired. Magnetic and electric fields have been explored as potential approaches to modify a traditional drug elution profile and increase drug release in the stimulation duration.

A MagneTherm (Nanotherics, UK) was used to provide a high frequency magnetic stimulus of 109.9 kHz at 25 mT. Various timelines were designed to provide stimulus as this research progressed. The short-term accelerated studies typically span a few minutes (for electrical) or a few hours (for magnetic). The long-term studies stretch over several days (for magnetic), with stimuli given to the samples when the antibiotic elution drops below therapeutic levels.

Both magnetic and electric stimuli were explored to alter normal drug elution profile and escalate its release from the chitosan microbeads. For each test, assuming μ_{stim} is the average drug concentration eluted by stimulated groups and μ_{ctrl} is the average drug concentration released by control groups in each time period under consideration, the null hypothesis (H_0) and alternate hypothesis (H_1) are defined as:

$H_0: \mu_{stim} = \mu_{ctrl}$

$H_1: \mu_{stim} > \mu_{ctrl}$

In descriptive terms, the null hypothesis H_0 is that the stimuli do not have any effect on the DDS and both groups have a similar drug elution profile. The alternative hypothesis H_1 is the stimuli is capable of influencing the DDS in such a way that the test groups release a significantly higher amount of drug compared to control. The raw data was analyzed with t-tests

or Wilcox non-parametric tests coded in R programming language, assuming 5% significance level. The results showed promise of developing a smart DDS that will allow control over dosage discipline, duration and strength by external non-invasive excitation.

1.4 ACHIEVEMENTS

Patent Application:

A. Mohapatra, M. A. Harris, B. I. Morshed, J. A. Jennings, J. Bumgardner, T. Fujiwara, S. R. Mishra, D. A. Levine, G. McGraw, W. O. Haggard, USPTO Provisional Patent Application, 52/401,751, Sep. 29, 2016.

Journals as first author:

- A. Mohapatra, B. I. Morshed, W. O. Haggard, R. A. Smith. "Stealth Engineering for in vivo Drug Delivery Systems", *Crit. Rev. Biomed. Engg.*, vol. 43, pp. 347-69, 2016
- A. Mohapatra, M. A. Harris, D. LeVine, M. Ghimire, J. A. Jennings, B. I. Morshed, W. O. Haggard, J. D. Bumgardner, S. R. Mishra, T. Fujiwara, "Magnetic Stimulus Responsive Vancomycin DDS Based on Chitosan Microbeads Embedded with Magnetic Nanoparticles", J. *Biomed. Mater. Res. Part B*, 2017
- A. Mohapatra, B. I. Morshed, J. A. Jennings, T Fujiwara, M. A. Harris, C. M. Wells, S R Mishra, "Electric Stimulus Responsive Chitosan/MNP Microbeads for a Smart Drug Delivery System", *IEEE Trans. Biomed. Eng*. (manuscript in preparation)

Other Journal Articles:

- M. Harris, H. Ahmed, B. Barr, A. Mohapatra, D. Levine, L. Pace, B. Morshed, J. Bumgardner, J. A. Jennings, "Magnetic Stimuli-Responsive Chitosan-based Drug Delivery Biocomposite for Multiple Triggered Release", *Int. J. Biol. Macromolec.*, vol. 104(Pt B), pp. 1407-1414, 2017

Refereed Conference Publications:

- A. Mohapatra, M. Harris, M. Ghimire, B. I. Morshed, J. A. Jennings, W. O. Haggard, J. Bumgardner, S. Mishra, T. Fujiwara, "Chitosan Microbeads with MNP on Printed Electrodes for Electric Stimulus Responsive Drug Delivery'', *IEEE Medical Measurements and Applications*, Rochester (MN), pp. 464-469, 2017.
- A. Mohapatra, G. McGraw, B. I. Morshed, J. A. Jennings, W. O. Haggard, J. D. Bumgardner, S. R. Mishra, "Electric Stimulus of Chitosan Microbeads Embedded with Magnetic Nanoparticles for Controlled Drug Delivery", *IEEE Healthcare Innovations and Point-of-Care Technologies Conference*, Seattle (WA), pp. 284-287, 2014.
- A. Mohapatra, M. N. Sahadat, B. I. Morshed, G. McGraw, A. P. Hoban, J. A. Jenning, W. O. Haggard, J. D. Bumgardner, S. R. Mishra, "Stimuli-Controlled Drug Delivery System Development with Implantable Biocompatible Chitosan Microbeads", *4th IAJC/ISAM Joint International Conference*, Orlando (FL), Paper 77, 2014.
- A. Hoban, G. McGraw, A. Mohapatra, et al. 2014, "Preliminary Results for the Addition of Fe3O4 Nanoparticle Impregnated Chitosan Microspheres to the Chitosan Sponge for Stimuli Responsive Antibiotic Delivery", *Society for Biomaterials Annual Meeting and Exposition*, 2014.

Other work published during this period (not part of this dissertation):

- A. Mohapatra, B. I. Morshed, S. Shamsir, S. K. Islam, " Inkjet Printed Thin Film Electronic Traces on Paper for Low-cost Body-worn Electronic Patch Sensors" in *IEEE Body Sensor Networks*, Las Vegas (NV), 2018 (in press).
- A. Mohapatra, S. K. Tuli, K. Liu, T. Fujiwara, R. W. Hewitt, F. Andrasik, B. I. Morshed, "Inkjet Printed Parallel Plate Capacitors Using PVP Polymer Dielectric Ink on Flexible

Polyimide Substrates", *IEEE Engineering in Medicine and Biology Society*, Honolulu (HI), 2018, submitted

Awards/Distinctions:

- Recipient of Herff Fellowship, Herff College of Engineering, University of Memphis, Fall 2013- Fall 2015
- Best presentation, IEEE Healthcare Innovation & Point of Care Technologies, Seattle (WA, USA), 2014.
- Received travel award, IEEE Body Sensor Networks, Las Vegas (NV), 2018

1.5 REFERENCES

[1] A. Mohapatra, B. I. Morshed, W. O. Haggard, R. A. Smith, "Stealth Engineering for in vivo Drug Delivery Systems", *Crit. Rev. Biomed. Engg.*, vol. 43, pp. 347-69, 2016.

[2] R. Cheng, F. Meng, C. Deng, H. Klok, Z. Zhong, "Dual and multi-stimuli responsive polymeric nanoparticles for programmed site-specific drug delivery", *Biomaterials*, vol. 34, pp. 3647-3627, 2013.

[3] M.N. Yasin, D. Svirskis, A. Seyfoddin, I.D. Rupenthal, "Implants for drug delivery to the posterior segment of the eye: A focus on stimuli-responsive and tunable release systems", *J. Control.* Rel., vol. 196, pp. 208-221, 2014.

[4] C.P. McCoy, N.J. Irwin, C. Brady, D.S. Jones, G.P. Andrews, S.P. Gorman, "Synthesis and release kinetics of polymerisable ester drug conjugates: towards pH-responsive infection-resistant urinary biomaterials". Tetrahedron Lett., vol. 54, pp. 2511-2514, 2013.

[5] Y. Shi, A. Wan, Y. Shi, Y. Zhang, Y. Chen, "Experimental and Mathematical studies on the drug release properties of aspirin loaded chitosan nanoparticles", BioMed. Res. Int., vol. 2014, 2014.

[6] R. K. Gilchrist, R. Medal, W. D. Shorey, R. C. Hanselman, J. C. Parrott, C. B. Taylor, "Selective inductive heating of lymph nodes", Annals of Surgery, vol. 146(4), pp. 596-606, 1957.

[7] H. S. Huang, J. F. Hainfeld, "Intravenous magnetic nanoparticle cancer hyperthermia", Int. J. Nanomedicine, vol. 8, pp. 2521-2532, 2013.

[8] M. Johannsen, U. Gneveckow, L. Eckelt, A. Feussner, N. Waldofner, R. Scholz, S. Deger, P. Wust, S. A. Loening, A. Jordan, "Clinical hyperthermia of prostate cancer using magnetic nanoparticles: presentation of a new interstitial technique", Int. J. Hyperthermia, vol. 21(7), pp. 637-647, 2005.

[9] K. M. Hauff, R. Rothe, R. Scholz, U. Gneveckow, P. Wust, B. Thiesen, A. Feussner, A. Deimling, N. Waldoefner, R. Felix, A. Jordan, "Intracranial thermotherapy using magnetic nanoparticles combined with external beam radiotherapy: Results of a feasibility study on patients with glioblastoma multiforme", J. Neurooncol., vol. 81, pp. 53-60, 2007.

[10] P. I. P. Soares et al, "Iron oxide nanoparticles stabilized with a bilayer of oleic acid for magnetic hyperthermia and MRI applications", Appl. Surf. Sci., vol. 383, pp. 240-247, 2016.

[11] J. Kost, J. Wolfrum, R. Langer, "Magnetically enhanced insulin release in diabetic rats", J. Biomed. Mater. Res. Part A, vol. 21, pp. 1367-73, 1987.

[12] P. V. Finotelli, D. D. Silva, M. Sola-Penna, A. M. Rossi, M. Farina, L. R. Andrade, A. Y. Takeuchi, M. H. Rocha-Leão, "Microcapsules of alginate/chitosan containing magnetic nanoparticles for controlled release of insulin", Colloids Surf. B: Biointerfaces, vol. 81, pp. 206-211, 2010.

[13] B. Koppolu, M. Rahimi, S. Nattama, A. Wadajkar, K. T. Nguyen, "Development of multiple-layer polymeric particles for targeted and controlled drug delivery", Nanomedicine, vol. 6, pp. 355-361, 2010.

[14] K. Katagiri, Y. Imai, K. Koumoto, "Variable on-demand release function of magnetoresponsive hybrid capsules", J. Colloid and Interface Sci., vol. 361, pp. 109-114, 2011.

[15] C. S. S. R. Kumar, F. Mohammad, "Magnetic nanomaterials for hyperthermia-based therapy and controlled drug delivery", Adv. Drug Deliv. Rev., vol. 63(9), pp. 789-808, 2011.

[16] A. M. Derfus, G. Maltzahn, T. J. Harris, T. Duza, K. S. Vecchio, E. Ruoslahti, S. N. Bhatia, "Remotely Triggered Release from Magnetic Nanoparticles", Adv. Mater., vol. 19, pp. 3932-3936, 2007.

[17] T. Hoare, B. P. Timko, J. Santamaria, G. F. Goya, S. Irusta, S. Lau, C. F. Stefanescu, D. Lin, R. Langer, D. S. Kohane. (Mar. 2011). Magnetically triggered nanocomposite membranes: a versatile platform for triggered drug release. Nano Lett. 11(3), pp. 1395-1400, 2011

[18] S. Hu, C. Tsai, C. Liao, D. Liu, S. Chen. (2008). Controlled Rupture of Magnetic Polyelectrolyte Microcapsules for Drug Delivery. Langmuir. 24, pp. 11811-11818, 2008

[19] B. Zinger, L. L. Miller, “Timed release of chemicals from polypyrrole films”, J. Am. Chem. Soc., vol. 106(22), pp. 6861-6863, 1984.

[20] S. Szenerits, F. Teodorescu, R. Boukherroub, “Electrochemically triggered release of drugs”, Eur. Polym. J., vol. 83, pp. 467-477, 2016.

[21] I. C. Kwon, Y. H. Bae, S. W. Kim, “Electrically erodible polymer gel for controlled release of drugs”, Nature, vol. 354, pp. 291-293, 1991.

[22] F. Fantozzi, E. Arturoni, R. Barbucci, “The effects of the electric fields on hydrogels to achieve antitumoral drug release”, Bioelectrochemistry, vol. 78, pp. 191-195, 2010.

[23] W. Li, X. Zeng, H. Wang, Q. Wang, Y. Yang, “Polyaniline-poly(stryrene sulfonate) conducting hydrogels reinforced by supramolecular nanofibers and used as drug carriers with electric-driven release”, Eur. Polym. J., vol. 66, pp. 513-519, 2015.

[24] Y. Liu, et al, “An electric-field responsive microsystem for controllable miniaturized drug delivery applications”, Sens. Actuators B-Chem., vol. 175. pp. 100-105, 2012.

Chapter 2

STEALTH ENGINEERING FOR *IN VIVO* DRUG DELIVERY SYSTEMS

2.1 INTRODUCTION

Since the later half of 20th century, there has been an escalating interest in developing an ideal drug carrier that could be injected intravenously, endure a long circulation period and release drug in a controllable manner. This could facilitate external monitoring and regulation over drug dosage without causing the discomfort of repeated bolus injections to the patient. In addition, target-specific drugs could be administered easily without degradation *in vivo* prior to the intended delivery period. Numerous types of systems have been developed for this purpose; however, most suffer from surface opsonisation by plasma proteins and are eliminated from circulation.

2.1(a) Mononuclear Phagocytic System:

The mononuclear phagocytic system (MPS), traditionally referred to as reticulo-endothelial system (RES), is a part of the immune system and consists of cells that originate in bone marrow and ultimately settle in tissues as macrophages. The monocyte/macrophage cell family plays a key role in the body's innate and adaptive immune responses and is on the front line for detection of foreign molecules and pathogens. Macrophages are a complex heterogeneous group of cells found throughout the body and provide a vast number of functions. The monocytes migrate from the blood into tissue to replenish long-lived tissue-specific macrophages of the bone (osteoclasts), alveoli, central nervous system (microglial cells), connective tissue (histiocytes), skin (Langerhans), gastrointestinal tract, liver (Kupffer cells), spleen and peritoneum[1]. These cells are phagocytic and search for older worn out or damaged cells such as erythrocytes (to conserve iron and hemoglobin) and virally infected cells to clear them from the

circulatory system[2]. They also remove cellular debris from cells, such as neutrophils, that have undergone apoptosis as well as foreign debris found in the body including that from implanted biomaterials[3]. The macrophage's phagocytic actions replenish this debris ceaselessly from the tissue without producing inflammatory or immune mediators[4]. However, debris from cells that have undergone necrosis give off molecular danger signals such as DNA and heat shock proteins that activate the macrophages to secrete pro-inflammatory cytokines[5]. The role of classically activated macrophages in host defense to intracellular pathogens has been well documented[1,6-8]. Classically activated macrophages release growth factors like PDGF and vascular endothelial growth factor (VEGF) to initiate repair, and produce inflammatory cytokines such as tumor necrosis factor α (TNFα), macrophage inflammatory protein, IL1-α, IL−6, IL-8, and inducible nitric oxide synthase (iNOS or NOS2) to activate cellular programs amplifying their own and other immune cells' antimicrobial activities and interleukin 1 (IL-1) and IL-6 to mobilize other immune cells[2].

The macrophages detect these danger signals through specific receptors such as the Toll-like receptors (TLRs), intracellular pattern recognition receptors and the IL-1 receptor[4,9-10]. These receptors have evolved over millions of years to detect pathogen associated molecular patterns (PAMPs) related to pathogenic molecules such as lipopolysaccharide, lipoteichoic acid and muramyl peptides derived from peptidylglycans. TLR activation then initiates signals (e.g. interleukin receptor associated kinases (IRAK)1 and 4) activating the transcription factor NFκB and regulating inflammatory gene expression[11-12]. These macrophages detect the bacteria in this process and become primed and activated giving off microbicidal oxygen radicals such as superoxide anions oxygen and nitrogen free radicals that kill pathogens as well as pro-inflammatory cytokines such as IL-6, IL-23, IL-1b and TNFα. Enhanced release of superoxide

has also been shown to occur in response to IFNg, irradiation, pH, osmolarity and temperature changes[13-16].

The body has a number of different molecules such as complement proteins, fibronectin, and vitronectin that may associate with biomaterials or introduced molecules[17]. The interactions of these endogenous proteins with the biomaterial may change the nature of the biomaterial or the endogenous protein such that local macrophages may become activated. Therefore, avoiding or regulating macrophage priming and activation in a way that would inhibit the activity of other immune cells is a goal of stealth molecule technology. One possible group of regulatory molecules is the prostaglandins (PG). High concentrations of PGE_2 are found at sites of infection where it inhibits macrophage proinflammatory functions such as phagocytosis, reactive oxygen species (ROS) production, release of antimicrobial peptides, and the production of TNFα, MIP-1α and LKT B4 while enhancing the production of anti-inflammatory IL-10[18-19]. PGE_2 also inhibits ROS and leukotriene production by neutrophils, may enhance production of endogenous IL-10, which down–regulates dendritic cell functions[20-21]. Finally, prostaglandins inhibit fibroblast collagen and fibronectin synthesis and PDGF-stimulated migration[22-23].

Stealth engineering is the generic term assigned to Drug Delivery System (DDS) modification to delay its opsonisation and ultimately renal elimination. This review provides a summary of recent research in stealth engineering for *in vivo* DDS that is of particularly high interest for many therapeutic applications including chemotherapy for cancer, tumor treatment, bone regeneration and blood sugar management.

2.1(b) Need for Stealth Engineering:

The foundation for DDS was probably laid by Bangham who reported selective restriction to diffusion of cations by swollen bilayer ovolecithin structures[24], also known as Bangasomes or

liposomes. It was followed by abundant research on these structures[25-32]. Several other researchers proposed other DDS structures, such as, dendrimers, polymer nanoparticles, micelles and red blood cells.

From ingestion to final therapeutic activation, a drug carrier has to encounter several deterrent factors. Segal *et al.* injected radio-labeled compounds entrapped by liposomes in rat testicle and recorded testicular radioactivity, attributing the liberation to probable macrophagal endocytosis[27]. Carrier characteristics like surface chemistry, charge, flexibility, size, and shape have an acute influence on its *in vivo* lifetime. Designing an optimal carrier for maximal efficacy is a vast research area in itself and has been explored extensively. It was suggested that adsorption of plasma protein on the surface of a drug particle caused clearance from circulation after observing protein binding behavior in vivo and *in vitro*; a higher capability to bind protein was associated with faster clearance kinetics[33-34]. The protein was suggested to consist of high amounts of opsonin which triggered the phagocytic uptake by the MPS. Particles of size greater than 200 nm were observed to accumulate in spleen while those smaller than 10 nm are prone to glomerular filtration[35-37]. Also, since the glomerular membrane contains anionic polysaccharides, cationic particles are sieved faster than anionic ones[37]. Hydrophobicity is another aspect that can prematurely terminate vasculature circulation and is usually solved by grafting hydrophilic polymers onto the carrier surface[36-40]. Increased flexibility and branching of these steric shields further decreases macrophagal recognition by creating a high-density conformational barrier. Nanoparticle shapes are also observed to affect pharmacokinetic behavior. Discher showed that filamentous micelles had longer circulation than chemically similar spherical polyethylene-glycolated (PEG) vesicles[41]. Champion and Mitragotri fabricated worm-like polystyrene particles with high aspect ratios (>20) and reported negligible phagocytosis compared to spherical

particles of the same volume (1-3μm diameter), when tested against a rat alveolar macrophage cell line[42]. They attributed this observation to reduction in curvature and limiting it to only the endpoints of the worm shapes, which theoretically in turn should decrease phagocytosis.

Early attempts to curb phagocytic reaction to drug carriers by temporarily causing MPS Blockade was by administering a pre-dose of similar particles. The effect of an intravenous high dose of empty multilamellar liposomes on opsonisation rate of a second dose encapsulating 14C-inulin injected at 1, 5 and 24 h was studied in 1980[43]. It was observed that compared to a control group where only the second dose was given, 14C-inulin level in blood increased by a factor of 29 and decreased by a factor of 6 in liver when a preemptive dose was administered 1hr prior to actual dose. A similar method describes injecting a pre-dose of large unilamellar liposomes to limit the clearance of the second drug dose[44]. Further, different sizes of liposomes were comparatively studied to understand the dependency, if any, of MPS flushing on particulate size of such consecutive doses[45-46]. Small liposomes (40-200 nm) were shown to have a relatively higher circulation as compared to their larger counterparts.

Dextran sulphate (DS) was also used to lower the rate of clearing foreign particles from the blood stream by impeding MPS functioning, in some cases even resulting in absolute cessation of immunological response[47-48]. Patel *et al.* demonstrated a suppression of liver uptake of multilamellar liposomes from the blood stream by injecting a maximal dose of 50 mg DS per kg of body weight that caused a temporary liver blockage lasting 48 hours[49]. Liver uptake was observed to have dropped as early as 2 hours after infusion of DS. Prior dosage of a monoclonal antibody such as 2.4G2 demonstrated an inhibition in clearance of liposomes loaded with Dinitrophenyl[50].

The half-life and area under the plasma-concentration time curve are an accurate assessment of how long the DDS survives *in vivo*. Toutain and Bousquet-Melou have defined plasma terminal half-life as "following intravenous (IV) administration, the terminal half-life is the time required for plasma/blood concentration to decrease by 50% after pseudo-equilibrium has been reached; then, terminal half-life is computed when the decrease in drug plasma concentration is due only to drug elimination, and the term elimination half-life is applicable"[51]. Zhang *et al.* have published a detailed review in 2013 of materials that have been tested for drug delivery along with the FDA approval dates for the successful ones[52].

In this paper, we have reviewed some DDS that have been widely studied . Table I summarizes important data of various formulations reported. The data provided are not intended to highlight a negative comparison between their adequacies; they just serve the purpose of providing knowledge about various developmental approaches to DDS. These data have been primarily collected and summarized from the databases maintained through FDA archives and Drugbank of Canada. Fig. 2.1 shows a layout of this review.

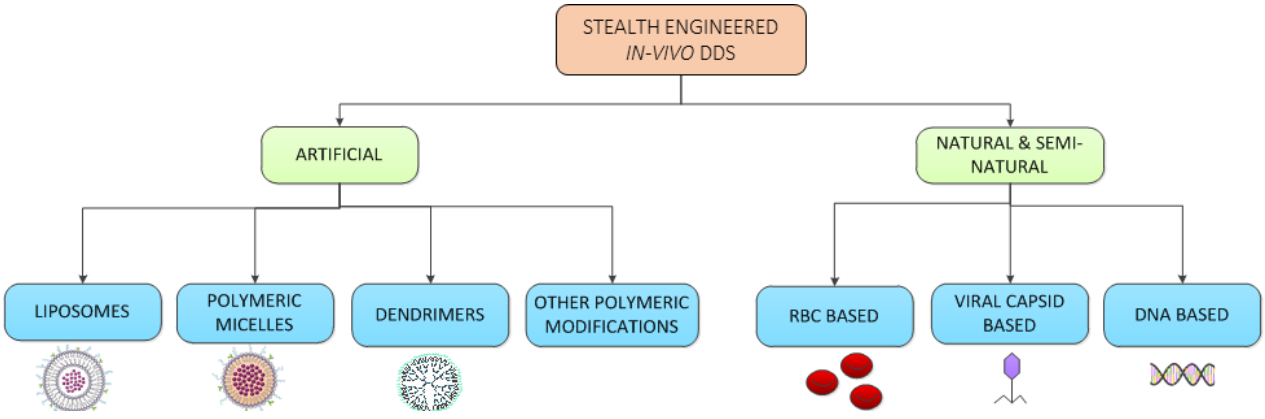

Fig. 2.1: Broad Classification of the types of DDS. Only major groups are shown here and discussed in this paper

2.2 ARTIFICIAL STEALTH ENGINEERING TECHNIQUES FOR *IN VIVO* DRUG DELIVERY

Various types of polymers and other biological entities have been artificially developed for the required camouflage ability of stealth engineered DDS for *in vivo* applications. Some of these techniques have shown promise and been tested through animal studies. Major stealth engineering techniques for *in vivo* DDS are discussed in this section.

2.2(a) Liposomes:

Liposomes are phospholipid bilayers that encapsulate drug in the inner compartment while the outer bilayer acts as its shield (Fig. 2.2). Some drugs can also be entrapped in the vesicular space. They were discovered by Bangham in 1961 and were extensively adopted as DDS, followed by various approaches to extend their short half-life *in vivo*. A comparative study of *in vivo* circulation time between non-entrapped neuraminidase and neuraminidase enclosed in liposomes with varying lipid concentration was done by Gregoriadis *et al.*[31]. They reported a higher circulation time for liposomes with a higher constituent of lipids, thus concluding that the rate of renal elimination is dictated by the drug carrier, rather than by the drug itself. Further, it was observed that cholesterol rich liposomes displayed enhanced *in vivo* lifetimes over cholesterol-poor or cholesterol-nil liposomes by impeding serum opsonin binding[53-55]. Semple *et al.* also noted that cholesterol inclusion improves packing density of liposomal phospholipid molecules thereby decreasing ion permeability[55].

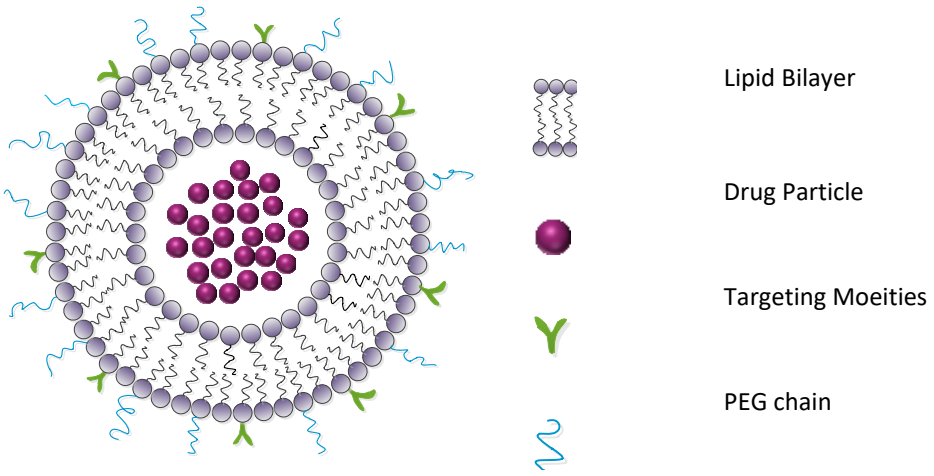

Fig. 2.2: Schematic of a copolymer liposome structure. The constituent building blocks have a hydrophobic tail and hydrophilic head which self-assemble to form the unique bilayer membrane. The liposomal surface can be conjugated to any functional molecule pertaining to the desired application. It can also be PEGylated for increased steric shielding

Negatively charged liposomes cleared faster compared to neutral or positively charged liposomes hence the negative charge on liposomes was labeled as a probable factor of recognition by MPS[34]. As a remedy for this, liposomes were structured with a low molar fraction of a negatively charged glycolipid, such as, GM1[34] or phosphatidylinositol, and a neutral phospholipid used as the major constituent[57]. These modified liposomes that were termed as sterically stabilized had a longer circulation time without MPS blockage. The effect of different concentrations of ganglioside and sphingomyelin (SM) modifications in liposomes on liver uptake was studied[34,58-59] where it was conclusively demonstrated that these modifications provided a longer life-time *in vivo* over classical liposomes. They were named as "Stealth Liposomes". The liposomes constituted of SM:PC:cholesterol:GM1 in the molar ratio 1 : 1 : 1 : 0.2 were classified as the first generation.

Abuchowski *et al.*[60] were among the first to covalently couple PEG to a bovine liver catalase which provided a hydrophilic shield around the enzyme and delayed recognition by the MPS. This method transcended to liposomal modification by PEG and performed better than earlier

methods that employed glycolipids. This was followed by several publications on superior performance of PEGylated liposomes *in vivo* tested with various drugs[61-75]. Allen and Hansen demonstrated an elaborate pharmacokinetic performance which was dependent on the dosage effect between the stealth and conventional liposomes; a comparison was also made between the half-lives of first generation GM1 liposomes and second generation PEG(1900)-distearoylphosphatidylethanoalamine[64,67,76]. Gabizon *et al.* were the first to demonstrate the extended blood lifetime of PEGylated liposomes encapsulating doxorubicin in human subjects[68]. It was followed by clinical trials of doxorubicin in Stealth Liposomes on 15 HIV infected patients for the treatment of Kaposi's sarcoma[69]. Liposomes modified with PEG were also employed as drug carrier devices for gene delivery, specifically for delivery of pDNA[77] and siRNA[78]. FDA approved Adagen, a polymer-drug conjugate of adenosine deaminase with PEG in 1990 was followed by approval for PEGylated liposomal doxorubicin for cancer treatment in 1995. Many researchers investigated the versatility of PEGylated liposomes for various drug deliveries, including those for cancer and conclusively established the higher lifetime of PEGylated DDS[78-94]. Compared to the first generation stealth liposomes such as monoganglioside (GM) and sphingomyelin (SM) liposomes mentioned above, PEGylated liposomes demonstrated the ability to evade activating the immune system. However, gradually several disadvantages were identified and associated with PEGylation in subsequent research, known as the "PEG Dilemma"[95]. Earlier the pharmacokinetics of PEG-liposomes were proven to be independent of dosage unless the quantity administered was too low, at which accelerated blood clearance, abbreviated as ABC-effect was observed. This phenomenon occurred in successive bolus injections of liposomes after a prior sample was already injected[96-105]. This event is attributed to production of anti-PEG immunoglobulin (IgM) from spleen in reaction to

the prior doses which increases uptake by Kupffer cells and can be suppressed to some extent by choosing antiproliferative drugs or moieties[37].

2.2(b) Polymeric Micelles (PM), Polymeric Nanoparticle, Solid Lipid Nanoparticles (SLN):

Micelles (Fig. 2.3) differ from liposomes in their structure. Liposomes are lipid bilayers (Fig. 2.2) that separate an internal aqueous phase from an external aqueous environment while PM are lipid monolayers (Fig. 2.3) with two functional parts, an inner hydrophobic core that determines loading efficiency of desired drugs and an outer hydrophilic shell that controls pharmacokinetic behavior of the micelle *in vivo*[39,106-7]. The outer polymeric corona acts as a steric shield, camouflaging the drug loaded in the solid inner core and can be conjugated to targeting or recognition moieties. They are smaller in size (<100 nm) and have superior stealth properties compared to liposomes. They are created by self-assembly of amphiphilic di-block or tri-block copolymeric molecules, which are in turn a mix of hydrophilic and hydrophobic components. Lee *et al.* showed the superior pharmacokinetic properties of polymeric vesicles over stealth liposomes[108]. This class of DDS has gathered much interest because of their similarity to natural biological transport systems; their unique characteristics delays uptake by RES while facilitating efficient intracellular drug delivery[109].

Any amphiphilic biocompatible polymer capable of significant steric hindrance such as PEG, PVP can be used to make micelles[39]. A popular class of micelles, marketed as Pluronics®, also known under the non-proprietary name of Poloxamers consist of polyethylene oxide (PEO) and PPO in an A-B-A tri-block structure and have relatively long elimination half-lives compared to liposomes[99]. For instance, P85 was shown to have a half-life between 60-90 h[110].

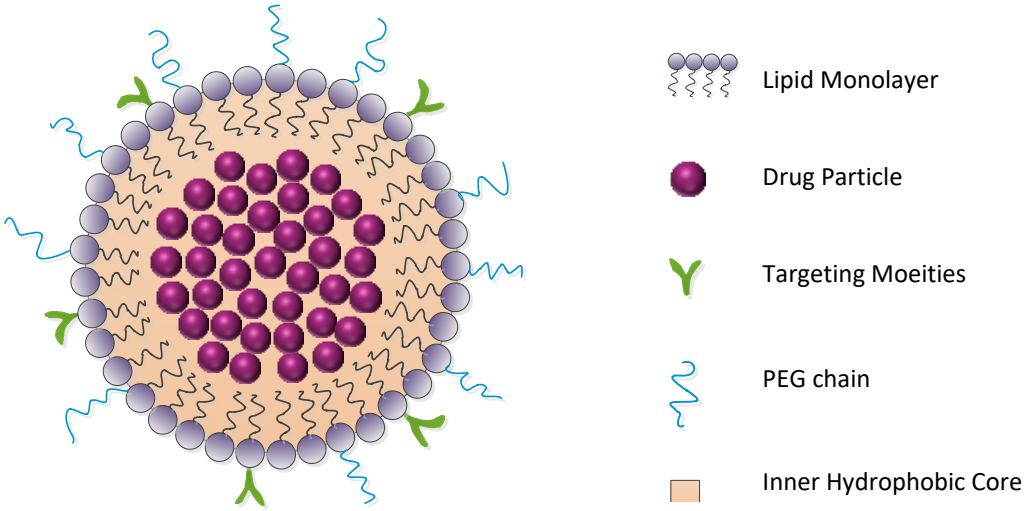

Fig. 2.3: Schematic of a Polymeric Micelle/ SLN. The inner matrix holds the drug cargo, protected by the outer shell that maybe activated by attachment of various molecules.

Poloxamine (PX) and poloxamer were noticed to impart stealth properties when coated on the drug particle. Illum and Davis were among the first to use them for modification of polystyrene and PMMA nanoparticle[111-112]. Uptake by liver was seen to decrease by 20% and 40% for nanoparticle (NP) coated with poloxamer-188 and poloxamer-338, respectively. Poloxamer-407 was seen to perform even better than either in terms of evading phagocytosis while PX proved to be superior over poloxamer[113]. Rudt and Muller conducted an assay of NP and microparticles pharmacokinetics affecting phagocytosis for polysterene modified by PX[114]. Furthermore, Moghimi *et al.* established that injecting PX-908 caused rapid clearance of a second dosage, most likely by resident macrophages and Kupffer cells from the previous dose. Such a behavior was noticed to be exactly similar to coating the particle with PX-908[115-116]. The modification with other polymers, such as, PLGA also exhibited enhanced circulation lifetimes[117-119].

PEG has also been widely used as a constituent of di-block and multi-block copolymer micelles and shown to have longer circulation life-times[109]. Several stimuli-responsive PM have

been designed[120] and some are in final stages of clinical trials[39]. Tri-block copolymer micelles of ABA and BAB combination of PEG and PLA were designed and tested as a DDS for paclitaxel in mice[121]. Moffatt *et al.* used one such copolymer, PLGA-PEG-PLGA as a gene delivery vehicle for encapsulated salicycl hydroxamic acid-PEI/pDNA[122]. Various other polymeric NP were formulated and tested for suitability as a drug carrier. Verrechia *et al.* modified the PLA/albumin to PLA-PEG copolymer and recorded an extended half-life of 6 hrs. over the former's few minutes[123]. Zhiqing *et al.* studied PEGylated PLGA NP (Stealth NP) as carriers for arsenic trioxide and showed it had lower uptake by murine peritoneal macrophages compared to naked arsenic trioxide[124]. Bazile *et al.* developed Methoxy based NP Me-PEG-PLA and recorded a longer half-life of 6 hours compared to a few minutes for F68 coated NP[125]. It was followed by other PLA-PEG complexed with NP for stealth delivery[126-127]. In addition, PEGylated PGLA microparticles encapsulating VEGF with improved circulation times was proposed recently[128]. Gref *et al.* structured nanoparticles with PLA and MPOE[129] followed by Perachhia *et al.* developing coated polycyanoacrylate NP and poly(isobutyl-2-cyanoacrylate) with PEG and observed an increased circulation time and decreased cytotoxicity[130-132]. Ahmed and Discher[133] designed PEG-PLA, PEG-polycaprolactone (PCL) and PEG-polybutadiene hydrolysis triggered polymerosomes. PEG was incorporated to improve *in vivo* circulation and a comparison between PEG-polymerosome and Stealth Liposome was presented. Lee *et al.* reported best half-life of 47.3±1.8 hours[108] for polymerosome-10 while Photos *et al.* reported a half-life of 28±10 h for OB16[134], both a significant improvement over stealth liposomes.

PEO was extensively studied as a prospective drug particle shield. Jaeghere *et al.* modified NP with PEO and the factors that determined MPS uptake were assayed[135]. Vittaz *et al.* conducted a similar study with a complex of PLA-PEO, and concluded that the decrease in

phagocytosis is directly proportional to surface density of PEO[136]. PLA nanoparticles when modified into a di-block copolymer by MPEO) were seen to undergo delayed phagocytosis in guinea pigs[137]. Butsele *et al.* tested (P2VP) (PEO) (PCL) tri-block copolymer as a pH-triggered drug delivery device and found it to possess stealth behavior[138]. A detailed review of various polymeric coatings and the behavior of complement activation mediated by polymeric structure is provided by Salmaso and Caliceti [139].

NK911, a micelle with a diameter of 40 nm constructed from PEG-poly(aspartic acid) block copolymer, encapsulating doxorubicin was the first polymeric micelle that was approved for clinical trial on 23 patients with malignant tumor[140]. While PEG formed the outer core, adding the "stealth" characteristic, the poly(aspartic acid) chain conjugated to doxorubicin built the inner hydrophobic core. The dosage was gradually increased from 6.0 to 67 mg doxorubicin equivalent m^{-2} in several levels. The half-life for NK911 was observed to be longer for NK911 compared to free drug. Following this, several other micelle structures were developed that proceeded to human trials[141]. Micelles have been conjugated to antibodies, nucleic acids, peptides and other biomolecules to augment target specificity and localization.

SLN are usually characterized by a solid lipid core proposed as an alternate drug carrier[142]. Following this Bocca *et al.*[143] modified SLN with two types of dipalmitoylphosphatidylethanolamine-PEG and stearic acid PEG as a stealth agent for fluorescent rhodamine B. Stealth SLN were noticed to be non-phagocytized after 60 min of administration compared to phagocytosis of plain SLN in few minutes. This was followed by the use of Stealth SLN to deliver doxorubicin in rats[144] and Icariin in mice[146]. Madan *et al.* also employed PEG nanoparticles to deliver noscapine across the blood-brain barrier (BBB) to glioblastoma cells[147].

2.2(c) Dendrimers:

Dendrimers (Fig. 2.4), a whole new class of drug carriers, were proposed in 1980s[148]. Since then, these highly branched macromolecules with low polydispersity have been extensively explored as drug carriers. They garnered much interest as a pharmaceutical vehicle because of their unique structural properties. They have a central core that can be loaded with hydrophobic drugs, a branched shell that can impart steric stability, and surface 3D moieties that can be conjugated with targeting bioactive molecules[149]. Polyamidoamine (PAMAM) dendrimers or STARBURST® dendrimers are the most common; dendrimers made of poly(lysine), poly(propyleneimine), polyester, polyol and triazine. PEGylated dendrimers with a comparatively longer terminal life-times have been reported too[150-152]. It was observed that cationic dendrimers were flushed out of circulation in Wistar rats at much accelerated rates compared anionic dendrimers, which re-confirmed that surface charge is a factor that significantly determines opsonisation rate[151]. Detailed pharmacokinetic dependency between dendrimer shape and drug content on its longevity *in vivo* has been studied[153-154].

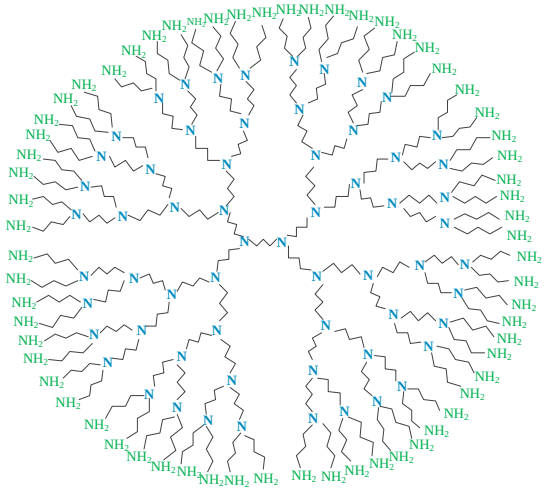

Fig. 2.4: Schematic of PAMAM dendrimer. Starting from an initiator core, the branching increases outwards in a tree like structure which is terminated by amine branches. The dendrimer surface can also be conjugated to other molecules by correct protonization

Vivagel™ from Starpharma, an amide based (SPL7013) dendrimer microbicide was cleared for clinical trials against herpes simplex viruses (HSV) and human immunodeficiency virus (HIV) in 2004[155-157]. SPL7013 has a core of benzhydrylamine amide of L-lysine bonded to four layers of L-lysine branches; each of the 32 amine groups on the surface were terminated by a sodium 1-(carboxymethoxy) naphthalene-3,6-disulfonate group It has been suggested that SPL7013 attached itself to gp120 proteins on viral surfaces, thus preventing it from adhering to human cells.

2.2(d) Polymeric Modifications of other Substrates:

Liu *et al.* grafted PEG onto single walled nanotubes (SWNT) and noticed an increase in circulation time with increase in chain length[158], recording 15 h for triple branched PEG grafted onto SWNT. Prencipe *et al.* reported 22.1 hr for PGA-pyrene-mPEG[159]. Niidome *et al.* layered gold nanorods with PEG to decrease its cytotoxicity and increase its lifetime with an objective of photo-thermal therapy and/or photo-controlled DDS[160-161]. Yokoyama *et al.* conjugated the anti-tumour drug, Adriamycin (ADR) with PEG and showed it to have a longer half-life of 70 mins over 18 min for non-complexed ADR[162]. Zhou *et al.* used camptothecin (CPT) to form PEG-block-dendritic polylysine-CPT nanospheres/nanorods of different sizes intended for drug delivery to cancerous cells[163]. PEG-tetra-CPT-nanorods with dimensions < 500 nm were found to have longest life-time and target specificity among all other sized nanorods.

In 1997, Cho *et al.* proposed a carbohydrate coating of NP that eluded phagocytic tagging by MPS[164]. Same year Maruyama *et al.* developed a new class of gene carrier with polysachharide and PLA grafted onto poly(L-lysine)[165]. Recently, super paramagnetic iron oxide (SPIO) nanoparticles are gaining popularity as MRI contrast agents and for treatment of cancer by hyperthermia. SPIO are not biocompatible and need to be shielded from phagocytosis. SPIO with

surface-modification with chitosan[166], PLA-PEG[167], PEG[168] and PEG-poly(amino) acid[169] have been proposed.

2.3. NATURAL AND SEMI-NATURAL STEALTH ENGINEERING TECHNIQUES FOR *IN VIVO* DRUG DELIVERY

Liposomes, PM, SLN and dendrimers are artificial DDS developed in an attempt to extend drug longevity *in vivo*. However they were still subjected to rapid elimination from the blood. This motivated several researchers to explore natural biological structures as potential DDS like erythrocytes, and capsids. The following section is a short review on such developments.

2.3(a) Red Blood Cells (RBC/Erythrocytes) based:

RBC are anucleate cells that transport oxygen and carbon-dioxide between lungs and body tissues via the circulatory system. In humans, healthy mature RBCs are bi-concave shaped, around 7.7 μm in diameter and have a lifetime of approximately 120 days. Their cytoplasm contain haemoglobin, a metalloprotein of iron which binds with oxygen. RBCs are found in all vertebrates (except the family Channichthyidae) and a few invertebrates. The discocytes are biocompatible, abundant, non-toxic and normally do not instigate MPS for opsonisation. Additionally their anucleate nature allows a considerably inert intracellular condition and high loadability of drugs. These aspects make it a probable DDS with extended vascular circulation, thereby reducing the frequency and intensity of dosage[170-171]. A common method to insert a load in RBC is lysis of RBC in hypotonic solutions, followed by drug absorption and membrane resealing. However this method almost always caused haemolysis, irreversible morphological damage to RBC structure and phosphatidyl sterine (PS) exposure. PS has been associated with early removal of RBC by MPS[172]. RBC can also be loaded by pre-treating with chlorpromazine, which causes reversible swelling and endocytosis of payload. In other research, RBC membranes

were fused with liposomes containing the therapeutic load, the liposomes then release it gradually inside the erythrocytic cell[172-173]. Other common methods are electroporation by exposure to a strong electric field and drug induced endocytosis[170]. In 2014, Yang *et al.* proposed a novel method of loading protein into RBC by using covalent bonding between the protein and a cell-penetrating peptide (CPP) via a disulfide link[174]. The CPP penetrates the RBC without any membrane disruption. Once inside the RBC, the disulfide bond dissociates, thus successfully enclosing the protein inside the cell and ensuring its structural and functional integrity.

RBCs have surface antigens that react with antibodies present in the blood of a different type. This necessitates proper matching during transfusion. To facilitate easy transfusion without cross-matching, shielding the antigens by modifying RBC with mPEG was first achieved by a group of Korean researchers in 1996[175]. This was soon followed by other researchers, some attempting to optimize polymer structure with respect to cytotoxicity[176-183]. Scott and Chen extended PEGylation to other allogenic and xenogenic cells including white blood cells[184].

Several drugs have also been successfully encapsulated and tested *in vivo*[170-171]. One of the early clinical studies on 9 volunteers using 51Cr labeled autologous RBC had a normal *in vivo* half-life of 19-29 days[185]. It was succeeded by another clinical study of PEG-conjugated adenosine deaminase (pegademase) and native adenosine deaminase (ADA) loaded 51Cr labeled RBC by hypo-osmotic dialysis. They reported a half-life of 20 d and 12.5 d for erythrocyte-entrapped pegademase and ADA respectively, compared to 3-6 d of exposed pegademase[186]. Mitragotri and Chambers attempted non-covalently binding of polystyrene nanoparticles of 200-450 nm size to RBC membrane and injected in Sprague-Dawley rats. They observed an increment in circulation time for the RBC-nanoparticles; around 5 % of them were still circulating after 12 h whereas >99.9 % of unbound particles were cleared in 2 min[187]. In a

clinical trial to evaluate potency of low doses of corticosteroid in cystic fibrosis patients, autologous erythrocytes were loaded with dexamethasone 21-phosphate and administered to 17 patients in two phases over a time interval. While no side-effects or toxicity were recorded, a persistent level of dexamethasone was detected in plasma at least up to 10 days after injection, proving efficacy of these low dexamethasone doses over standard direct therapeutic dosage[188]. Amikacin, an aminoglycoside antibiotic, was encapsulated in RBC for protection against enzymatic degradation and targeted to peritoneal macrophages in rats. The study revealed a significant improvement in pharmacokinetics of the antibiotic with more than five-fold increase in half-life of enclosed drug over the free drug[189,190]. Phenylalanine hydroxylase (PAH) is an enzyme that initiates and controls processing of phenylalanine, an essential amino acid. Deficiency of PAH can cause phenylketonuria. To find a sustained alternate enzyme replacement therapy for PAH, Yew *et al.* enclosed PAH in RBC by hypotonic dialysis and injected in mice. They observed a persistent level of PAH in circulation for at least 10days and a decrease of phenylalanine levels by 80%[191]. Chitosan is another popular colloidal drug delivery substrate, however as an intravascular DDS, they are flushed out from circulation easily. To extend its lifetime, low molecular weight chitosan was attached onto RBC surface by electrostatic attraction and the combination was demonstrated as a feasible DDS[192]. Among several such therapeutic molecules enclosed in RBC, some are immunophilin[193], paclitaxel[194], bovine serum albumin[195], piperine[196] and interferon-alpha 2b[197]. Apart from drugs, they have also been used to encapsulate gold nanoparticles to facilitate high contrast in dynamic X-ray imaging[198] which indicate the flexibility and lucrativeness of RBC as a functional DDS.

2.3(b) Viral Capsids based:

Viruses are submicroscopic parasitic agents that are characterized by an RNA/DNA core encapsulated by a protein coat. They can effortlessly penetrate living cells and cause unwanted effects, such as, infection or mutation. However, because of this same property, platforms derived from viral sources have been evaluated as a likely DDS[199]. Capsid is the outer shell of a virus composed of protein sub-units called capsomeres. The viral genetic material is extracted and substituted by the desired load and the capsid is re-assembled again[199]. Such a process prevents them from replicating and infecting the host, while still retaining their MPS evasive properties. Viral vectors are slowly gaining preference as a carrier of transgenes for gene therapy because they enable efficient transfer and sustained gene expression. Cooper and Shaul utilized hepatitis B viral capsid to enclose Oligonucleotides (ON). They first permeabilized the virus and treated it with ribonuclease, causing evacuation of endogenous RNA. This process was followed by incubation with ON and capsid restructuring which successfully encapsidated ON[200]. They also tested these particles on cultured HeLa cells and observed a higher cell uptake than naked ON and no cytotoxicity, providing proof of it being a viable DDS. Adeno-associated viral (AAV) serotypes were obtained by transfection of 293T cells[201]. AAV was then injected into neonatal mice brain at delivery and sacrificed after 30 days. An examination of the brain sections has affirmed efficient transduction. AAV have also been used to provide a media for conjugation and delivery of paclitaxel[202]. This could eliminate the potential virulence of chemical solvents currently used to deliver paclitaxel, which has a low water solubility. Several viral vectors were modified for gene transportation in lacrimal glands and have been thoroughly reviewed by Trousdale *et al*.[203]. Plant viruses are expected to be less pathogenic and immunostimulatory than animal virus and several of them have been used to show viability as a DDS. A group of

investigators encapsulated doxorubicin in hibiscus chlorotic ringspot virus and targeted it to ovarian cancer cell line, observing a statistically higher uptake and cytotoxicity in cancer cells[204]. Cucumber mosaic virus was also loaded with doxorubicin and conjugated with folic acid as a targeting moiety[205]. It was tested both *in vitro* and *in vivo* and exhibited enhanced antitumour action and lesser cardiotoxicity.

2.3(c) Deoxyribonucleic Acid (DNA) Based Drug Delivery Systems:

The quest to develop an ideal DDS that avoids opsonisation and renal flushing by MPS recognition as a native molecule has seen the design of a novel group of delivery structures based on the endogenous structure of DNA. DNA is a biopolymer that encodes genetic information uniquely characterized to every living organism. It is inherently biocompatible, biodegradable, physiologically stable and has engaged much interest over the past few years as an efficient DDS[206]. DNA consists of two polynucleotide strands coiled helically. Each nucleotide in a strand is constructed from either one from purine bases (adenine, guanine) or one of pyrimidine bases (cytosine, thymine) on a deoxyribose sugar and phosphate backbone. The phosphate of one nucleotide covalently binds to the sugar of adjoining nucleotide while its nitrogenous base forms a pair with the base of the other strand, together also known as base pairs. Base pairs can only be formed between adenine and guanine or cytosine and thymine and this is commonly termed as complementary base pairing.

The famous DNA origami technique proposed by Paul Rothemund[207] is contingent upon the unique base pairing feature of DNA (Fig. 2.5(a)). He manipulated DNA strands by short complementary synthetic oligonucleotide staples into various shapes and patterns such as smiley face, map of China/North America and stars. Joyce and group were the first to use DNA origami to create three dimensional structures and were followed by other research groups[208]. Ko *et al.*

utilized 52-base long, single-stranded DNA with four palindrome segments to self-assemble into DNA-nanotubes of length 50-200 nm and diameter 40 μm to delivered Cy3 to cancer cells[209]. Krishnan *et al.* described the potential of these nano-structures for cargo delivery by designing DNA icosahedra using a modular assembly approach and encapsulated it with gold nanoparticles (Fig. 2.4)[210]. These structures are suitable for drug delivery because of their high capacity to carry drug, well defined structure, biocompatibility, stability in physiological environment and commendable half-lives[211]. 2D triangular and 3D tubular origami structures were independently loaded with doxorubicin by intercalation and exposed to regular and doxorubicin resistant human adenocarcinoma breast cells (MC7)[212]. It was observed that while the DNA nanostructures, by themselves were not cytotoxic to the cell line, the ones loaded with drug induced cell-death in both types of MC7, whereas free doxorubicin was ineffective against the resistant type. Another group conjugated DNA tetrahedron with doxorubicin and it to both receptive and resitive MC7 cell lines. They obtained similar results which confirmed that DNA nanostructures had an enhanced intracellular uptake and were thus capable of reversing their drug resistivity[213]. Huang *et al.* incorporated doxorubicin in DNA-icosahedra (Doxo@DNA-icosa) and aptamer conjugated DNA-icosahedra (Doxo@Apt-DNA-icosa) and exposed it to MUC-1 negative Chinese hamster ovary cell (CHO-K1) and MUC1-positive human breast cancer cell (MCF-7) cultures[214]. Doxo@Apt-DNA-icosa showed a higher intracellular absorption in MCF-7 but not CHO-K1 cells, compared to Doxo@DNA-icosa and a higher cell lethality to MCF-7 compared with free-doxorubicin and Doxo@DNA-icosa. These data indicate the possibility of an efficient targeted DDS. Ahn *et al.* formulated a cancer cell-targeting DNA hybrid duplex of DNA-cholesterol and DNA-peptide which self-assembled into liposomal NP in solution and was then loaded with doxorubicin[215]. These NP released drug at acidic pH, thus demonstrating their capability of

functioning as a controllable smart drug. Another research group loaded similar DNA complex with circumin and docetaxel at a high loading efficiency and studied its cytotoxicity against human lung cancer cell line A549[216].

Chitosan, another biocompatible polymer sourced from chitin was paired with DNA and doxorubicin as a nanocomplex and was seen to have an extended half-life compared to naked DOX. Its efficacy was also verified against various cell lines[217]. Rolling circle amplification (RCA) is an isothermal process that generates very long periodically sequenced single stranded DNA. DNA nanoribbons were fabricated by RCA and a few staple oligonucleotides[218]. They were the coupled with CpG oligodeoxynucleotides as a model drug to prove functionality as a viable DDS. DNA hydrogels composed of CpG DNA were used to deliver doxorubicin and CpG motifs[219]. Andersen *et al.* proposed an advanced delivery system in which they designed a "DNA-box" of dimensions 42 × 36 × 36 nm^3 that could only be opened by a matching oligonucleotide "key"[220] (Fig. 2.5(b)).

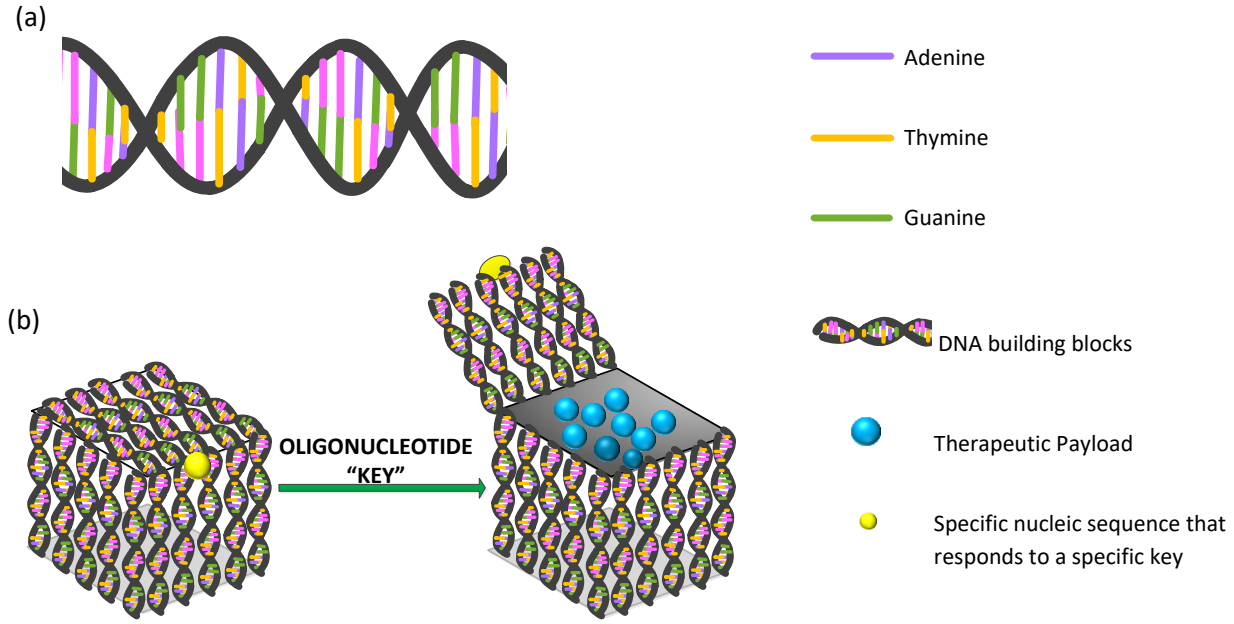

Fig. 2.5: (a) Structure of a DNA showing Watson-Crick complementary pairing. Adenine can bond only with Thymine and Guanine with Cytosine. (b) DNA box that can ideally be used to store drug molecules until the lid is opened by an oligonucleotide chain complementary to the "lock"

TABLE 2.I: Summary of DDS products developed for in-vivo applications in recent years that utilize stealth engineering technique

Type	Name of Product	Drug Load	Constituents of modification	Size	Elimination Half-life (of drug) before modification	Elimination Half-life after modification	Plasma AUC (before)	Plasma AUC (after)	Injected Dose	Test Subjects	Ref No.
Polymeric Micelle	Genexol	Paclitaxel	mPEG-PDLLA	<50 nm	0.98-1.84 h (dose dependent)	11.0-17.9 h (dose dependent)	n.a	27490±8.297 ng h/ml	390 mg/mm^2	Humans	145, 146, 147
	NK105	Paclitaxel	PEG-P(Asp)	85 nm	0.98-1.84 h (dose dependent)	5.99 h - 6.82h (dose dependent)	309.0 µg h/ml	15573.6 µg h/ml	100 mg /kg	26-Bearing CDF1 mice	145, 147
	NC-6004	Cisplatin	PEG-P(Glu)	30 nm	20-30 min	6.43h	75.73 ±26.13 µg h/ml	1335.47 ± 75.99 µg h/ml	5 mg/kg	BALB/c nude Rats implanted with MKN-45 cancer cell line	145,148, drugbank
	NK911	Doxorubicin	PEG-P(Asp)	40 nm	5-10 min	1.6-4.7 h	1620.3 ±1062.9 ng h/ml	4174.1 ± 471.2 ng h/ml	50 mg/mm^2	Humans	145, 149
	SP1049C	Doxorubicin	Pluronic F127,L61	30 nm	5-10 min	48.8 h	1620.3 ±1062.9 ng h/ml	2190 ng h/ml (approx)	50 mg/mm^2	Humans	145, 149, 150
	Pluronic 85	Doxorubicin	A-B-A type of PPO and PEO	n.a.	5-10 min	90 h (for 1 % wt dose)	n.a.	1045 µg h/ml	1% wt	C57/Bl/6 mice	145, 144
	Ps10	FITC-Dextran	PEG-PDLLA :: 10:90	96.3±6.6 nm	< 2h	47 ±12.7 h	n.a	2634±258 %ID h/ml	100 mg/kg	C57Bl/6J female mice	101
	-	Adriamycin	PEG-P(Asp)	50 nm	18 min (at 10 mg/kg)	70 min	n.a	n.a	0.1 ml/10 g	C57BL/6 male mice	179

TABLE 2.I (continued)

Type	Name of Product	Drug Load	Constituents of modification	Size	Elimination Half-life (of drug) before modification	Elimination Half-life after modification	Plasma AUC (before)	Plasma AUC (after)	Injected Dose	Test Subjects	Ref No.
Liposome	tHA-LIP	Doxorubicin	Hyaluronan	81 nm	5-10 min	139 h	-	tHA-LIP/free DXR = 47	10 mg/kg	Mice	192
	Stealth Liposome ®	1-β-D-Arabinofuranosylcytosine	HSPC:CH:PEG-DSPE :: 2:1:0.1	400 nm	16-20 min	12h	n.a	n.a	0.5 μmol	Leukemia Bearing Mice	59
	Conventional Liposomes	-	PC:CH::2:1	92-123 nm	-	13 h	-	89295 nmol h/ml	10 μmol	Female Mice	56
	Stealth Liposome ®		SM: PC:CH :GM1::1:1:1:10 %			21.6 h		138754 nmol h/ml			
	Stealth Liposome ®		SM:PC:CH:PEG-DSPE :: 1:1:1:10%			24.8 h		170150 nmol h/ml			
	Conventional Liposomes	Flurbiprofen	SPC : cholesterol :: 4:1	168 nm	2.31 h	7.36 h	151650.7 ± 16.760 ng/ml/h	43924.1 ± 24.440 ng/ml/h	2.5 mg/kg	Male Albone Wistar Arthritic Rats	193
	DSPC Liposomes		DSPC : cholesterol :: 4:1	182 nm		7.84		512669 ± 21.640 ng/ml/h			
	Stealth Liposome ®		DSPC : cholesterol : DSPE-PEG :: 4:1:0.2	192 nm		19.87 h		704408.3 ± 77.430 ng/ml/h			
	Stealth Liposome ®	Mitoxantrone	DSPC/Chol/DPPE-PEG_{2000} :: 50:45:5	n.a	<30 min	n.a	n.a	*10.95 μ mol h ml-1	10 mg kg^{-1}	female BDF1 mice	68
	Conventional Liposomes	-	PC:Chol :: 1:1	0.2μm	-	<30min	n.a.	n.a	0.12-0.14 mg	male Balb/c mice	54
	Stealth Liposome ®		PC:chol:PEG-PE::1:1:0.16			5h					

TABLE 2.I (continued)

Type	Name of Product	Drug Load	Constituents of modification	Size	Elimination Half-life (of drug) before modification	Elimination Half-life after modification	Plasma AUC (before)	Plasma AUC (after)	Injected Dose	Test Subjects	Ref No.
Liposome	Stealth Liposome ®	Doxorubicin	DSPC:chol:DSPE–PEG–COOH ::6:3:0.6	62 ± 17 nm	5.476 ± 1.690 h	20.584 ± 0.905	0.538 ± 0.145 µg h/ml	1276.458 ± 195.444 µg h/ml	5 mg/kg	male ICR mice	67
	Targeted Stealth Liposome ® (Transferin)			70 ± 19 nm		22.238 ± 2.059		1221.262 ± 80.795 µg h/ml			
	Stealth Liposome ®	FITC-Dextran	DPPC:chol:PEG-DSPE::1.85:1:0.15)	103 nm	< 2h	10.6±1.8 h	n.a.	797±46 (%ID h/ml)	70 mg/kg	C57Bl/6J female mice	101
	Conventional Liposomes	IBP 5823	PLA:Albumin	160 nm	n.a.	2-3 min	n.a.	10 h µg/ml	8 mg/kg	Sprague-Dawley rats	116
	Stealth Liposome ®		PLA:PEG	120 nm		6 h		120 h µg/ml	7 mg/kg		
	Stealth Liposome ®	Monensin	DPPC:chol:DSPE-PEG	114 ± 32nm	n.a.	7-8 h	n.a.	n.a.	0.7 M lipid (total)	BALB/c mice	80
	Stealth ImmunoLiposome ®		DPPC:chol:DSPE-PEG + anti-MY9 antibody	127 ± 41 nm							
	Stealth Liposome ®	Radio-labeled	PHEPC:PEGDSPE:HYNIC-	900 nm	n.a.	43 h	n.a.	n.a.	0.5 µmol/kg	Humans	88
						28 h			0.1 µmol/kg		
	OB2	-	1200 Da PEG	100 nm	-	15.8 ± 2.2 h	n.a.	n.a.	5 mg	Sprague–Dawley and Wistar rats	127
	OE7		1840 Da PEG			18.5 ± 4.7 h					
	OB16		2300 Da PEG			28.0 ± 10 h					
	OB18		3680 Da PEG			25.5 ± 2.7 h					
Solid Lipid NP	Stealth SLN (SSLN)	Icariin	Chol, PEG, Lecithin	50.03 ± 0.90 nm	0.21 h	1.40 h	0.82 mg h/L	3.34 mg h/L	7.46 mg/kg	Kunming Mice	136
	Non-Stealth SLN (NSLN)	Doxorubicin	Stearic Acid, Epikuron 200	80 ± 5 nm	5-10 min	241.7 ± 95.3 min	83:70 ± 19:82 µg min/ml	814.45 ± 46.11 µg min/ml	6 mg/kg	Rats	135
	Stealth SLN (SSLN)		Stearic Acid, Epikuron 200, PEG	90 ± 5 nm		211.2 ± 44.3 min		1121.10 ± 75.85 µg min/ml			

TABLE 2.I (continued)

Type	Name of Product	Drug Load	Constituents of modification	Size	Elimination Half-life (of drug) before modification	Elimination Half-life after modification	Plasma AUC (before)	Plasma AUC (after)	Injected Dose	Test Subjects	Ref No.
Dendrimers	Liposomal Doxorubicin (L-Dox) / Caelyx	Doxorubicin	PC, PEG-40-carbonyl-distearoylphosphatidylethanolamine	12 nm	0.5 ± 0.1 h	23.6 ± 3.0 h	0.42 ± 0.07 μg h/ml	1786 ± 367 μg h/ml	2 mg/kg (dox equiv)	Walker 256 tumor-bearing rats	142
	Dendrimer Doxorubicin (D-Dox)		Polylysine, PEG1100	89 nm		19.3 ± 3.1 h		341 ± 39 μg h/ml			
	PEG_{45}-DiCPT	Camptothecin	Polylysine, PEG	100 nm nanosphere	-	1.61 h	-	47.13 %ID h/g	10 mg CPT-eq./kg	BALB/c mice	143
	PEG_{45}-TetraCPT			60 nm dia. 500		5.82 h		239.71 %ID h/g			
	PEG_{45}-OctaCPT			100 nm dia 1 μm		1.70 h		58.2 %ID h/g			
	DN1	Indomethacin (intraperitoneal administration)	Folate-PAMAM conjugate, Indomethacin = 932.0 ± 12.52 μg/ml	n.a.	3.09 ± 0.13 h	6.12 ± 0.78 h	91.93 ± 10.35 μg h/ml	125.94 ± 22.34 μg h/ml	3.3 mg/kg Indomethacin equiv.	Arthritic Wistar rats	144
	FN1		Folate-PAMAM conjugate, Indomethacin = 964.8 ± 14.96 μg/ml			7.80 ± 0.15 h		127.56 ± 25.19 μg h/ml			
	FN2		Folate-PAMAM conjugate, Indomethacin = 1393.8 ± 21.75 μg/ml			8.89 ± 1.94 h		121.22 ± 1.86 μg h/ml			
	FN3		Folate-PAMAM conjugate, Indomethacin = 1457.5 ± 20.28 μg/ml			8.17 ± 1.63 h		166.59 ± 0.20 μg h/ml			

TABLE 2.I (continued)

Type	Name of Product	Drug Load	Constituents of modification	Size	Elimination Half-life (of drug) before modification	Elimination Half-life after modification	Plasma AUC (before)	Plasma AUC (after)	Injected Dose	Test Subjects	Ref No.
Dendrimers	DN1	Indomethacin (in inflamed paw)	Folate-PAMAM conjugate, Indomethacin = 932.0 ± 12.52 µg/ml	n.a.	5.06 ± 0.42 h	11.79 ± 2.68 h	207.51 ± 15.42 µg h/ml	396.44 ± 18.65 µg h/ml	3.3 mg/kg Indomethacin equiv.	Arthritic Wistar rats	144
	FN1		Folate-PAMAM conjugate, Indomethacin = 964.8 ± 14.96 µg/ml			22.79 ± 3.15 h		579.01 ± 19.25 µg h/ml			
	FN2		Folate-PAMAM conjugate, Indomethacin = 1393.8 ± 21.75 µg/ml			29.92 ± 2.36 h		602.89 ± 22.18 µg h/ml			
	FN3		Folate-PAMAM conjugate, Indomethacin = 1457.5 ± 20.28 µg/ml			37.08 ± 2.94 h		850.73 ± 20.59 µg h/ml			

2.4 CONCLUSIONS

Stealth engineering for DDS to prolong circulation time and maintain therapeutic levels of drugs in blood by camouflaging the substrate from MPS has been a topic of interest over the past 50 years. From surface PEGylation to designing DNA boxes, there have been many optimistic attempts to create the perfect DDS. This review paper describes the progression of engineering techniques used for DDS, and the key results from *in vitro*, *in vivo* and clinical studies. Such research has many therapeutic applications in humans including systemic cancer treatment, bone regeneration, gene therapy, curing pathogenic infections and insulin control. It has allowed initiation of advanced research in several vistas such as completely controllable drug delivery, where the dose intensity, duration and instant can be precisely and monitored. An exponential growth of such smart DDS can be predicted.

2.5 REFERENCES

[1] S. Gordon, P. R. Taylor, "Monocyte and macrophage heterogeneity", Nat. Rev. Immunol., vol. 5(12), pp. 953-964, 2005.

[2] D. M. Mosser, J. P. Edwards, "Exploring the full spectrum of macrophage activation", Nat Rev Immunol., vol. 8(12), pp. 958-969, 2008.

[3] C. Nich, Y. Takakubo, J. Pajarinen, M. Ainola, A. Salem, T. Sillat, A. J. Rao, M. Raska, Y. Tamaki, M. Takagi, Y. T. Konttinen, S. B. Goodman, J. Gallo, "Macrophages-Key cells in the response to wear debris from joint replacements", J. Biomed. Mater. Res. A., vol. 101(10), pp. 3033-3045, 2013.

[4] H. Kono, K. L. Rock, "How dying cells alert the immune system to danger", Nat. Rev. Immunol., vol. 8(4), pp. 279-289, 2008.

[5] X. Zhang, D. M. Mosser, "Macrophage activation by endogenous danger signals", J Pathol., vol. 214(2), pp. 161-178, 2008.

[6] C. Nathan, "Metchnikoff's legacy in 2008", Nat Immunol., vol. 9(7), pp. 695-698, 2008.

[7] G. B. Mackaness, "Cellular immunity and the parasite", Adv Exp Med Biol., vol. 93, pp. 65-73, 1977.

[8] D. C. Dale, L. Boxer, W. C. Liles, “The phagocytes: neutrophils and monocytes”, Blood, vol. 112(4), pp. 935-945, 2008.

[9] C. J. Chen, H. Kono, D. Golenbock, G. Reed, S. Akira, K. L. Rock, “Identification of a key pathway required for the sterile inflammatory response triggered by dying cells”, Nat Med, vol. 13(7), pp. 851-856, 2007.

[10] J. S. Park, D. Svetkauskaite, Q. He, J. Y. Kim, D. Strassheim, A. Ishizaka, E. Abraham, “Involvement of Toll-like receptors 2 and 4 in cellular activation by high mobility group box 1 protein”, J Biol Chem., vol. 279(9), pp. 7370-7377, 2004.

[11] S. Akira, “Toll-like receptor signaling”, J Biol Chem., vol. 278(40), pp. 38105-38108, 2003.

[12] S. L. Doyle, L. A. J. O'Neill, “Toll-like receptors: From the discovery of NF[kappa]B to new insights into transcriptional regulations in innate immunity”, Biochem Pharmacol., vol. 72(9), pp. 1102-1113, 2006.

[13] R. Duerst, K. Werberig, “Cells of the J774 macrophage cell line are primed for antibody-dependent cell-mediated cytotoxicity following exposure to gamma-irradiation”, Cell Immunol., vol. 136(2), pp. 361-372, 1991.

[14] L. E. Lambert, D. M. Paulnock, “Modulation of macrophage function by gamma-irradiation- Acquisition of the primed cell intermediate stage of the macrophage tumoricidal activation pathway”, J Immunol., vol. 139(8), pp. 2834-2841, 1987.

[15] S. Carozzi, P. M. Caviglia, M. G. Nasini, C. Schelotto, O. Santoni, A. Pietrucci, “Peritoneal dialysis solution pH and Ca2+ concentration regulate peritoneal macrophage and mesothelial cell activation”, Asaio J., vol. 40(1), pp. 20-23, 1994.

[16] M. J. Pabst, K. M. Pabst, D. B. Handsman, S. Beranova-Giorgianni, F. Giorgianni, “Proteome of monocyte priming by lipopolysaccharide, including changes in interleukin-1beta and leukocyte elastase inhibitor”, Proteome Sci., vol. 6(13), 2008.

[17] L. Tang, W. Hu W, “Molecular determinants of biocompatibility”, Expert Rev Med Devices., vol. 2(4), pp. 493–500, 2005.

[18] M. Peters-Golden, “Putting on the brakes: Cyclic AMP as a multipronged controller of macrophage function”, Sci. Signal, vol. 2(75), pp. 37, 2009.

[19] E. A. Wall, J. R. Zavzavadjian, M. S. Chang, B. Randhawa, X. Zhu, R. C. Hsueh, J. Liu, A. Driver, X. R. Bao, P. C. Sternweis, M. I. Simon, I. D. Fraser, “Suppression of LPS-induced TNF-α production in macrophages by cAMP is mediated by PKA-AKAP95”, Sci Signal, vol. 2(75), pp. 28, 2009.

[20] E. A. Ham, D. D. Soderman, M. E. Zanetti, H. W. Dougherty, E. McCauley, F. A. Kuehl, “Inhibition by prostaglandins of leukotriene B4 release from activated neutrophils”, Proc Natl Acad Sci USA., vol. 80(14), pp. 4349-4353, 1983.

[21] H. Harizi, M. Juzan, V. Pitard, J. F. Moreau, N. Gualde, “Cyclooxygenase-2-issued prostaglandin E2 enhances the production of endogenous IL-10, which down-regulates dendritic cell functions”, J Immunol., vol. 168(5), pp. 2255-2263, 2002.

[22] A. Diaz, J. Varga, S. A. Jimenez, “Transforming growth factor-beta stimulation of lung fibroblast prostaglandin E2 production”, J Biol Chem., vol. 264(20), pp. 11554-11557, 1989.

[23] T. Kohyama, X. Liu, H. J. Kim, T. Kobayashi, R. F. Ertl, F. Q. Wen, H. Takizawa, S. I. Rennard, “Prostacyclin analogs inhibit fibroblast migration”, Am J Physiol Lung Cell Mol Physiol., vol. 283(2), pp. 428-432, 2002.

[24] A. D. Bangham, M. M. Standish, J. C. Watkins, “Diffusion of univalent ions across the lamellae of swollen phospholipids”, J Mol Biol., vol. 13(1), pp. 238-252, 1965.

[25] G. Gregoriadis, “Liposomes In Drug Delivery: Present and Future”, Liposome Dermatics, pp. 346-352, 1992.

[26] G. Gregoriadis, B. E. Ryman, “Liposomes as carrier of enzymes or drugs: a new approach to the treatment of storage diseases”, Biochem J., vol. 124(5), pp. 58, 1971.

[27] A. W. Segal, G. Gregoriadis, C. D. V. Black, “Liposomes as vehicles for local release of drugs”, Clin Sci Mol Med., vol. 49(2), pp. 99-106, 1975.

[28] G. Gregoriadis, “The carrier potential of liposomes in biology and medicine (first of two parts)”, N Engl J Med., vol. 295(14), pp. 704-710, 1976.

[29] G. Gregoriadis G, “The carrier potential of liposomes in biology and medicine (second of two parts)”, N Engl J Med., vol. 295(14), pp. 765-770, 1976.

[30] G. Gregoriadis, “Drug Entrapment in Liposomes”, FEBS Lett., vol. 36(3), pp. 292-296, 1973.

[31] G. Gregoriadis, D. Putman, L. Louis, D. Neerunjun, “Comparative effect and fate of non-entrapped and liposome-entrapped neuraminidase injected into rats”, Biochem J., vol. 140(2), pp. 323-330, 1974.

[32] T. M. Allen, P. R. Cullis, “Liposomal Drug Delivery Systems: From concept to clinical applications”, Adv Drug Deliv Rev., vol. 65(1), pp. 36-48, 2013.

[33] D. Hoekstra, C. Scherpof, “Effect of fetal calf serum and serum protein fractions on the uptake of liposomal phosphatidylcholine by rat hepatocytes in primary monolayer culture”, Biochim Biophys Acta., vol. 551(1), pp. 109-121, 1979.

[34] A. Chonn, S. C. Semple, P. R. Cullis, “Association of blood proteins with large unilamellar liposomes in vivo (Relation to circulation lifetimes)”, J Biol Chem., vol. 267(26), pp. 18759-18765, 1992.

[35] S. Stolnik, L. Illum, S. S. Davis, “Long circulating microparticle drug carriers”, Adv Drug Deliv Rev., vol. 16(2-3), pp. 195-214, 1995.

[36] J. Yoo, N. Doshi, S. Mitragotri, “Adaptive micro and nanoparticles: Temporal control over carrier properties to facilitate drug delivery”, Adv Drug Del Rev., vol. 63(14-15), pp. 1247-1256, 2011.

[37] F. Yamashita, M. Hashida, “Pharmacokinetic considerations for targeted drug delivery”, Adv Drug Del Rev., vol. 65(1), pp. 139-147, 2013.

[38] V. P. Torchilin, V. S. Trubetskoy, “Which polymers can make nanoparticulate drug carriers long-circulating?”, Adv Drug Deliv Rev., vol. 16(2-3), pp. 141-155, 1995.

[39] J. Gong, M. Chen, Y. Zheng, S. Wang, Y. Wang, “Polymeric micelles drug delivery system in oncology”, J Control Rel., vol. 159(3), pp. 312-323, 2012.

[40] S. Venkataraman, J. L. Hedrick, Z. Y. Ong, C. Yang, P. L. R. Ee, P. T. Hammond, Y. Y. Yang, “The effects of polymeric nanostructure shape on drug delivery”, Adv Drug Del Rev., vol. 63(14-15), pp. 1228-1246, 2011.

[41] Y. Geng, P. Dalhaimer, S. Cai, R. Tsai, M. Tewari, T. Minko, D. E. Discher, “Shape effects of filaments versus spherical particles in flow and drug delivery”, Nat Nanotechnol., vol. 2(4), pp. 249–255, 2007.

[42] J. A. Champion, S. Mitragotri, “Shape induced inhibition of phagocytosis of polymer particles”, Pharm. Res., vol. 26(1), pp. 244-249, 2009.

[43] R. M. Abra, M. E. Bosworth, C. A. Hunt, “Liposome Deposition in vivo: effects of pre-dosing with liposomes”, Res Commun Chem Pathol Pharmacol., vol. 29(2), pp. 349-360, 1980.

[44] Y. J. Kao, K. L. Juliano, “Interactions of liposomes with reticuloendothelial system. Effects of reticulothelial blockade on clearance of large unilamellar vesicles”, Biochim Biophys Acta., vol. 677(3-4), pp. 453-61, 1981.

[45] R. M. Abra, C. A. Hunt, “Liposome Disposition in vivo III: Dose and vesicle size effects”, Biochim Biophys Acta., vol. 666(3), pp. 493-503, 1981.

[46] R. M. Abra, C. A. Hunt, “Liposome disposition in vivo IV: the interaction of sequential doses of liposomes having different diameters”, Res Commun Chem Pathol Pharmacol., vol. 6(1), pp. 17-31, 1982.

[47] J. W. B. Bradfield, R. L. Souhami, I. E. Addison, “Mechanism of adjuvant effect of dextran sulphate”, Immunology, vol. 26(2), pp. 383-392, 1974.

[48] J. L’Age-Stehr, T. Diamantstein, “Suppression and potentiation of expression of delayed type hypersensitivity by dextran sulphate”, Immunology, vol. 33(2), pp. 179-183, 1977.

[49] K. R. Patel, M. P. Li, J. D. Baldeschwieler, “Suppression of liver uptake of liposomes by dextran sulphate 500”, Proc Natl Acad Sci. USA, vol. 80(21), pp. 6518-6522, 1983.

[50] D. Aragnol, L. D. Leserman, “Immune Clearance of Liposomes inhibited by an anti-Fc receptor antibody in vivo”, Proc Natl Acad Sci. USA, vol. 83(8), pp. 2699-2703, 1986.

[51] P. L. Toutain, A. Bousquet-Melou, “Plasma terminal half-life”, J vet Pharmacol Ther., vol. 27(6), pp. 427-439, 2004.

[52] Y. Zhang, H. F. Chan, K. W. Leong, “Advanced materials and processing for drug delivery: The past and the future”, Adv Drug Deliv Rev., vol. 65(1), pp. 104-120, 2013.

[53] C. Kirby, J. Clarke, G. Gregoriadis, “Effect of the cholesterol content of small unilamellar liposomes on their stability in vivo and in vitro”, Biochem J., vol. 186(2), pp. 591-598, 1980.

[54] G. Gregoriadis, C. Davis, “Stability of Liposomes in vivo and in vitro is promoted by their cholesterol content and presence of blood cells”, Biochem Biophys Res Commun., vol. 89(4), pp. 1287-1293, 1979.

[55] S. C. Semple, A. Chonn, P. R. Cullis, “Influence of Cholesterol on the association of plasma proteins with liposomes”, Biochemistry, vol. 35(8), pp. 2521-2525, 1996.

[56] W. Zhou, Z. An, J. Wang, W. Shen, Z. Chen, X. Wang, “Characteristics, phase behaviour and control release for copolymer-liposome with both pH and temperature sensitivities”, Colloids Surf A, vol. 395(5), pp. 225-23, 2012.

[57] A. Gabizon, D. Papahadjopoulos, “Liposome Formulations with prolonged circulation time in blood and enhanced uptake by tumors”, Proc Natl Acad Sci. USA, vol. 85(18), pp. 6949-6953, 1988.

[58] T. M. Allen, A. Chonn, “Large unilamellar liposomes with low uptake into the reticuloendothelial system”, FEBS Lett., vol. 223(1), pp. 42-46, 1987.

[59] T. M. Allen, “Stealth Lipsomes: avoiding reticuloendothelial uptake. UCLA symposium in Molecular and Cellular Biology”, vol. 405-415, 1989.

[60] A. Abuchowski, J. R. McCoy, N. C. Palczuk, T. V. Es, F. F. Davis, “Effect of covalent attachment of polyethylene glycol on immunogenicity and circulating life of bovine liver catalase”, J Biol Chem., vol. 25(11), pp. 3582-3586, 1977.

[61] G. Blume, G. Cevc, “Liposomes for the sustained drug release in vivo”, Biochim Biophys Acta., vol. 1029(1), pp. 91-97, 1990.

[62] A. L. Klibanov, K. Maruyama, V. P. Torchilin, L. Huang L, “Amphipathic polyethylene glycol effectively prolong the circulation time of liposomes”, FEBS Lett., vol. 268(1), pp. 235-237, 1990.

[63] J. Senior, C. Delgado, D. Fisher, C. Tilcock, G. Gregoriadis, “Influence of surface, hydrophilicity of liposomes on their interaction with plasma protein and clearance from the circulation: studies with poly(ethylene glycol) coated vesicles”, Biochim Biophys Acta., vol. 1062(1), pp. 77-82, 1991.

[64] T. M. Allen, C. Hansen, “Pharmacokinetics of stealth versus conventional liposomes: effect of dose”, Biochim Biophys Acta., vol. 1068, pp. 133-141, 1991.

[65] K. Maruyama, T. Yuda, A. Okamoto, S. Kojima, A. Suginaka, M. Iwatsuru, “Prolonged circulation time in vivo of large unilamellar liposomes composed of distearoylphosphatidylcholine and cholesterol containing amphipathic poly(ethylene glycol)”, Biochim Biophysics Acta., vol. 1128(1), pp. 44-49, 1992.

[66] M. C. Woodle, G. Storm, M. S. Newman, J. J. Jekot, L. R. Collins, F. J. Martin, F. J. Szoka, “Prolonged systemic delivery of peptide drugs by long circulating liposomes: Illustration with Vasopressin in the Brattleboro rat”, Pharma Res., vol. 9(2), pp. 260-265, 1992.

[67] T. M. Allen, T. Mehra, C. Hansen, “Stealth Liposomes: An improved sustained release system for 1-β-d-Arabinofuranosyl cytosine”, Cancer Res., vol. 52, pp. 2431-2439, 1992.

[68] A. Gabizon, R. Catane, B. Uziely, B. Kaufman, T. Safra, R. Cohem, F. Martin, A. Huang, Y. Barenholz, “Prolonged circulation time and enhanced accumulation in malignant exudates of doxorubin encapsulated in polyethylene-glycol coated liposomes”, Cancer Res., vol. 54(4), pp. 987-992, 1994.

[69] N. D. James, R. J. Coker, D. Tomilinson, J. R. Harris, M. Gompels, A. J. Pinching, J. S. Stewart, “Liposomal doxorubicin (doxil): an effective new treatment for Kaposi’s sarcoma in AIDS”, Clin Oncol (R Coll Radiol), vol. 6(5), pp. 294-296, 1994.

[70] J. Vaage, D. Donovan, P. Uster, P. Working, “Tumour uptake of doxorubin in polyethylene glycol-coated liposomes and therapeutic effect against a xenografted human pancreatic carcinoma”, Br J Cancer., vol. 75(4), pp. 482-486, 1997.

[71] C. W. Chang, L. Barber, C. Ouyang, D. Masin, M. B. Bally, T. D. Madden, “Plasma clearance, biodistribution and therapeutic properties of mitoxantrone encapsulated in conventional and sterically stabilized liposomes after intravenous administration in BDF1 mice”, Br J Cancer, vol. 75(2), pp. 169-177, 1997.

[72] P. Deol, G. K. Khuller, “Lung specific stealth lipsomes: stability, biodistribution and toxicity of liposomal antitubercular drugs in mice”, Biochim Biophys Acta., vol. 1334(2-3), pp. 161-172, 1997.

[73] A. Etzerodt, M. B. Maniecki, J. H. Graversen, H. J. Moller, V. P. Torchilin, S. K. Moestrup, “Efficient intracellular drug targeting of macrophages using stealth liposomes directed to the hemoglobin scavenger receptor CD163”, J Control Release, vol. 160, pp. 72-80, 2012.

[74] L. L. Timo, L. M. ten Hagen, M. Hossann, R. Suss, G. C. van Rhoon, A. M. M. Eggermont, D. Hammerich, G. A. Koning, “Mild hyperthermia triggered doxorubicin release from optimized stealth thermosensitive liposomes improves intratumoral drug delivery and efficacy”, J Control Release, vol. 168, pp. 142-150, 2013.

[75] X. Li, L. Ding, Y. Xu, Y. Wang, Q. Ping, “Targeted delivery of doxorubicin using stealth liposomes modified with transferrin”, Int J Pharm., vol. 373, pp. 116-123, 2009.

[76] C. W. Chang, L. Barber, C. Ouyang, D. Masin, M.B. Bally, T. D. Madden, “Plasma clearance, biodistribution and therapeutic properties of mitoxantrone encapsulated in conventional and sterically stabilized liposomes after intravenous administration in BDF1 mice”, Br J Cancer., vol. 75(2), pp. 169-177, 1997.

[77] Z. Y. He, X. Zheng, X. H. Wu, X. R. Song, G. He, W. F. Wu, S. Yu, S. J. Mao, Y. Q. Wei, “Development oglycyrrhetinic acid-modified stealth cationic liposomes for gene delivery”, Int J Pharm., vol. 397, pp. 147-154, 2010.

[78] T. P. Herringson, J. G. Altin, “Convenient targeting of stealth si RNA-lipoplexes to cells with chelator lipid-anchored molecules”, J Control Release, vol. 139, pp. 229-238, 2009.

[79] Y. Namiki, T. Namiki, M. Date, K. Yanagihira, M. Yashiro, H. Takahashi, “Enhanced photodynamic antitumour effect on gastric cancer by a novel photosensitive stealth liposome”, Pharmacol Res., vol. 50, pp. 65-76, 2004.

[80] W. Dai, T. Yang, Y. Wang, X. Wang, J. Wang, X. Zhang, Q. Zhang, “Peptide PHSCNK as an integrin α5β1 antagonist targets stealth liposomes to integrin-overexpressing melanoma”, J Nanomed Nanotechnol., vol. 8, pp. 1152-1161, 2012.

[81] E. Ducat, J. Deprez, A. Gillet, A. Noel, B. Evrard, O. Peulen, G. Piel, “Nuclear delivery of a therapeutic peptide by long circulating pH-sensitive liposomes : Benefits over classical vesicles”, Int J Pharm., vol. 420, pp. 319-332, 2011.

[82] A. Gabizon, D. Goren, A. T. Horowitz, D. Tzemach, A. Lossos, T. Siegal, “Long-circulating liposomes for drug delivery in cancer therapy: a review of biodistribution studies in tumor bearing animals”, Adv Drug Deliv Rev., vol. 24, pp. 337-344, 1997.

[83] H. Yanagie, K. Maruyama, T. Takizawa, O. Ishida, K. Ogura, T. Matsumoto, Y. Sakurai, T. Kobayashi, A. Shinohara, J. Rant, J. Skvarc, R. Illic, G. Kuhne, M. Chiba, Y. Furuya, H. Sugiyama, T. Hisa, K. Ono, H. Kobayashi, M. Eriguchi, “Application of boron-entrapped stealth liposomes to inhibition of growth of tumor cells in the in vivo boron neutron-capture therapy model”, Biomed Pharmacother., vol. 60, pp. 43-50, 2006.

[84] A. V. Doi, H. Ishiwata, K. Miyajima, “Binding and uptake of liposomes containing a poly (ethylene glycol) derivative of cholesterol (stealth liposomes) by the macrophage cell line J774: influence of PEG content and its molecular weight”, Biochim Biophys Acta., vol. 1278, pp. 19-28, 1996.

[85] M. R. Ranson, S. Cheeseman, S. White, J. Margison, “Caelyx (stealth liposomal doxorubicin) in the treatment of advanced breast cancer”, Crit Rev Oncol Hematol., vol. 37, pp. 115-120, 2001.

[86] T. M. Allen, E. H. Moase, “Therapeutic opportunities for targeted liposomal drug delivery”, Adv Drug Deliv Rev., vol. 21, pp. 117-133, 1996.

[87] K. Jorgensen, J. Davidsen, O. G. Mouritsen, “Biophysical mechanisms of phospholipase A2 activation and their use in liposome-based drug delivery”, FEBS Lett., vol. 531, pp. 23-27, 2002.

[88] M. Singh, A. J. Ferdous, N. Kannikkannan, G. Faulkner, “Stealth monensin immunoliposomes as potentiator of immunotoxins in vitro”, Eur J Pharm Biopharm., vol. 52, pp. 13-20, 2001.

[89] A. Junior, L. G. Mota, E. A. Nunan, A. J. A. Wainstein, A. P. D. L. Wainstein, A. S. Leal, V. N. Cardoso, M. C. De Oliveira, “Tissue distribution evaluation of stealth pH-sensitive liposomal cisplatin versus free cisplatin in Ehrlich tumor-bearing mice”, Life Sci., vol. 80, pp. 659-664, 2007.

[90] L. L. Timo, L. M. Hagen, D. Schipper, T. M. Wijnberg, G. C. van Rhoon, A. M. M. Eggermont, L. H. Lindner, G. A. Koning, “Triggered content release from optimized stealth thermosensitive liposomes using mild hyperthermia”, J Control Release, vol. 143, pp. 274-279, 2010.

[91] R. Li, X. Ying, Y. Zhang, R. Ju, X. Wang, H. Yao, Y. Men, W. Tian, Y. Yu, L. Zhang, R. Huang, W. Lu, “All-trans retinoic acid stealth liposomes prevent the relapse of breast cancer arising from the cancer stem cells”, J Control Release, vol. 149, pp. 281-291, 2011.

[92] T. Ishida, D. L. Iden, T. M. Allen, “A combinatorial approach to producing sterically stabilized (stealth) immunoliposomal drugs”, FEBS Lett., vol. 460, pp. 129-133, 1999.

[93] S. K. Singh, P. S. Bisen, “Adjuvanticity of stealth liposomes on the immunogenicity of synthetic gp41 epitope of HIV-1”, Vaccine, vol. 24, pp. 4161-4166, 2006.

[94] J. C. Wang, X. Y. Liu, W. L. Lu, A. Chang, Q. Zhang, B. C. Goh, H. S. Lee, “Pharmacokinetics of intravenously administered stealth liposomal doxorubicin modulated with verapamil in rats”, Eur J Pharm Biopharm., vol. 62, pp. 44-51, 2006.

[95] Z. Amoozgar, Y. Yeo, “Recent advances in stealth coating of nanoparticles drug delivery systems”, Wiley Interdiscip Rev Nanomed Nanobiotechnol., vol. 4, pp. 219-233, 2012.

[96] P. Laverman, A. H. Brouwers, C. T. M. Dams, W. J. G. Oyen, G. Storm, N. V. Rooijen, F. H. M. Corstens, O. C. Boerman, “Preclinical and clinical evidence for disappearance of long-circulating characteristics of polyethylene glycol liposomes at low lipid dose”, J Pharmacol Exp Ther., vol. 293, pp. 996-1001, 2000.

[97] E. T. Dams, P. Laverman, W. J. Oyen, G. Storm, G. L. Scherphof, J. W. Van Der Meir, F. H. Corstens, O. C. Boerman, “Accelerated blood clearance and altered biodistribution of repeated injections of sterically stabilized liposomes”, J Pharmacol Exp Ther., vol. 292(3), pp. 1071-1079, 2000.

[98] P. Laverman, M. G. Carstens, O. C. Boerman, E. T. Dams, W. J. Oyen, N. V. Rooijen, F. H. Corstens, G. Storm, “Factors affecting the accelerated blood clearance of polyethylene glycol-liposomes upon repeated injection”, J Pharmacol Exp Ther., vol. 298(2), pp. 607-612, 2001.

[99] T. Ishida, R. Maeda, M. Ichihara, K. Irimura, H. Kiwada, “Accelerated clearance of PEGylated liposomes in rats after repeated injections”, J Control Release, vol. 88, pp. 35-42, 2003.

[100] T. Ishida, K. Masuda, T. Ichikawa, M. Ichihara, K. Irimura, H. Kiwada, “Accelerated clearance of a second injection of PEGylated liposomes in mice”, Int J Pharm., vol. 255(1-2), pp. 167-174, 2003.

[101] T. Ishida, T. Ichikawa, M. Ichihara, Y. Sadzuka, H. Kiwada, “Effect of physicochemical properties of initially injected liposomes on the clearance of subsequently injected PEGylated liposomes in mice”, J Control Release, vol. 95(3), pp. 403-412, 2004.

[102] T. Ishida, M. Harada, X. Y. Wang, M. Ichihara, K. Irimura, H. Kiwada, "Accelerated blood release of PEGylated liposomes following preceding liposome injection: effects of lipid dose and PEG surface-density and chain length of first-dose liposomes", J Control Release, vol. 105(3), pp. 305-317, 2005.

[103] X. Y. Wang, T. Ishida, M. Ichihara, H. Kiwada, "Influence of the physicochemical properties of liposomes on the accelerated blood clearance phenomenon in rats", J Control Release, vol. 104(1), pp. 91-102, 2005.

[104] T. Ishida, M. Ichihara, X. Wang, K. Yamamoto, J. Kimura, E. Majima, H. Kiwada, "Injection of PEGylated liposomes in rat elicits PEG-specific IgM, which is responsible for rapid elimination of a second dose of PEGylated liposomes", J Control Release, vol. 112(1), pp. 15-25, 2006.

[105] T. Ishida, K. Atobe, X. Wang, H. Kiwada, "Accelerated blood clearance of PEGylated liposomes upon repeated injections: effect of doxorubin-encapsulation and high dose first injection", J Control Release, vol. 155(3), pp. 251-258, 2006.

[106] A. Lavasanifar, J. Samuel, G. S. Kwon, "Poly(ethylene oxide)-block-poly(L-amino acid) micelles for drug delivery", Adv Drug Deliv Rev., vol. 54, pp. 169-190, 2002.

[107] E. V. Batrakova, A. V. Kabanov, "Pluronic Block Copolymers: Evolution of drug delivery concept from inert nanocarriers to biological response modifiers", J Control Release, vol. 130(2), pp. 98-106, 2008.

[108] J. S. Lee, M. Ankone, E. Pieters, R. M. Schiffelers, W. E. Hennink, J. Feijen, "Circulation kinetics and biodistribution of dual-labeled polymerosomes with modulated surface charge in tumor-bearing mice : comparison with stealth liposomes", J Control Release, vol. 155, pp. 282-288, 2011.

[109] G. Gaucher, M. H. Dufresne, V. P. Sant, N. Kang, D. Maysinger, J. C. Leroux, "Block copolymer micelles: preparation, characterization and application in drug delivery", J Control Release, vol. 109, pp. 169-188, 2005.

[110] E. V. Batrakova, S. Li, Y. Li, V. Y. Alakhov, W. F. Elmquist, A. V. Kabanov, "Distribution kinetics of a micelle-forming block copolymer Pluronic P85", J Control Release, vol. 100(3), pp. 389-397, 2004.

[111] L. Illum, S. S. Davis, "Effect of nonionic surfactant poloxamer 338 on the fate and deposition of polystyrene microspheres following intravenous administration", J Pharm Sci., vol. 72, pp. 1086-1089, 1983.

[112] L. Illum, S. S. Davis, "The organ uptake of intravenously administered colloidal particles can be altered using a non-ionic surfactant (poloxamer 338)", FEBS Lett., vol. 167, pp. 79-82, 1984.

[113] L. Illum, S. S. Davis, R. H. Muller, E. Mak, P. West, "The organ distribution and circulation time of intravenously injected colloidal carriers sterically stabilized with a block copolymer poloxamine 908", Int J Pharm., vol. 89, pp. 25-31, 1993.

[114] S. Rudt, R. H. Muller, "In vitro phagocytosis assay of nano and micro-particles by chemiluminescence III. Uptake of differently sized surface-modified particles and its correlation to particle properties and in vivo distribution", Eur J Pharm Sci., vol. 1, pp. 31-39, 1993.

[115] S. Moghimi, T. Gray, "A single dose of intravenously injected poloxamine-coated long-circulating particles triggers macrophage clearance of subsequent dosage in rats", Clin Sci (Lond), vol. 93(4), pp. 371-379, 1997.

[116] S. M. Moghimi, K. D. Pavey, A. C. Hunter, "Real time evidence of surface modification of polysterene lattices by poloxamine 908 in the presence of serum : in vivo conversion of macrophage prone nanoparticles to stealth entities by poloxamine 908", FEBS Lett., vol. 547, pp. 177-182, 2003.

[117] S. E. Dunn, A. G. A. Coombes, M. C. Garnett, S. S. Davis, L. Illum, "In vitro cell interaction and in vivo distribution of poly(lactide-co-glycolide) nanosphere surface modified by poloxamer and poloxamine copolymers", J Control Release, vol. 44, pp. 65-76, 1997.

[118] L. Araujo, R. Lobenberg, J. Kreuter, "Influence of the surfactant concentration on the body distribution of nanoparticles", J Drug Target., vol. 6(5), pp. 373-385, 1999.

[119] D. Jain, R. Athawale, A. Bajaj, S. Shrikhande, P. N. Goel, "Studies on stabilization mechanism and stealth effect of poloxamer 188 onto PLGA nanoparticles", Colloids Surf B: Biointer., vol. 109, pp. 59-67, 2013.

[120] N. Rapoport, "Physical stimuli-responsive polymeric micelles for anti-cancer drug delivery", Prog Polym Sci., vol. 32, pp. 962-990, 2007.

[121] G. He, L. L. Ma, J. Pan, S. Venkataraman, "ABA and BAB type tri-block copolymer of PEG and PLA: A comparative study of drug release properties and "stealth" particle characteristics", Int J Pharm., vol. 334, pp. 48-55, 2007.

[122] S. Moffatt, R. J. Cristiano, "Uptake characteristics of NGR coupled stealth PEI/pDNA nanoparticles loaded with PLGA-PEG-PLGA tri-block copolymer for targeted delivery to human monocyte-derived dendritic cells", Int J Pharm., vol. 321, pp. 143-154, 2006.

[123] T. Verrecchia, G. Spenlehauer, D. V. Bazile, A. Murry-Brelier, Y. A. Archimbaud, M. Veillard, "Non-stealth (poly(lactic acid) albumin)) and stealth (poly(lactic acid-polyethylene glycol)) nanoparticles as injectable drug carriers", J Control Release, vol. 36, pp. 49-61, 1995.

[124] W. Zhiqing, L. Wei, X. Huibi, Y. Xiangliang, “Preparation and in vitro studies of stealth PEGylated PLGA nanoparticles as carriers for Arsenic Trioxide”, Chin J Chem Eng, vol. 15(6), pp. 795-801, 2007.

[125] D. Bazile, C. Prud Homme, M. Bassoullet, M. Marlard, G. Spenlehauer, M. Veillard, “Stealth Me-PEG–PLA nanoparticles avoid uptake by the mononuclear phagocyte system”, J Pharm Sci, vol. 84, pp. 493–498, 1995.

[126] M. Tobio, R. Gref, A. Sanchez, R. Langer, M. T. Alonso, “Stealth PLA–PEG nanoparticles as protein carriers for nasal administration”, Pharm Res., vol. 15, pp. 270–275, 1998.

[127] T. Govender, T. Riley, S. Stolnik, M. C. Garnett, L. Illum, S. S. Davis, “PLA–PEG nanoparticles for site specific delivery: drug incorporation studies”, J Control Release, vol. 64, pp. 269–347, 2000.

[128] T. S. Yarza, F. R. Formiga, E. Tamayo, B. Pelacho, F. Prosper, M. J. Blanco-Prieto, “PEGylated-PLGA microparticles containing VEGF for long term drug delivery”, Int J Pharm., vol. 440, pp. 13-18, 2013.

[129] R. Gref, G. Miralles, E. Dellacherie, “Polyoxyethylene coated nanospheres: effect of coating on zeta potential and phagocytosis”, Polymer Int., vol. 48, pp. 251–256, 1999.

[130] M. T. Peracchia, E. Fattal, D. Desmaele, M. Bensard, J. P. Noel, J. M. Gomis, M. Appel, J. d’Angelo, P. Couvreur, “Stealth PEGylated polycyanoacrylate nano-particles for intravenous administration and splenic targeting”, J Control Release, vol. 60, pp. 121–128, 1999.

[131] M. T. Peracchia, C. Vauthier, F. Puisieux, P. Couvreur, “Development of sterically stabilized poly(isobutyl-2-cyanoacrylate) nanoparticles by chemical coupling of poly-(ethylene glycol)”, J Biomed Mater Res., vol. 34, pp. 317–326, 1997.

[132] M. T. Peracchia, C. Vauthier, C. Passirani, P. Couvreur, D. Labarre, “Compliment consumption by poly(ethylene glycol)in different conformations chemically coupled topoly(isobutyl-2-cyanoacrylate) nanoparticles”, Life Sci., vol. 61, pp. 741–761, 1997.

[133] F. Ahmed, D. W. Discher, “Self-porating polymerosomes of PEG-PLA and PEG-PCL: hydrolysis-triggered controlled release vesicles”, J Control Release, vol. 96, pp. 37-53, 2004.

[134] P. Photos, L. Bacakova, B. Discher, F. S. Bates, D. E. Discher, “Polymer vesicles in vivo: correlations with PEG molecular weight”, J Control Release, vol. 90(3), pp. 323-334, 2003.

[135] F. D. Jaeghere, E. Allemann, J. C. Leroux, W. Stevels, J. Feijen, E. Doelker, R. Gurny, “Formulation and lyoprotection of poly(lactic acid-co-ethylene oxide) nanoparticles:

Influence on the physical stability and in vitro cell uptake", Pharm Res., vol. 16, pp. 859–866, 1999.

[136] M. Vittaz, D. Razile, G. Spenlehauer, T. Verrecchia, M. Veillard, F. Puisieux, D. Labarre, "Effect of PEO surface density on long-circulating PLA–PEO nanoparticles which are very low complement activators", Biomaterials, vol. 17, pp. 1575–1581, 1996.

[137] M. F. Zambaux, B. F. Fiorina, F. Bonneaux, S. Marchal, J. L. Merlin, E. Dellacherie, P. Labrude, C. Vigneron, "Involvement of neutrophilic granulocytes in the uptake of biodegradable non-stealth and stealth nanoparticles in guinea pig", Biomaterials, vol. 21, pp. 975-980, 2000.

[138] K. V. Butsele, M. Morille, C. Passirani, P. Legras, J. P. Benoit, S. K. Varshney, R. Jerome, C. Jerome, "Stealth properties of poly(ethylene oxide) based triblock copolymer micelles : A prerequisite for a pH-triggered targeting system", Acta Biomaterialia., vol. 7, pp. 3700-3707, 2011.

[139] S. Salmaso, P. Caliceti P, "Stealth properties to improve therapeutic efficacy of drug nanocarriers", Drug Deliv., vol. 2013, pp. 1-19, 2013.

[140] Y. Matsumura, T. Hamaguchi, T. Ura, K. Muro, Y. Yamada, Y. Shimada, K. Shirao, T. Okusaka, H. Ueno, M. Ikeda, N. Watanabe, "Phase I clinical trial and pharmacokinetic evaluation of NK911, a micelle encapsulated doxorubicin", Br J Cancer., vol. 91, pp. 1775-1781, 2004.

[141] H. Cabral, K. Kataoka, "Progress of drug-loaded polymeric micelles into clinical studies", J Control Rel., vol. 190, pp. 465-476, 2014.

[142] A. Muhlen, C. Schwarz, W. Mehnert, "Solid lipid nanoparticles (SLN) for controlled drug delivery: drug release and release mechanism", Eur J Pharm Biopharm., vol. 45(2), pp. 149-155, 1998.

[143] C. Bocca, D. Caputo, R. Cavalli, L. Gabriel, A. Miglietta, M. R. Gasco, "Phagocytic uptake of fluorescent stealth and non-stealth solid lipid nanoparticles", Int J Pharm., vol. 175, pp. 185-193, 1998.

[144] A. Fundaro, R. Cavalli, A. Bargoni, D. Vighetto, G. P. Zara, M. R. Gasco, "Non-stealth and stealth solid lipid nanoparticles (SLN) carrying doxorubicin: pharmacokinetics and tissue distribution after i.v. administration to rats", Pharmacol Res., vol. 42(4), pp. 337-343, 2000.

[146] K. Liu, L. Wang, Y. Li, B. Yang, C. Du, Y. Wang, "Preparation. Pharmacokinetics and tissue distribution properties of icariin-loaded stealth solid lipid nanoparticles in mice", Chin Herb Med., vol. 4(2), pp. 170-174, 2012.

[147] J. Madan, R. S. Pandey, V. Jain, O. P. Katare, R. Chandra, A. Katyal, "Poly(ethylene)-glycol conjugated solid lipid nanoparticles improve biological half-life, brain delivery and efficacy in glioblastoma cells", Nanomed. Nanotechnol., vol. 9(4), pp. 492-503, 2013.

[148] D. A. Tomalia, H. Baker, J. Dewald, M. Hall, G. Kallos, S. Martin, J. Roeck, J. Ryder, P. Smith, "A new class of polymers: Starburst-dendritic macromolecules", Polym J., vol. 17, pp. 117–132, 1985.

[149] S. Mignani, S. E. Kazzouli, M. Bousmina, J. P. Majoral JP, "Expand classical drug administration ways by emerging routes using dendrimer drug delivery systems: A concise overview", Adv Drug Deliv Rev., vol. 65, pp. 1316-1330, 2013.

[150] C. Kojima, K. Kono, K. Maruyama, T. Takagashi, "Synthesis of polyamidoamine dendrimers having poly(ethylene glycol) grafts and their ability to encapsulate anticancer drugs", Bioconj Chem., vol. 11, pp. 910-917, 2000.

[151] N. Mallik, R. Wiwattanapatapee, R. Klopsch, K. Lorenz, H. Frey, J. W. Weener, E. W. Meijer, W. Paulus, R. Duncan, "Dendrimers: Relationship between structure and biocompatibility in vitro, and preliminary studies on the biodistribution of 125I-labelled polyamidoaminedendrimers in vivo", J Control Release, vol. 65, pp. 133-148, 2000.

[152] L. M. Kaminskas, V. M. McLeod, B. D. Kelly, G. Sberna, B. J. Boyd, M. Williamson, D. J. Owen, C. J. H. Porter, "A comparison of changes to doxorubicin pharmacokinetics, antitumor activity and toxicity mediated by PEGylated dendrimer and PEGylated liposome drug delivery systems", Nanomed., vol. 8, pp. 103-111, 2010.

[153] Z. Zhou, X. Ma, E. Jin, J. Tang, M. Sui, Y. Shen, E. A. V. Kirk, W. J. Murdoch, M. Radosz, "Linear-dendritic drug conjugates forming long-circulating nanorods for cancer drug delivery", Biomaterials, vol. 34(22), pp. 1-14, 2013.

[154] D. Chandrasekar, R. Sistla, F. J. Ahmad, R. K. Khar, P. V. Diwan, "The development of folate-PAMAM dendrimer conjugates for targeted delivery of anti-arthritic drugs and their pharmacokinetics and biodistribution in arthritic rats", Biomaterials, vol. 28, pp. 504-512, 2007.

[155] V. Gajbhiye, V. K. Palanirajan, R. K. Tekade, N. K. Jain, "Dendrimers as therapeutic agents: a systematic review", J Pharm Pharmacol., vol. 61, pp. 989-1003, 2009.

[156] E. Gong, B. Matthews, T. McCarthy, J. Chu, G. Holan, J. Raff, S. Sacks, "Evaluation of dendrimer SPL7013, a lead microbicide candidate against herpes simplex viruses", Antiviral Res., vol. 68, pp. 139-146, 2005.

[157] R. Rupp, S. L. Rosenthal, L. R. Stanberry, "VivaGel™ (SPL7013 Gel): A candidate dendrimer – microbicide for the prevention of HIV and HSV infection", Int J Nanomed., vol. 2(4), pp. 561-566, 2007.

[158] Z. Liu, C. Davis, W. Cai, L. He, X. Chen, H. Dai, "Circulation and long-term fate of functionalized, biocompatible single-walled carbon nanotubes in mice probed by Raman spectroscopy", Proc Natl Acad Sci. USA, vol. 105(5), pp. 1410-1415, 2008.

[159] G. Prencipe, S. M. Tabakman, K. Welsher, Z. Liu, A. P. Goodwin, L. Zhang, J. Henry, H. Dai, "PEG branched polymer for functionalization of nanomaterials with ultra-long blood circulation", J Am Chem Soc., vol. 131, pp. 4783-4787, 2009.

[160] T. Niidome, M. Yamagata, Y. Okamoto, Y. Akiyama, H. Takahashi, T. Kawano, Y. Katayama, Y. Niidome, "PEG modified gold nanorods with a stealth character for in vivo applications", J Control Release, vol. 114, pp. 343-347, 2006.

[161] Y. Akiyama, T. Mori, Y. Katayama, T. Niidome, "The effects of PEG grafting level and injection dose on gold nanorod biodistribution in tumor-bearing mice", J Control Release, vol. 139(1), pp. 81-84, 2009.

[162] M. Yokoyama, T. Okano, Y. Sakurai, H. Ekimoto, C. Shibazaki, K. Kataoka, "Toxicity and antitumour activity against solid tumours of micelle forming polymeric anticancer drug and its extremely long circulation in blood", Cancer Res., vol.51, pp. 3229-3236, 1991.

[163] Z. Zhou, X. Ma, E. Jin, J. Tang, M. Sui, Y. Shen, E. A. V. Kirk, W. J. Murdoch, M. Radosz, "Linear-dendritic drug conjugates forming long-circulating nanorods for cancer drug delivery", Biomaterials, vol. 34(22), pp. 1-14, 2013.

[164] C. S. Cho, Y. I. Jeong, T. Ishihara, R. Takei, J. U. Park, K. H. Park, A. Maruyama, T. Akaike, "Simple preparation of nanoparticles coated with carbohydrate carrying polymers", Biomaterials, vol. 18, pp. 323-326, 1997.

[165] A. Maruyama, T. Ishihara, S. W. Kim, T. Akaike, "Nanoparticle DNA carrier with poly(L-lysine) grafted polysaccharide copolymer and poly(D,L-lactic acid)", Bioconjug Chem., vol. 8, pp. 735-742, 1997.

[166] C. Fan, W. Gao, Z. Chen, H. Fan, M. Li, F. Deng, Z. Chen, "Tumor selectivity of stealth multi-functionalized superparamagnetic iron oxide nanoparticles", Int J Pharm., vol. 404, pp. 180-190, 2011.

[167] E. S. Lee, C. Lim, H. T. Song, J. M. Yun, K. S. Lee, B. J. Lee, Y. S. Youn, Y. T. Oh, K. T. Oh, "A nanosized delivery system of superparamagnetic iron oxide for tumor MR imaging", Int J Pharm., vol. 439, pp. 342-348, 2012.

[168] L. Zhu, D. Wang, X. Wei, X. Zhu, J. Li, C. Tu, Y. Su, J. Wu, B. Zhu, D. Yan, "Multifunctional pH-sensitive superparamagnetic iron-oxide nanocomposites for targeted drug delivery and MR imaging", J Control Release, vol. 169(3), pp. 228-238, 2013.

[169] D. Kokuryo, Y. Anraku, A. Kishimura, S. Tanaka, M. R. Kano, J. Kershaw, N. Nishiyama, T. Saga, I. Aoki, K. Kataoka, "SPIO-PICosome : Development of a highly sensitive and stealth-capable MRI nano-agent for tumor detection using SPIO-loaded unilamellar polyion complex vesicles (PICsomes)", J Control Release, vol. 169(3), pp. 220-227, 2013.

[170] C. G. Millan, M. L. S. Marinero, A. Z. Castaneda, J. M. Lanao, "Drug, enzyme and peptide delivery using erythrocytes as carriers", J Control Release, vol. 95, pp. 27-49, 2004.

[171] M. Hamidi, A. Zarrin, M. Forrozesh, S. Mohammadi-Samani, "Application of carrier erythrocytes in delivery of biopharmaceuticals", J Control Release, vol. 118, pp. 145-160, 2007.

[172] M. E. Favretto, J. C. A. Cluitmans, G. J. C. G. M. Bosman, R. Brock, "Human erythrocytes as drug carriers: Loading efficiency and side effects of hypotonic dialysis, chlorpromazine treatment and fusion with liposomes", J Control Release, vol. 170, pp. 343-351, 2013.

[173] J. L. Holovati, M. I. C. Gyongyossy-Issa, J. P. Acker, "Effects of trehalose-loaded liposomes on red blood cell response to freezing and post-thaw membrane quality", Cryobiol., vol. 58(1), pp. 75-83, 2009.

[174] H. He, J. Ye, Y. Wang, Q. Liu, H. S. Chung, Y. M. Kwon, M. C. Shin, K. Lee, V. C. Yang, "Cell-penetrating peptides meditated encapsulation of protein therapeutics into intact red blood cells and its application", J Control Release, vol. 176, pp. 123-132, 2014.

[175] J. S. Bae, M. W. Hwang, I. T. Kim, C. S. Lim, K. R. Ma, Y. K. Kim, K. N. Lee, D. H. Kim, S. M. Byun, "Chemical modifications of RBC surface antigen with methoxy polyethylene glycol", Korean J Clin Pathol., vol. 19, pp. 723-728, 1999.

[176] M. D. Scott, K. Murad, F. Koumpouras, M. Talbot, J. W. Eaton, "Chemical camouflage of antigenic determinants: Stealth erythrocytes", Proc Natl Acad Sci USA, vol. 94, pp. 7566-7571, 1997.

[177] K. L. Murad, K. L. Mahany, C. Brugnara, F. A. Kuypers, J. W. Eaton, M. D. Scott, "Structural and functional consequences of antigenic modulation of red blood cells with methoxypoly(ethylene glycol)", Blood, vol. 93, vol. 2121-2127, 1999.

[178] A. J. Bradley, K. L. Murad, K. L. Regan, M. D. Scott, "Biophysical consequences of linker chemistry and polymer size on stealth erythrocytes: size does matter", Biochim Biophys Acta., vol. 1561, pp. 147-158, 2002.

[179] A. J. Bradley, M. D. Scott, "Immune complex binding by immune camouflaged [poly(ethylene glycol)-grafted] erythrocytes", Am J Hematol., vol. 82(11), pp. 970-975, 2007.

[180] W. Duncheng, D. L. Kyluik, K. Murad, W. M. Toyofuku, M. D. Scott, "Polymer-mediated immunocamouflage of RBC: Effects of polymer size on antigenic and immunogenic recognition of allogeneic donor blood cells", Sci China Life Sci., vol. 54, pp. 589-598, 2011.

[181] D. Wang, W. M. Toyofuku, M. D. Scott, "The potential utility of methoxypoly(ethylene glycol)-mediated prevention of rhesus blood group antigen RhD recognition in transfusion medicine", Biomaterials, vol. 33, pp. 3002-3012, 2012.

[182] R. Chapanian, I. Constantinescu, D. E. Brooks, M. D. Scott, J. N. Kizhakkedathu, "In vivo circulation, clearance and biodistribution of polyglycerol grafted red blood cells", Biomaterials, vol. 33, pp. 3047-3057, 2012.

[183] N. A. Rossi, I. Constantinescu, R. K. Kainthan, D. E. Brooks, M. D. Scott, J. N. Kizhakkedathu, "Red blood cell membrane grafting of multi-functional hyperbranched polyglycerols", Biomaterials, vol. 31, pp. 4167-4178, 2010.

[184] M. D. Scott, A. M. Chen, "Beyond the red cell: PEGylation of other blood cells and tissues", Transfusion Clinique et Biologique., vol. 11, pp. 40-46, 2004.

[185] B. E. Bax, M. D. Bain, P. J. Talbot, E. J. Parker-Williams, R. A. Chalmers, "Survival of human carrier erythrocytes in vivo", Clin Sci., vol. 96, pp. 171-178., 1999

[186] B. E. Bax, M. D. Bain, L. D. Fairbanks, A. D. B. Webster, R. A. Chalmers, "In vitro and in vivo studies with human carrier erythrocytes loaded with polyethylene glycol-conjugated and native adenosine deaminase", Brit J Haematol., vol. 109, pp. 549-554, 2000.

[187] E. Chambers, S. Mitragotri, "Prolonged circulation of large polymeric nanoparticles by non-covalent adsorption on erythrocytes", J Control Release, vol. 100, pp. 111-119, 2004.

[188] L. Rossi, M. Castro, F. D'Orio, G. Damonte, S. Serafini, L. Bigi, I. Panzani, G. Novelli, B. Dallapiccola, S. Panunzi, P. Di Carlo, S. Bella, M. Magnania, "Low doses of dexamethasone constantly delivered by autologous erythrocytes slow the progression of lung disease in cystic fibrosis patients", Blood cells Mol. Dis., vol. 33, pp. 57-63, 2004.

[189] E. Briones, C. I. Colino, C. G. Millan, J. M. Lanao, "Increasing the selectivity of amikacin in rat peritoneal macrophages using carrier erythrocytes", Eur. J. Pharm. Sci., vol. 38, pp. 320-324, 2009.

[190] C. G. Millan, A. Z. Castaneda, F. G. Lopez, M. L. S. Marinero, J. M. Lanao, "Pharmacokinetics and biodistribution of amikacin encapsulated in carrier erythrocytes", J Antimicrob Chmeother., vol. 61, pp. 375-381, 2008.

[191] N. S. Yew, E. Dufour, M. Przybylska, J. Putelat, C. Crawlet, M. Foster, S. Gentry, D. Reczek, A. Kloss, A. Meyzaud, F. Horand, S. H. Cheng, Y. Godfrin, "Erythrocytes

encapsulated with phenylalanine hydroxylase exhibit improved pharmacokinetics and lowered plasma phenylalanine levels in normal mice", Mol Genet Metab., vol. 109, pp. 339-344, 2013.

[192] W. Fan, W. Yan, Z. Xu, H. Ni, "Erythrocytes load of low molecular weight chitosan nanoparticles as a potential vascular drug delivery system", Colloids Surf. B., vol. 95, pp. 258-265, 2012.

[193] S. Biagiotti, L. Rossi, M. Bianchi, E. Giacomini, F. Pierige, G. Serafini, P. G. Conaldi, M. Magnani, "Immunophilin-loaded erythrocytes as a new delivery strategy for immunosuppressive drugs", J Control Release, vol. 154, pp. 306-313, 2011.

[194] G. I. Harisa, M. F. Ibrahim, F. Alanazi, G. A. Shazly, "Engineering erythrocytes as a novel carrier for the targeted delivery of the anticancer drug paclitaxel", Saudi Pharm J., vol. 22, pp. 223-230, 2014.

[195] M. Hamidi, N. Zarei, A. H. Zarrin, S. Mohammadi-Samani, "Preparation and in vitro characterization of carrier erythrocytes for vaccine delivery", Int J Pharm., vol. 338, pp. 70-78, 2007.

[196] B. B. Madhavi, M. Bhavana, A. R. Nath, M. Prasad, K. S. Vennela, "In vitro evaluation of piperine enclosed erythrocyte Carriers", Drug Invention Today, vol. 5(3), pp. 169-174, 2013.

[197] M. Hamidi, A. H. Zarrin, M. Forrozesh, N. Zarei, S. Mohammadi-Samani, "Preparation and in vitro evaluation of carrier erythrocytes for RES-targeted delivery of interferon-alpha 2b", Int J Pharm., vol. 341, pp. 125-133, 2007.

[198] S. Ahn, S. Y. Jung, E. Seo, S. J. Lee, "Gold nanoparticle-incorporated human red blood cells (RBCs) for X-ray dynamic imaging", Biomaterials, vol. 32, pp. 7191-7199, 2011.

[199] Y. Ma, R. J. M. Nolte, J. J. L. M. Cornelissen, "Virus-based nanocarriers for drug delivery", Adv Drug Del Rev., vol. 64, pp. 811-825, 2012.

[200] A. Cooper, Y. Shaul, "Recombinant viral capsids as an efficient vehicle of oligonucleotide delivery into cells", Biochem Biophys Res Commun., vol. 327(4), pp. 1094-1099, 2005.

[201] M. L. D. Broekman, L. A. Comer, B. T. Hyman, M. Sena-Esteves, "Adeno-associated virus vectors serotypes with AAV8 capsid are more efficient than AAV-1 or -2 serotypes for widespread gene delivery to the neonatal mouse brain", Neuroscience, vol. 138, pp. 501-510, 2006.

[202] F. Wei, K. I. McConnell, T. Yu, J. Suh, "Cojugation of paclitaxel on adeno-associated virus (AAV) nanoparticles for co-delivery of genes and drugs", Eur J Pharm Sci., vol. 46, pp. 167-172, 2012.

[203] S. Selvam, P. B. Thomas, S. F. Hamm-Alvarez, J. E. Schechter, D. Stevenson, A. K. Mircheff, M. D. Trousdale, "Current status of gene delivery and gene therapy in lacrimal gland using viral vectors", Adv Drug Del Rev., vol. 58, pp. 1243-1257, 2006.

[204] Y. Ren, S. M. Wong, L. Lim, "Folic acid-conjugated protein cages of a plant virus: A novel delivery platform for doxorubicin", Bioconjug Chem., vol. 18, pp. 836-843, 2007.

[205] Q. Zeng, H. Wen, Q. Wen, X. Chen, Y. Wang, W. Xuan, J. Liang, S. Wan, "Cucumber mosaic virus as drug delivery vehicle for doxorubicin", Biomaterials, vol. 34, pp. 4632-4642, 2013.

[206] P. Charoenphol, H. Bermudez, "Design and application of multifunctional DNA nanocarriers for therapeutic delivery", Acta Biomaterialia, vol. 10, pp. 1683-1691, 2014.

[207] P. W. K. Rothemund, "Folding DNA to create nanoscale shapes and patterns", Nature, vol. 440(16), pp. 297-302, 2006.

[208] P. K. Lo, K. L. Metera, H. F. Sleiman, "Self-assembly of three dimensional DNA nanostructures and potential biological applications", Current opinion in chemical biology, vol. 14, pp. 597-607, 2010.

[209] S. H. Ko, H. Liu, Y. Chen, C. Mao, "DNA nanotubes (DNA-NTs) as combinatorial vehicles for cellular delivery", Biomacromolecules, vol. 9(11), pp. 3039-3043, 2006.

[210] D. Bhatia, S. Mehtab, R. Krishnan, S. S. Indi, A. Basu, Y. Krishnan, "Icosahedral DNA Nanocapsules by Modular Assembly", Angew Chem Int Ed Engl., vol. 48(23), pp. 4134-4137, 2009.

[211] J. Li, C. Fan, H. Pei, J. Shi, Q. Huang, "Smart drug delivery nanocarriers with self-assembled DNA nanostructures", Adv Mater., vol. 25, pp. 4386-4396, 2013.

[212] Q. Jiang, C. Song, J. Nangreave, X. Liu, L. Lin, D. Qiu, Z. Wang, G. Zou, X. Liang, H. Yan, B. Ding, "DNA origami as a carrier for circumvention of drug resistance", J Am Chem Soc., vol. 134, pp. 13396-13403, 2012.

[213] K. Kim, D. Kim, T. Lee, J. Y. Yhee, B. Kim, I. C. Kwon, D. Ahn, "Drug delivery by self-assembled DNA tetrahedron for overcoming drug resistance in breast cancer cells", Chem Commun., vol. 49, pp. 2010-2012, 2013.

[214] M. Chang, C. Yang, D. Huang, "Aptamer-conjugated DNA icosahedral nanoparticles as a carrier of doxorubicin for cancer therapy", ACS nano, vol. 5(8), pp. 6156-6163, 2011.

[215] K. Choi, I. C. Kwon, H. J. Ahn, "Self-assembled amphiphilic DNA-cholesterol/DNA-peptide hybrid duplexes with liposome-like structure for doxorubicin delivery", Biomaterials, vol. 34, pp. 4183-4190, 2013.

[216] T. H. La, T. T. T. Nguyen, V. P. Pham, T. M. H. Nguyen, Q. H. Le, "Using DNA nanotechnology to produce a drug delivery system", Adv Nat Sci: Nanosci Nanotechnol., vol. 4, pp. 015002, 2013.

[217] X. Cheng, F. Zhang, G. Zhou, S. Gao, L. Dong, W. Jiang, Z. Ding, J. Chen, J. Zhang, "DNA/chitosan nanocomplex as a novel drug carrier for doxorubicin", Drug Deliv., vol. 16(3), pp. 135-144, 2009.

[218] X. Ouyang, J. Li, H. Liu, B. Zhao, J. Yan, D. He, C. Fan, J. Chao, "Self-assembly of DNA-based drug delivery nanocarriers with rolling circle amplification", Methods, vol. 67, pp. 198-204, 2014.

[219] M. Nishikawa, Y. Mizuno, K. Mohri, N. Matsuoka, S. Rattanakiat, Y. Takahashi, H. Funabashi, D. Luo, Y. Takakura, "Biodegradable CpG DNA hydrogels for sustained delivery of doxorubicin and immonostimulatory signals in tumor-bearing mice", Biomaterials, vol. 32, pp. 488-494, 2011.

[220] E. S. Andersen, M. Dong, M. M. Nielsen, K. Jahn, R. Subramani, W. Mamdouh, M. M. Golas, B. Sander, H. Stark, C. L. P. Oliveira, J. S. Pedersen, V. Birkedal, F. Besenbacher, K. V. Gothelf, J. Kjems, "Self-assembly of a nanoscale DNA box with a controllable lid", Nature Lett., vol. 459, pp. 73-77, 2009.

[221] T. Y. Kim, D. W. Kim, J. Y. Chung, S. G. Shin, S. C. Kim, D. S. Heo, N. K. Kim, Y. J. Bang, "Phase I and pharmacokinetic study of genexol-PM, a cremophor-free, polymeric micelle-formulated paclitaxel, in patients with advanced malignancies", Clin Cancer Res., vol. 10, pp. 3708-3716, 2004.

[222] T. Hamaguchi, Y. Matsumura, M. Suzuki, K. Shimizu, R. Goda, I. Nakamura, I. Nakatomi, M. Yokoyama, K. Kataoka, T. Kakizoe, "NK105, a paclitaxel-incorporating micellar nanoparticle formulation, can extend in vivo antitumour activity and reduce the neurotoxicity of paclitaxel", Br J Cancer, vol.92, pp. 1240-1246, 2005.

[223] H. Uchino, Y. Matsumura, T. Negishi, F. Koizumi, T. Hayashi, T. Honda, N. Nishiyama, K. Kataoka, S. Naito, T. Kakizoe, "Cisplatin-incorporating polymeric micelles (NC-6004) can reduce nephrotoxicity and neurotoxicity of cisplatin in rats", Br J Cancer., vol. 93, pp. 678-687, 2005.

[224] S. Danson, D. Ferry, V. Alakhov, J. Margison, D. Kerr, D. Jowle, M. Brampton, G. Halbert, M. Ranson, "Phase I dose escalation and pharmacokinetic study of pluronic polymer-bound doxorubicin (SP1049C) in patients with advanced cancer", Br J Cancer., vol.90, pp. 2085-2091, 2004.

[225] D. Peer, R. Margalit, "Tumor-targeted hyaluronannano liposomes increase the antitumour activity of liposomal doxorubicin in syngeneic and human xenograft mouse tumor models", Neoplasia., vol. 6(4), pp. 343-353, 2004.

[226] M. Y. Begum, K. Abbulu, M. Sudhakar, “Flurbiprofen-Loaded stealth liposomes: studies on the development, characterization, pharmacokinetics and biodistribution”, J. Young Pharmacists., vol. 4(4), pp. 209-219, 2012

Chapter 3

MAGNETIC STIMULUS RESPONSIVE VANCOMYCIN DDS BASED ON CHITOSAN MICROBEADS EMBEDDED WITH MAGNETIC NANOPARTICLES

3.1 INTRODUCTION:

In the past few decades, pharmaceutical research has progressed significantly in various smart drug delivery systems (DDS) that are aimed at controlling dosage and drug localization.[1] Traditional systemic delivery of antibiotics is not always effective in achieving minimum inhibitory concentration (MIC) required for sustained treatment at the target site of injured tissue, thereby requiring stronger or repetitive dosages for efficacy in preventing infection.[2] The reason for insufficient concentration is usually due to avascular nature of the injured tissue, dissipation of drug into non-targeted tissues, dilution due to vascular circulation, or opsonisation by Mononuclear Phagocytic System (MPS). There have been numerous approaches to enhance pharmacokinetic efficiency and longevity of pharmaceutical products *in vivo*.[1] A popular method is to use a biocompatible, biodegradable DDS that allows longer bioavailability and localization of drug at potent concentrations at the site of interest. Chitosan has been extensively studied as a drug carrier because of positive characteristics such as biodegradability, non-cytotoxicity, intracellular permeability, biocompatibility, and its ability to entrap drugs.[3-5]

Although these DDS prolong the lifetime and efficacy of drug compared to naked drug, these DDS characteristically have a continuous first-order elution profile until the drug reserve is exhausted.[6] Slow degrading or non-degrading carriers such as poly-methylmethacrylate may continue releasing antibiotics at sub therapeutic levels after the drug payload is drained, increasing the risk of antibiotic resistance.[7] Several modifications have been proposed to make

such DDS responsive to a variety of stimuli, which would enable on-demand dosage optimization to actual therapeutic requirement.[8-10] Also, a drug boost at later time points may increase drug elution to therapeutic levels, thereby increasing efficacy and reducing the risk of drug-resistant bacterial strains.[11]

A DDS that is responsive to an exogenous stimulus of high-frequency alternating magnetic field, for on-demand drug releases has been developed (Fig. 3.1).[12] The DDS is in the form of microbeads fabricated from chitosan, cross-linked with poly-ethylene glycol dimethacrylate (PEGDMA) and embedded with magnetic nano-particles (MNP). As chitosan microbead itself does not respond to an external magnetic stimuli, MNP were embedded at the time of chitosan microbead preparation to enable the DDS to demonstrate hyperthermia phenomenon. The antibiotic vancomycin was loaded into microspheres to study drug release profiles with and without magnetic stimulation. A long term study was also performed via magnetic stimulation applied to microbeads after 12 to 15 days *in vitro*, in which a controlled increased drug delivery occurred even after initial first order elution profiles had been reached. This external non-invasive stimulation approach may have the benefit of using a non-invasive stimulus to maintain the antibiotic release profile for extended durations of infection prevention.

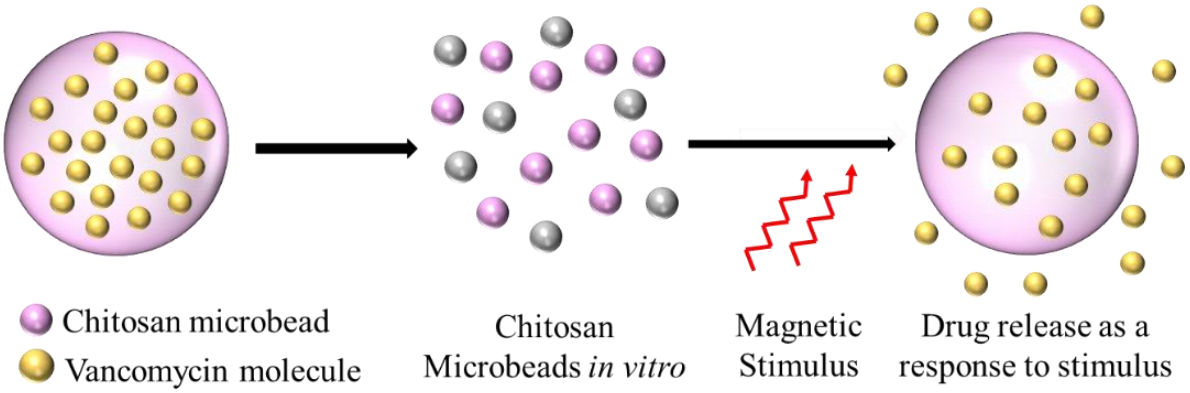

Fig. 3.1: Conceptualized framework for the DDS responsive to external stimuli.

3.2 MATERIALS AND METHODS:

MNP-loaded chitosan microbeads were prepared by an emulsion cross-linking method as described below, followed by the setup used for providing magnetic stimulus.

3.2(a) Preparation of Magnetic Nanoparticle [MNP]:

The Fe_3O_4 MNP were made by following the non-surfactants method described by Kang *et al.* [13] MNP were imaged by a Transmission Electron Microscope (Jeol JEM 1200) and the sizes of 500 individual particles in random fields of view were measured with ImageJ. D8 Advance (Bruker Inc.) diffractometer was used to measure x-ray diffraction (XRD) with Cu-Kα (λ = 0.15418 nm) radiation. A magnetization curve for the same samples was obtained by VSM-130 (Dexing Magnet Tech. Co.) at room temperature.

3.2(b) Preparation of Chitosan Microbead:

A modified water-oil emulsification technique reported by Jain *et al* was followed to make chitosan microbeads.[14] The preparation of the chitosan DDS can be divided into three phases: (1) Preparation of chitosan solution, (2) Emulsification/cross-linking step of chitosan microbeads, and (3) Washing stage.

In Phase 1, a solution of 4% wt. chitosan, 2% wt. MNP (Fe_3O_4), 1% volume glacial acetic acid and 0.8% vancomycin was made. Then, 1g MNP was added to 46 ml DI water in a 50 ml centrifuge tube and sonicated. The mixture was then added to 2 g chitosan (Chitopharm S) and 0.4 g vancomycin (MP Biomedicals). After that, 0.5 ml glacial acidic acid was added and the solution was stirred well. The solution was set up on an impeller and left to stir overnight.

In Phase 2, 2 g Span 80 surfactant (Sigma Aldrich), 75 ml light mineral oil, 75 ml heavy mineral oil (Fisher Scientific) and 15 ml PEGDMA Mn=550 (Sigma Aldrich) were combined in a beaker. This solution was placed on a hot plate and stirred by an impeller for a few hours.

Then, 15 ml chitosan solution from Phase 1 was injected into the mixture. The hot plate was set to 60^{O} C and left for 24 hr.

In the last phase, the excess oil was drained and the beads were centrifuged, followed by thorough washing with hexane, methanol, and acetone. After the final wash, the beads were re-suspended in approximately 10 ml of acetone and poured into a glass petri dish to dry.

The same process was followed without adding the Fe_3O_4 nanoparticles for making chitosan microbeads without MNP. Both kind of microbeads were imaged with a Scanning Electron Microscope (XL30 ESEM) after fixing them on a carbon tape and coating with 5 nm Au/Pd on a sputter-coater (EMS 5502X).

3.2(c) Procedure for stimulus:

A MagneTherm instrument (nanoTherics, UK) was used to provide magnetic stimulation (Fig. 3.2). It consists of interchangeable 9 and 17 turn coils with 10 different capacitor banks, each of which is characterized by a specific resonant frequency and maximum magnetic flux density. The coil is water-cooled and positioned around a sample holder. A fiber optic thermometer (Optocon, Germany) was used for temperature measurements of media surrounding the samples.

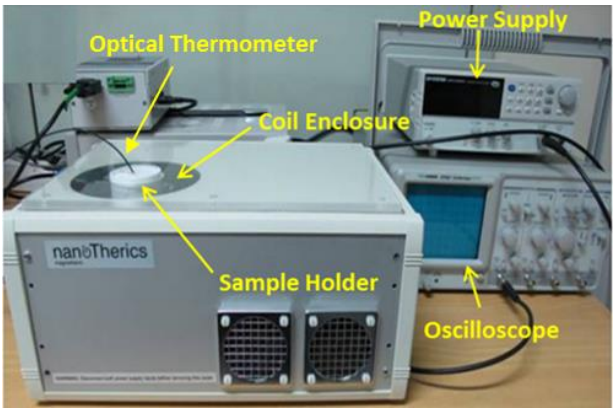

Fig. 3.2: Photograph of the Magnetherm equipment for magnetic stimulation.

A preliminary temperature rise test with 5 frequency/intensity combinations was performed and compared to determine the setting that caused the highest temperature rise in a sample of MNP. Based on results of this test, stimulus parameters for all DDS experiments were set at 109.9 kHz/25 mT, as this setting has produced the maximum temperature rise in this test.

3.2(d) Experiments on Chitosan microbeads with magnetic nano-particles:

(i) *Short term elution study:* The total duration of this experiment was 8 hrs, with test groups stimulated at 3rd, 5th and 7th hr for 30 min as shown in Fig. 3.3. The DDS was divided into 10 samples of 100 mg each, of which 5 were assigned as control (non-stimulated) and 5 as test groups. 4 ml was added to each sample. The PBS is completely refreshed with the same volume of fresh PBS every 1 hr.

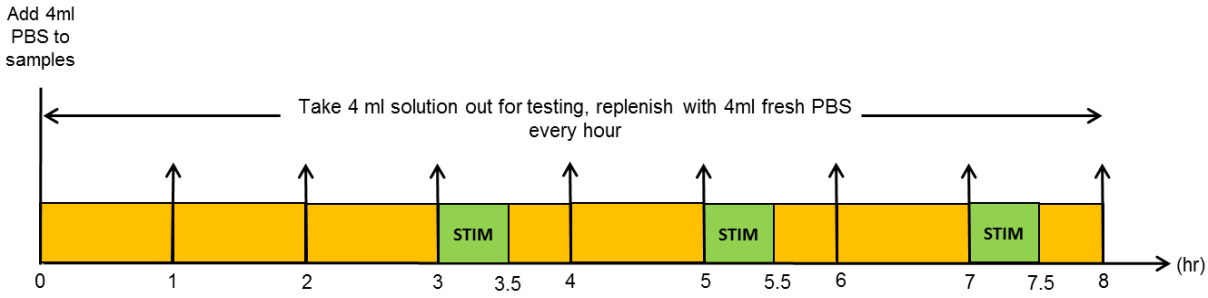

Fig. 3.3: Short time elution study timeline of hyperthermia experiments on samples with MNP.

(ii) *Long term elution study:* To evaluate clinically relevant application of this DDS elution and stimulation over a period of several days at a point when drug release is depleted or below active concentrations, the DDS samples were placed in 4 mL PBS and media was refreshed daily for 11 days and were then stimulated for 60 min on Day 12 and Day 15, as depicted in Fig. 3.4. The experiments consisted of 6 control (non-stimulated) and 6 test samples, each with 100 mg MNP-chitosan microbeads. 100 µl from the PBS was collected before and after stimulation on day 12 and 15. Additional 100 µl samples were also collected on day 13 and day 16.

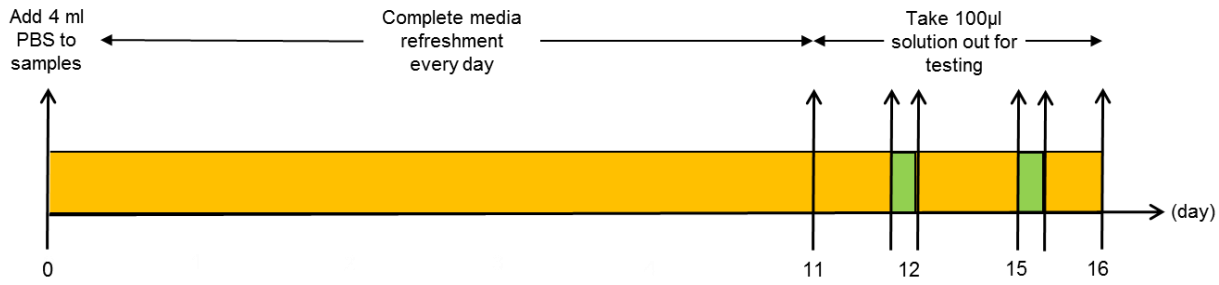

Fig. 3.4: Long term elution study timeline of hyperthermia experiments on samples with MNP

(iii) *General Hyperthermia Study:* To investigate if the samples would exhibit a similar drug release when treated to the same temperature increment by other means, 5 DDS samples (test groups) were also subjected to a rapid temperature rise of 16°C in an incubator, which was the same temperature rise observed via magnetic hyperthermia. The experimental timeline was same as showed in Fig. 3.3. A separate batch of 5 samples was not given any stimulation and were labelled as control groups for comparing drug elution. All samples in both groups had 100 mg microbeads in 4 ml PBS.

3.2(e) Experiments on Chitosan microbeads without MNP:

In order to demonstrate the role of MNP in aiding drug release, experiments above were conducted on beads without MNP. In these set of experiments, there were 5 control and 5 test samples containing 100 mg of microbeads. Due to the very fine and light nature of these beads, complete media refreshment was not possible without pipetting out several microbeads each time. To avoid introducing errors due to non-consistent sample weight, a slightly different timeline was followed, as shown in Fig. 3.5. Stimulations were given at 3rd, 5th and 24th hr, each session of 30 mins. At t = 0, 10 ml of PBS was added to all samples. Then, 120µl of the supernatant was collected before and after the stimulation sessions.

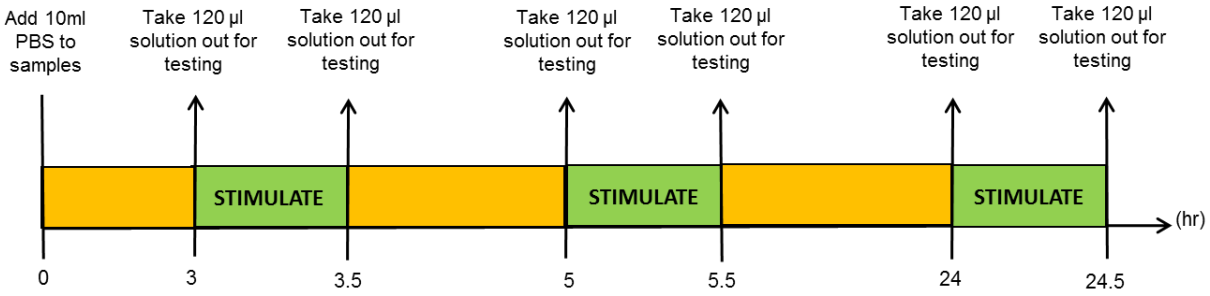

Fig. 3.5: Timeline of hyperthermia experiments on samples without MNP. Vertical arrows represent sampling instances for HPLC tests.

3.2(f) Data Collection, Calibration and Analysis:

High performance liquid chromatography (Dionex UltiMate 3000 HPLC, Thermo Scientific, Waltham, MA) was used for analyzing vancomycin amount released from the collected supernatant. The release data between stimulated and non-stimulated groups were analyzed by the non-parametric Mann Whitney test. The significance level for assessing significant differences in drug elution was fixed at 5%.

3.3 RESULTS

3.3(a) MNP characterization:

The XRD (Fig. 3.6(a)) confirms the presence of Fe3O4 phase and magnetization curve (Fig. 3.6(b)) show magnetic nature of the MNP up to 1.2 T field. Size analysis of TEM imaging (Fig. 3.6(c)) revealed the size of MNP distribution to be 10.89±2.67 nm.

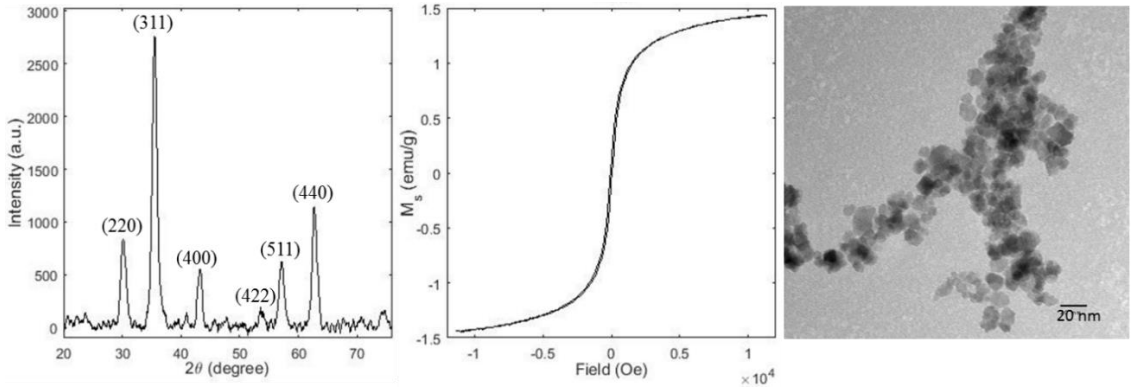

Fig. 3.6: (a) XRD pattern, (b) magnetization versus field curve, and (c) TEM image of Fe3O4 MNP.

3.3(b) Chitosan microbead characterization:

The microbeads were imaged using an SEM (Fig. 3.7) and the size distribution of these particles was 288.4 ± 62.2 µm.

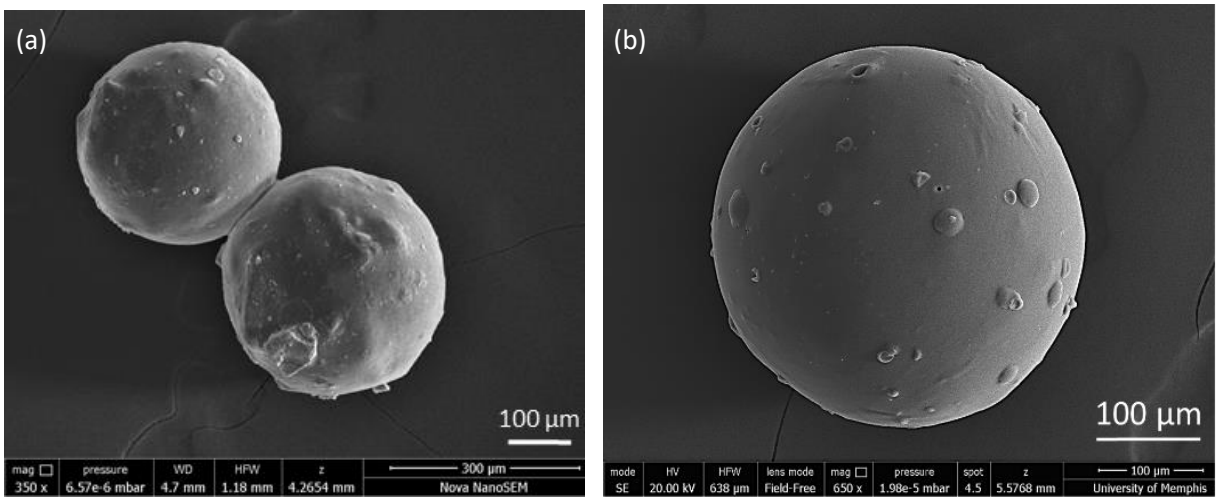

Fig. 3.7: SEM image of chitosan microbeads (a) with MNP and (b) without MNP.

A Fourier Transform Infrared Spectroscopy (FTIR) for the chitosan/MNP microbeads is shown (Fig. 3.8). The observed peaks were C-O-C Stretching(1070 cm^{-1}), C-H rocking (1400 cm^{-1}), Amide II (1530 cm^{-1}), N-H Scissor (1550 cm^{-1}), C=O (1640,1720 cm^{-1}), C-H (2850,2920 cm^{-1}) and N-H Stretch (3350-3280 cm^{-1}), OH (2700-3600 cm^{-1}). The XRD of chitosan, vancomycin and chitosan microbeads with MNP are shown in Fig. 3.9.

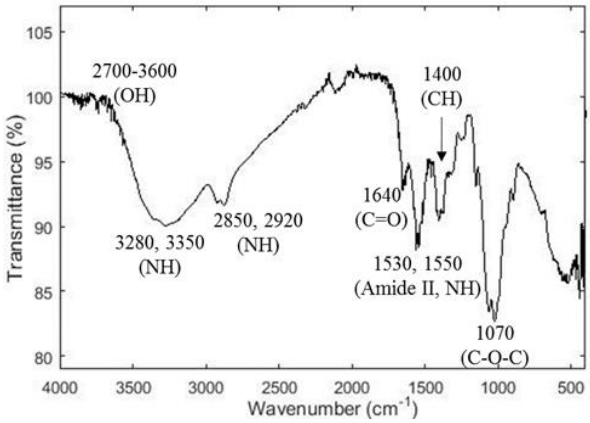

Fig. 3.8: FTIR of chitosan microbead containing MNP, vancomycin and PEGDMA.

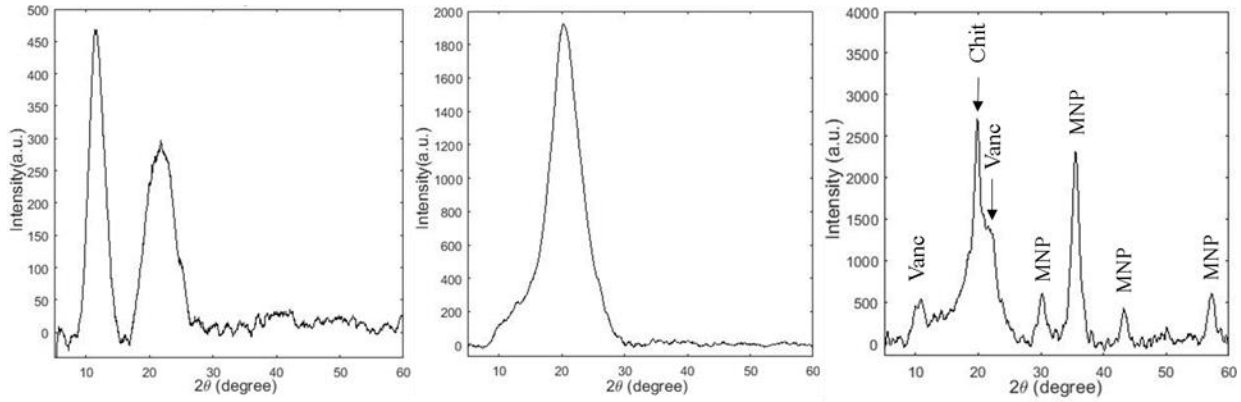

Fig. 3.9: XRD plots of (a) vancomycin, (b) chitosan with PEGDMA and vancomycin, and (c) chitosan with PEGDMA, vancomycin, and MNP.

3.3(c) Experiments on Chitosan microbeads with MNP:

A temperature elevation of 16ºC was recorded after each magnetic stimulation from MNP loaded chitosan.

(i) *Short term elution study*: The eluted concentration as a function of time is graphed in Fig. 3.10, which shows a statistically significant drug increase in stimulated samples. After stimulation at each of the 3 instances, the test groups released significantly higher amount of vancomycin compared to control ($p \leq 0.008$). In the periods when no stimulation was given, the test groups released similar amounts of drug to control levels ($p > 0.05$).

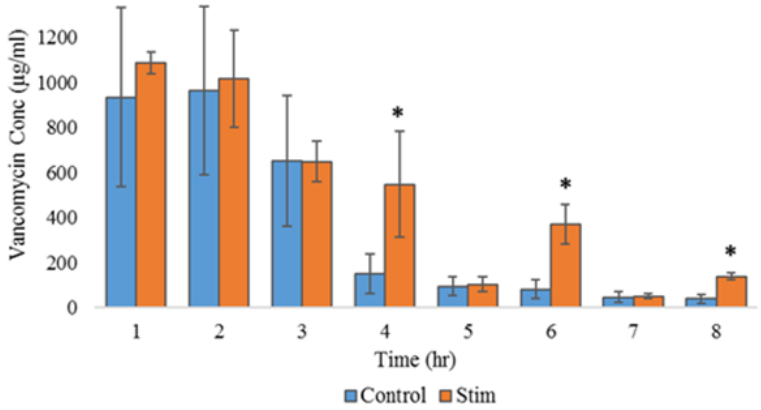

Fig. 3.10: Concentration of vancomycin over time with (Stim) and without (Control) stimulation for short term elution study with stimulation given at third, fifth and seventh hour. Data represented is average6standard deviation. Asterisks (*) represent statistically significant differences between stimulated and control groups, $p<0.05$.

(ii) *Long term elution study:* After 12 days of passive dissolution of antibiotics, vancomycin release from microparticles dropped below theoretically effective minimum inhibitory values against *S.aureus*. Magnetic stimulation of these microbeads for 30 minutes at days 12 and 15 caused an increase in vancomycin release to above the theoretically effective minimum inhibitory concentration of 1µg/ml against *S. aureus* (Fig. 3.11). For both stimulation events on Day 12 and Day 15, the test groups released statistically significant higher amounts of vancomycin ($p = 0.002$). In the non-stimulation periods, there was no statistical difference in drug elution between both groups ($p > 0.05$).

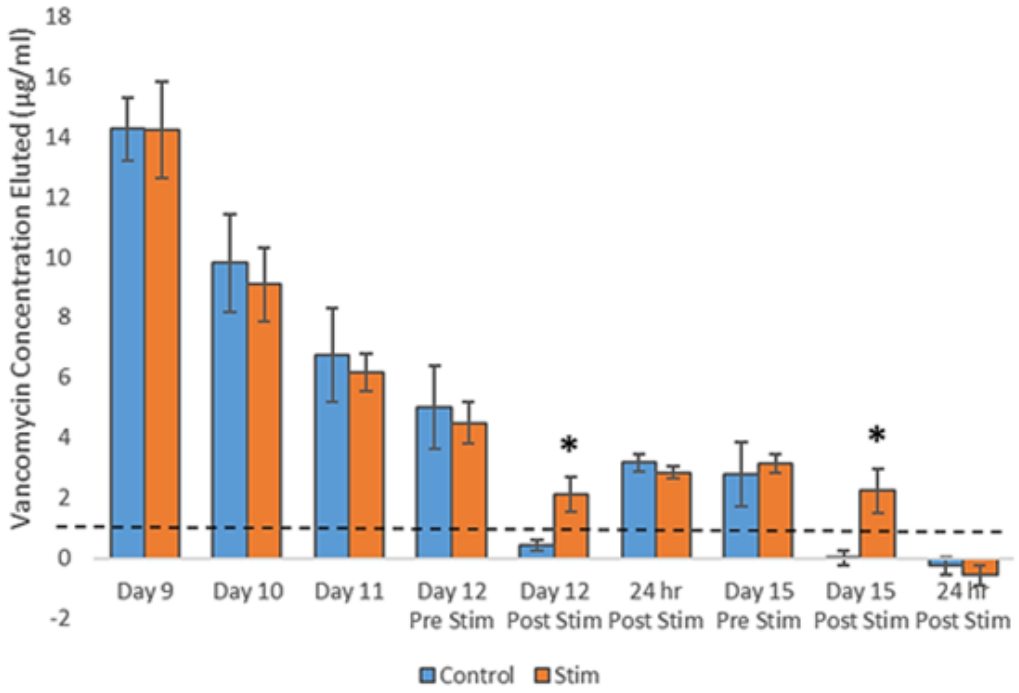

Fig. 3.11: Concentration of vancomycin over time with (Stim) and without (Control) stimulation for a long term elution study with stimulus given on day 12 and day 15. Data represented is average ± standard deviation. Asterisks (*) represent statistically significant differences between stimulated and control groups, $p<0.05$.

(iii) *General Hyperthermia Study***:** No significance differences were detected between both groups (Fig. 3.12).

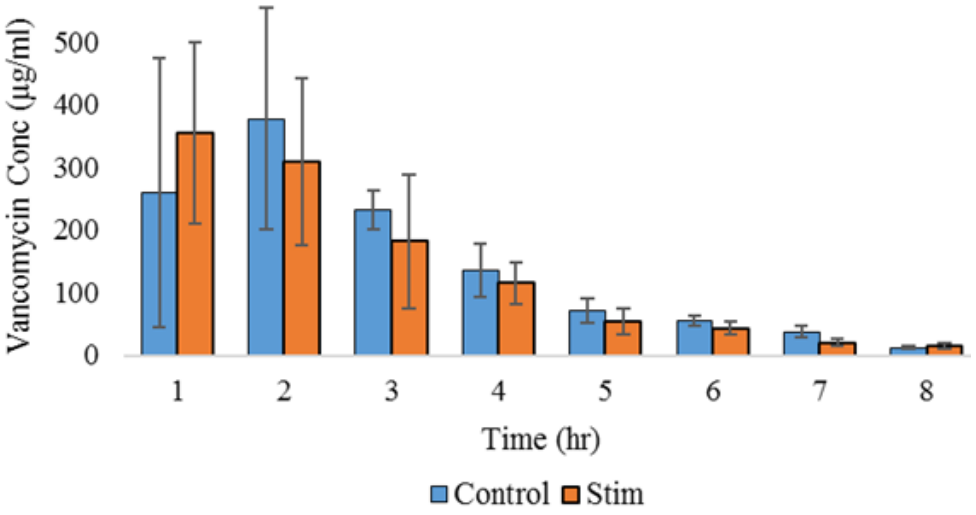

Fig. 3.12: Concentration of vancomycin over timewith and without stimulation in an incubator. Data represented is average ± standard deviation. Asterisks (*) represent statistically significant differences between stimulated and control groups, $p<0.05$.

3.3(d) Experiments on Chitosan microbeads without MNP:

The vancomycin concentration detected at each sampling points is shown in Fig. 3.13. There was no statistically significant difference in drug release between magnetically stimulated and non-stimulated MNP-free chitosan beads ($p > 0.05$). The temperature rise did not exceed 3ºC, which was the normal temperature rise observed in the MagneTherm chamber when the coil is generating a 25 mT magnetic field at 109.9 kHz, without any samples.

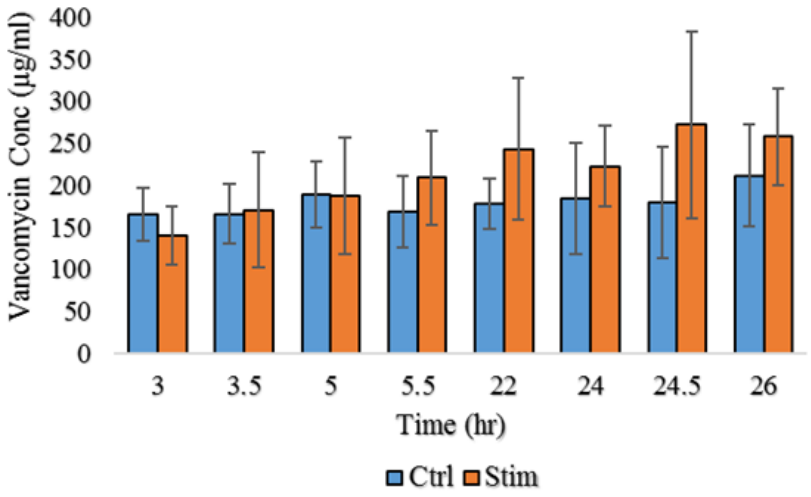

Fig. 3.13: Amount of vancomycin eluted by chitosan microbeads without MNPs. Assuming 5% significance level, the difference in vancomycin elution were not significant between test and control groups.

3.4 DISCUSSION

The DDS developed was responsive to a high frequency magnetic field, releasing increased amounts of antibiotics when stimulated. We were also able to boost antibiotic levels above MIC after several days by stimulation. Magnetic excitation was chosen over other stimulation modalities because this stimulation approach does not require any direct physical contact with the patient and is already being used for other needed clinical external stimulations, such as regenerating bone by stimulating external fixation devices.[15] The cross-linking process produced microbeads of the size that could be delivered through larger gauge syringes. While general diffusion of drug occurred between these stimulations, the ability to increase release with external, non-invasive means shows promise clinically.

XRD of the Fe_3O_4 MNP (Fig. 3.6(a)) show the peaks are consistent with those reported in literature.[16,17] Size of MNP produced were similar to other reported nanoparticles.[16,17] The hysteris loop of the MNP (Fig. 3.6(b)) confirms its superparamagnetic behavior. The major peaks of chitosan (Fig. 3.9(a)), vancomycin (Fig. 3.9(b)) and MNP (Fig. 3.6(a)) are prominent

in XRD of the chitosan-MNP microbeads (Fig. 3.9(c)), supporting the presence of these constituents in the DDS.[18,19] It was further affirmed by FTIR (Fig. 3.8) which showed amine groups and hydroxyl groups corresponding to chitosan and vancomycin respectively. The C-O-C stretching confirms the inclusion of polyethylene glycol in the DDS.

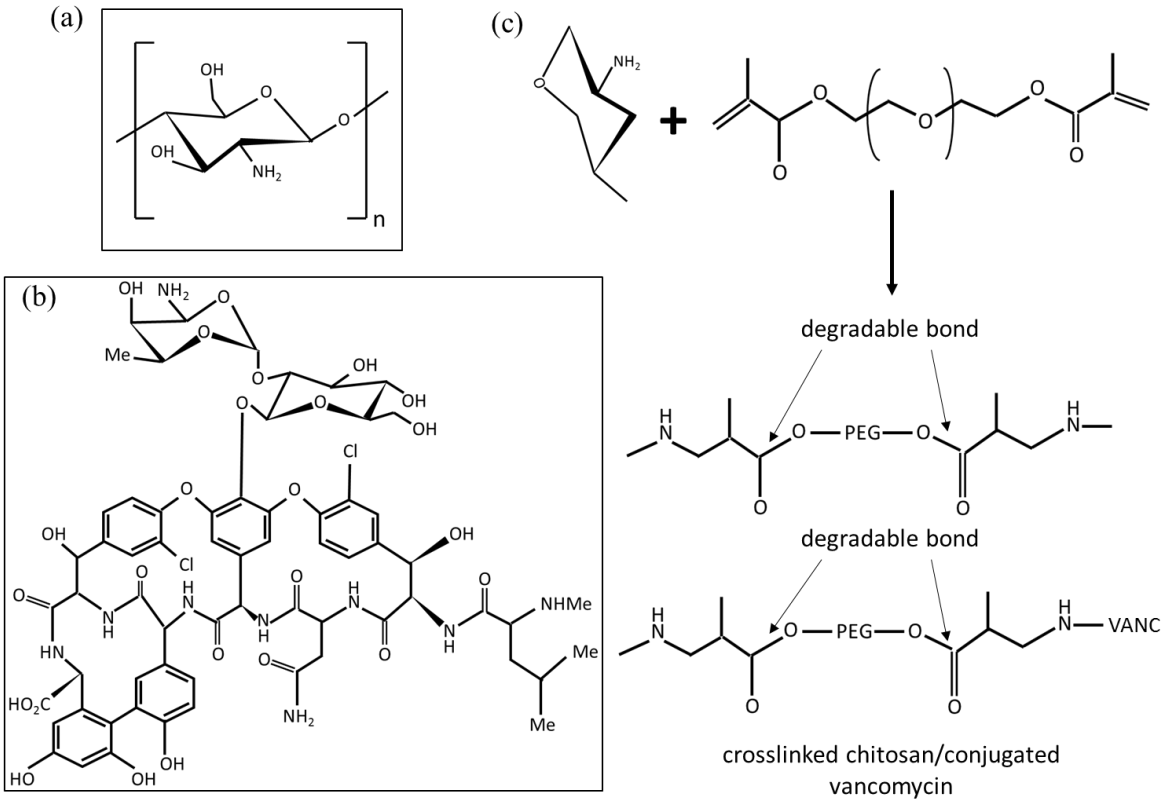

Fig. 3.14: Chemical structures of (a) chitosan, (b) vancomycin, and (c) reaction mechanism of PEGDMA crosslinker with chitosan and vancomycin.

In this DDS, vancomycin as well as chitosan can bind to PEGDMA through Michael addition reactions. Fig. 3.14 (a, b) show chemical structures of chitosan and vancomycin respectively. Similar to chitosan, vancomycin has two amino groups. Those amino groups react with the crosslinker PEGDMA as shown in Fig. 3.14 (c), in the phase 2 step of microbeads preparation. After the reaction, some vancomycin should be immobilized via degradable ester bond. Ester hydrolysis is known to accelerate at elevated temperature in the presence of acidic water. The chitosan microbeads may have confined slightly acidic water from the emulsion

procedure. Therefore, it is very likely that this conjugated ester bond was cleaved as a result of hyperthermia, causing vancomycin release. In addition, as the crosslinked chitosan-PEG bond is also cleaved by heat, diffusion of vancomycin could also be promoted by this stimulus.

In general hyperthermia tests on chitosan/MNP beads (Fig. 3.12), although the samples underwent the same elevation in temperature, the absence of a significant difference in vancomycin elution from test groups compared to test groups suggests that magnetic field is necessary for causing response. The dependence of drug release on magnetic field was further confirmed when chitosan microbeads without MNP were subjected to the same stimulation parameters (Fig. 3.13) but failed to show a significant variation in elution profile of vancomycin in comparison to control groups. It is known that on excitation with an alternating magnetic field, magnetic nanoparticles generate and dissipate heat due to core relaxation losses.[20-23] In the chitosan/MNP DDS, the localized temperature rise around the MNP on a nano-scale is likely to be much higher than 16ºC, which might be sufficient for cleaving the bonds. Further tests are needed to explore the exact mechanism causing vancomycin release.

Magnetic hyperthermia has been extensively explored for smart therapeutic applications like cancer therapy and drug delivery, leading to successful clinical trials on human subjects with brain/prostate cancer.[24,25] Also, since MNP, like magnetite, have been proven to be efficient MRI contrast agents[26-28], they facilitate drug targeting, localization and confinement.[29] Some of our preliminary tests further indicated that the DDS exhibits favorable cyto-compatibility.[12]

The repeated increases in release upon stimulation in the elution studies is relevant clinically because it gives the care provider freedom to administer dosage as per each patient's unique needs, without intravenous procedures each time.) Ethylene-vinyl acetate copolymer polymeric matrices loaded with insulin and MNP showed similar passive elution of active insulin as

release of antibiotic in this DDS, with higher activity in glucose lowering after stimulus of magnetic field.[30] Finotelli et al. loaded insulin in alginate/chitosan microbeads with magnetite nanoparticles and showed insulin release tripled in stimulated groups with respect to non-stimulated groups in response to a magnetic field.[31]

Katagiri and his group designed polyelectrolyte hollow multilayered shells containing dye, coated with Fe_3O_4 MNP and an amphiphilic bilayer that released dye upon magnetic stimulation which was attributed to heat-induced change in phase of amphiphile membrane, rather than any structural fissure.[32] Preliminary SEM and macroscopic observations of the DDS used in this study suggests that stimulation does not cause damage to the structure of microbeads. This is in contrast to some magnetically responsive DDS, such as Fe_3O_4/poly(allylamine) polyelectrolyte microcapsules, that formed microcavities on the DDS surface on application of a high frequency magnetic field and exacerbated into major ruptures with time, eluting drug in significant amounts.[33] Koppolu et al. designed MNP cores with outer multilayered shells of the temperature-responsive polymer poly(N-isopropylacrylamaide) (PNIPAAm) and poly(D,L-lactideco-glycolide) (PLGA) as carriers of both curcumin and bovine serum albumin (BSA); while curcumin showed a sustained release profile over 13 d, BSA could be burst-released from PNIPAAm layer by elevating temperature.[34]

3.5 CONCLUSION

The results demonstrated that the DDS responded to stimulus by discharging significant amount of drug compared to control non-simulated samples. It was also observed that the DDS did not respond to general hyperthermia, indicating that any in vivo thermal fluctuations will not affect drug elution. The experiments further suggest that this DDS has the potential to burst-release higher amount of drugs on multiple instances of stimulus, several hours or days apart as

needed, and thus might enable us to maintain or control drug concentrations in the targeted treatment location. It can aid in targeting drug directly to problem areas, preventing systemic toxicity. The DDS also has the capability to be guided, localized and confined at the target site by a static magnetic field35. Once at the site, drug can be released, when required, by an external alternating magnetic field as demonstrated in this work. These features would greatly assist clinicians in controlling drug delivery, dosage timings and local concentration to match the clinical needs of the patient.

3.6 References

[1] Mohapatra, B. I. Morshed, W. O. Haggard, R. A. Smith. “Stealth Engineering for in vivo Drug Delivery Systems”, Crit. Rev. Biomed. Eng., vol. 43, pp. 347-69, 2016.

[2] K. Belfield, R. Bayston, J. P. Birchall, M. Daniel. “Do orally administered antibiotics reach concentrations in the middle ear sufficient to eradicate planktonic and biofilm bacteria? A review”, Int. J. Pediatr. Otorhinolaryngol., vol. 79, pp. 296-300, 2015.

[3] Bernkop-Schnürch, S. Dünnhaupt, “Chitosan-based drug delivery systems”, Eur. J. Pharm. Biopharm., vol. 81, pp. 463-469, 2012.

[4] T. Jiang, R. James, S. G. Kumbar, C. T. Laurencin, “Chitosan as a Biomaterial: Structure, Properties, and Applications in Tissue Engineering and Drug Delivery”, Natural and Synthetic Biomedical Polymers, 1st Ed., Elsevier, pp. 91-107, 2014.

[5] Y. Luo, Q. Wang, “Recent developments of chitosan-based polyelectrolyte complexes with natural polysachharides for drug delivery”, Int. J. Biol. Macromolec., vol. 64, pp. 353-367, 2014.

[6] M. P. Patel, R. R. Patel, J. K. Patel, “Chitosan Mediated Targeted Drug Delivery System: A Review”, J. Pharm. Sci., vol. 13, pp. 536-557, 2010.

[7] Y. Shi, A. Wan, Y. Shi, Y. Zhang, Y. Chen, “Experimental and Mathematical studies on the drug release properties of aspirin loaded chitosan nanoparticles”, BioMed. Res. Int., vol. 2014, pp. 1-8, 2014.

[8] W. A. Jiranek, A. D. Hanssen, A. S. Greenwald, “Antibiotic-loaded bone cement for infection prophylaxis in total joint replacement”, J. Bone Joint Surg. Am., vol. 88, pp. 2487-2500, 2006.

[9] R. Cheng, F. Meng, C. Deng, H. Klok, Z. Zhong, “Dual and multi-stimuli responsive polymeric nanoparticles for programmed site-specific drug delivery”, Biomaterials, vol. 34, pp. 3647-3627, 2013.

[10] M. N. Yasin, D. Svirskis, A. Seyfoddin, I. D. Rupenthal, “Implants for drug delivery to the posterior segment of the eye: A focus on stimuli-responsive and tunable release systems”, J. Control Rel., vol. 196, pp. 208-221, 2014.

[11] P. McCoy, N. J. Irwin, C. Brady, D. S. Jones, G. P. Andrews, S. P. Gorman, “Synthesis and release kinetics of polymerisable ester drug conjugates: towards pH-responsive infection-resistant urinary biomaterials”, Tetrahedron Lett., vol. 54, pp. 2511-2514, 2013.

[12] M. Harris et al, “Magnetic Stimuli-Responsive Chitosan-based Drug Delivery Biocomposite for Multiple Triggered Release”, Int. J. Biol. Macromol, vol. 104(Pt B), pp. 1407-1414, 2017.

[13] Y. S. Kang, S. Risbud, J. F. Rabolt, P. Stroeve, “Synthesis and Characterization of Nanometer-Size Fe3O4 and γ-Fe2O3”, Chem. Mater., vol. 8, pp. 2209-2211, 1996.

[14] S. K. Jain, N. K. Jain, Y. Gupta, A. Jain, D. Jain, M. Chaurasia, “Mucoadhesive chitosan microspheres for non-invasive and improved nasal delivery of insulin”, Ind. J. Pharm. Sci., vol. 69, pp. 498-504, 2007.

[15] F. L. Gonzalez, R. L. Arevalo, S. M. Coretti, V. U. Labajos, B. D. Rufino, “Pulsed electromagnetic stimulation of regenerate bone in lengthening procedures”, Acta. Orthop. Belg., vol. 71, pp. 571-576, 2005.

[16] H. Li, L. Qin, Y. Feng, L. Hu, C. Zhou, “Preparation and characterization of highly water-soluble magnetic Fe3O4 nanoparticles via surface double-layered self-assembly method of sodium alpha-olefin sulfonate”, J. Magn. Magn. Mater., vol. 384, pp. 213-218, 2015.

[17] H. Lv, R. Jiang, Y. Li, X. Zhang, J. Wang, “Microemulsion-mediated hydrothermal growth of pagoda-like Fe3O4 microstructures and their application in a lithium-air battery”, Ceram. Int., vol. 41, pp. 8843-8848, 2015.

[18] Branca, G. D’Angelo, C. Crupi, K. Khouzami, S. Rifici, G. Ruello, U. Wanderlingh, “Role of the OH and NH vibrational groups in polysaccharide-nanocomposite interactions: A FTIR-ATR study on chitosan and chitosan/clay films”, Polymer, vol. 99, pp. 614-622, 2016.

[19] F. Ma, P. Li, B. Zhang, X. Zhao, Q. Fu, Z. Wang, C. Gu, “Effect of solution plasma process with bubbling gas on physicochemical properties of chitosan”, Int. J. Biol. Macromol., vol. 98, pp. 201-207, 2017.

[20] R. E. Rosensweig, “Heating magnetic fluid with alternating magnetic field”, J. Magn. Magn. Mater., vol. 252, pp. 370-374, 2002.

[21] R. Kötitz, W. Weitschies, L. Trahms, W. Semmler, “Investigation of Brownian and Néel relaxation in magnetic fluids”, J. Magn. Magn. Mater., vol. 201, pp. 102-104, 1999.

[22] E. Deatsch, B. A. Evans, “Heating efficiency in magnetic nanoparticle hyperthermia”, J. Magn. Magn. Mater., vol. 354, pp. 163-172, 2014.

[23] R. Hergt, W. Andra, C. G. d’Ambly, I. Hilger, W. A. Kaiser, U. Richter, H. Schmidt, “Physical limits of hyperthermia using magnetite fine particles”, IEEE Trans. Magn., vol. 34, pp. 3745-3754, 1998.

[24] B. Chertok, A. E. David, V. C. Yang, “Polyethyleneimine-modified iron oxide nanoparticles for brain tumor drug delivery using magnetic targeting and intra-carotid administration”, Biomaterials, vol. 31, pp. 6317-6324, 2010.

[25] Q. A. Pankhurst, N. K. T. Thanh, S. K. Jones, J. Dobson, “Progress in applications of magnetic nanoparticles in biomedicine”, J. Phys. D: Appl. Phys., vol. 42, pp. 1-15, 2009.

[26] W. Xu, K. Kattel, J. Y. Park, Y. Chang, T. J. Kim, G. H. Lee, “Paramagnetic nanoparticle T1 and T2 MRI contrast agents”, Phys. Chem. Chem. Phys., vol. 14, pp. 12687-12700, 2012.

[27] S. H. Lee, B. H. Kim, H. B. Na, T. Hyeon, “Paramagnetic inorganic nanoparticles as T1 MRI contrast agents”, Wiley Interdiscip. Rev. Nanomed. Nanobiotechnol., vol. 6, pp. 196-209, 2014.

[28] K. Ohno, C. Mori, T. Akashi, S. Yoshida, Y. Tago, Y. Tsujii, Y. Tabata, “Fabrication of contrast agents for magnetic resonance imaging from polymer-brush-afforded iron oxide magnetic nanoparticles prepared by surface-initiated living radical polymerization”, Biomacromolecules, vol. 14, pp. 3453-3462, 2013.

[29] Q. L. Jiang, S. W. Zheng, R. Y. Hong, S. M. Deng, L. Guo, R. L. Hu, B. Gao, M. Huang, L. F. Cheng, G. H. Liu, Y. Q. Wang, “Folic acid-conjugated Fe3O4 magnetic nanoparticles for hyperthermia and MRI in vitro and in vivo”, Appl. Surf. Sci., vol. 307, pp. 224-233, 2014.

[30] J. Kost, J. Wolfrum, R. Langer, “Magnetically enhanced insulin release in diabetic rats”, J. Biomed. Mater. Res. Part A, vol. 21, pp. 1367-73, 1987.

[31] P. V. Finotelli, D. D. Silva, M. Sola-Penna, A. M. Rossi, M. Farina, L. R. Andrade, A. Y. Takeuchi, M. H. Rocha-Leão, “Microcapsules of alginate/chitosan containing magnetic nanoparticles for controlled release of insulin”, Colloids Surf. B, vol. 81, pp. 206-211, 2010.

[31] K. Katagiri, Y. Imai, K. Koumoto, “Variable on-demand release function of magnetoresponsive hybrid capsules”, J. Colloid. Interface Sci., vol. 361, pp. 109-114, 2011.

[33] S. Hu, C. Tsai, C. Liao, D. Liu, S. Chen, “Controlled Rupture of Magnetic Polyelectrolyte Microcapsules for Drug Delivery”, Langmuir, vol. 24, pp. 11811-11818, 2008.

[34] B. Koppolu, M. Rahimi, S. Nattama, A. Wadajkar, K. T. Nguyen, “Development of multiple-layer polymeric particles for targeted and controlled drug delivery”, Nanomed., vol. 6, pp. 355-361, 2010.

[35] V. V. Mody, A. Cox, S. Shah, A. Singh, W. Bevins, H. Parihar, “Magnetic nanoparticle drug delivery systems for targeting tumor”, Appl. Nanosci., vol. 4(4), pp. 385-392, 2014.

Chapter 4

ELECTRIC STIMULUS RESPONSIVE CHITOSAN/MNP MICROBEADS FOR A SMART DRUG DELIVERY SYSTEM

4.1 INTRODUCTION:

Systemic drug delivery has several setbacks like rapid flushing out of circulation and low specificity to target site, thus usually requiring frequent invasive administration leading to patient discomfort. Sterically sheathing the drug in a biocompatible polymer substrate helped in remedying some of these shortcomings [1], however, such Drug Delivery System (DDS) were characterized by an initial burst release of their therapeutic payload and a subsequent first-order elution profile until the drug is exhausted.

Several researchers have proposed improvisations to the DDS to make the drug release responsive to stimuli [2-4]. A variety of electric stimuli such as pH, magnetic field, ultrasound, light etc. have been successfully demonstrated to be capable of altering the normal drug elution profile and cause a higher amount of drug release from the DDS [2-4].

The foundation for exploring drug release by electric stimulus was laid by Zinger and Miller who in 1984 applied 1V voltage to Polypyrrole (PPy) films loaded with glutamate to cause a controllable higher release of the drug [5]. Weaver *et al* electrodeposited PPy/graphene oxide films on glassy carbon electrodes. The films were loaded with dexamethasone, which was released by application of a biphasic voltage pulse [6]. Besides using PPy, another common method for electro-responsive drug release mechanisms is designing reservoirs containing the drug load of interest. These reservoirs are sealed off with a membrane that disintegrates or forms reversible pores when an electric current is passed through them [7-9]. Such reservoirs are made by complicated processes involving etching and lithography, and have a height up to a

few millimeters. Chitosan gels have also been explored for drug delivery by positioning electrodes on either side of the gel and applying a potential difference across the gel [10-11].

This paper explores a novel method of controlling drug release by electric stimulus applied to the DDS via silver Inter-Digitated Electrodes (IDE) printed on Polyimide substrate by an Inkjet printer (Fig. 4.1). The IDE were measured to be only a few microns in height [12], further enhancing their suitability as a thin, flexible implant for controllable drug release from the DDS. The DDS is chitosan based, crosslinked with Polyethylene Glycol Dimethacrylate (PEGDMA) and containing magnetic nanoparticles (MNP). Vancomycin was chosen as the drug of interest. In our previous work, we established the same DDS to be responsive to magnetic stimuli as well [13]. Either or both of these stimulation modes can be used to administer drug dosages according to unique therapeutic requirements of each patient, without repetitive invasive procedures to maintain potent drug concentration. Furthermore, we have previously demonstrated this DDS can release drug with magnetic stimulation [13], thus making it possible to use suitable stimulation modality as well as utilizing them in conjunction to increase efficacy is possible.

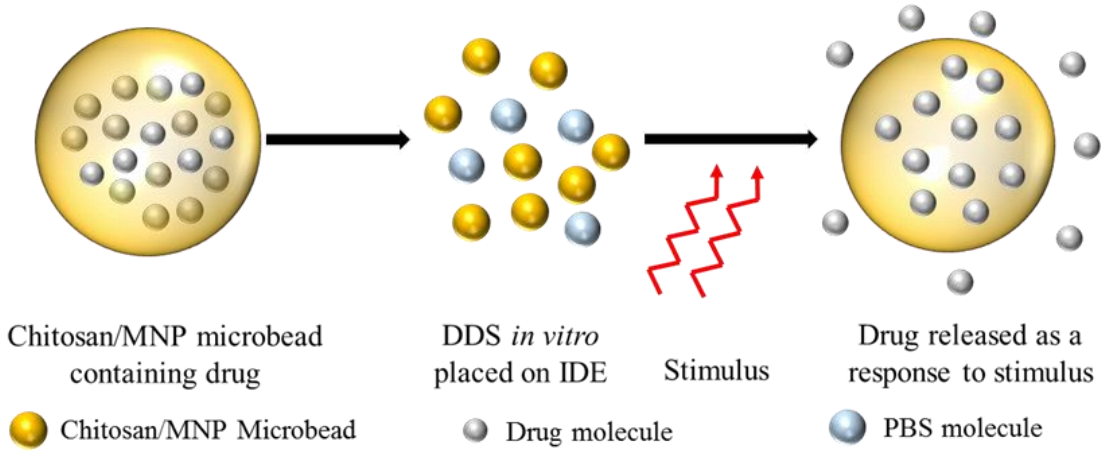

Fig. 4.1: Pictorial description of vancomycin release from chitosan microbeads by an electric stimulus

4.2 MATERIALS AND METHODS:

4.2(a) Chitosan Microbead Preparation and Characterization:

The chitosan DDS were made by a modified water-oil emulsification method [13-14]. The MNP and chitosan microbeads were scanned with an X-Ray Diffractometer (XRD) (D8/Advance, Bruker Advance X-Ray solutions) with Cu-Kα radiation, λ = 0.15418 nm. Further, the microbeads were also scanned by a Fourier Transform Infrared Spectrometer (FTIR) (Nicolet iS 10 FTIR Spectrometer) in the mid IR range of 400-4000cm^{-1}.

4.2(b) Preliminary Drug Delivery results using SAW resonators to apply stimulation:

In one of our initial studies [15] to explore the viability of using IDE as a stimulation modality, we used off the shelf Surface Acoustic Wave (SAW) resonators (Model:R880, EPCOS AG, Germany) which contain pre-designed IDE inside the cavity (Fig. 4.2).

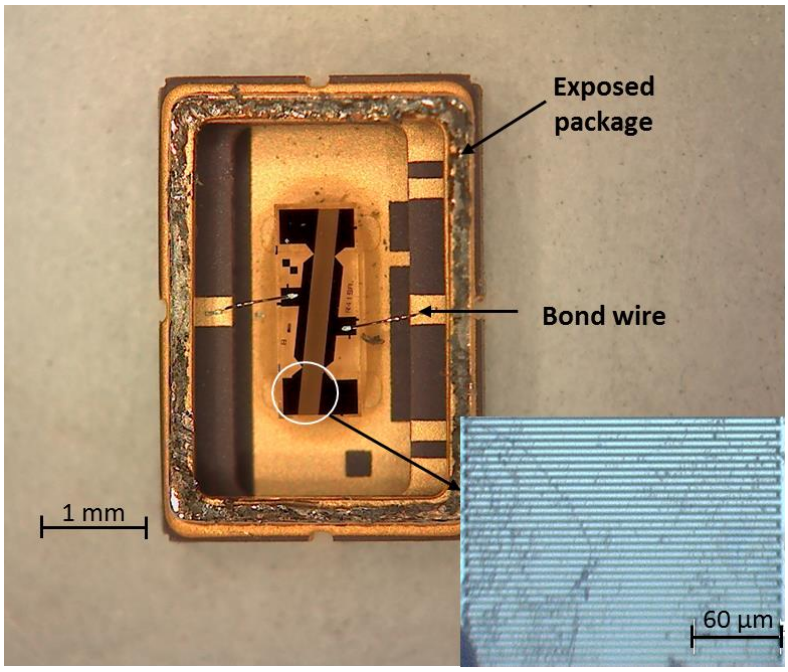

Fig. 4.2: Exposed SAW resonator with inter-digitated electrodes encircled (inset) Portion of interdigitated electrodes, viewed at 20x under a light microscope.

The DDS was in form of chitosan microbeads with MNP, cross-linked with glyoxal and containing Alizarin red S. After exposing these IDEs, the DDS samples were mixed with 10 µl Phosphate Buffered Solution (PBS) and carefully placed inside the cavity. Electrical stimulation was applied for 30 s. The Alizarin red S released was measured by a spectrophotometer (Model: Synergy H1 microplate reader, BioTek US, Winooski, VT) at 350 nm. Three different stimulation waveforms were applied to the IDE, along with control groups that did not undergo any stimulation. The test numbers for them were labelled as follows:

Table 4.1: Different stimulation waveforms applied to microbeads in SAW resonators

Test Number	Pulse type
1	None (control)
2	20 Vpp, 1 kHz, 10% duty cycle, bipolar rectangular
3	20 Vpp, 500 Hz, 10% duty cycle, bipolar rectangular
4	20 Vpp, 1 kHz, sinusoidal

4.2(c) Printing IDE and test setup:

After demonstrating the proof-of-concept, we explored stimulating larger volume by using IDEs to cause drug release. We adopted an approach to print IDEs on flexible substrates. A Fujifilm DMP-2831 material deposition printer (Fujifilm Dimatix, NH) was used to print IDEs on Polyimide (PI) tape with Silver ink. The silver ink was purchased from Novacentrix (Metalon JS-B40HV). After printing, the PI tape was shifted from printing platen to a glass substrate and thermally cured at 180°C to make the silver traces conductive and adhere to the PI.

The silver ink has a propensity to spread on PI tape, thus actual printed electrodes' width is wider than the width specified in design parameters. The fingers need to be reliably placed in closest possible proximity to each other to generate a high electric field, without causing an electric short. Several designs with different dimension were printed and tested. The layout shown in Fig. 4.3 was observed to be optimal and yielded consistent, reliable prints each time. This IDE pattern has a length of 35 mm and a width of 18.7 mm. Both terminals have 8 fingers and each finger is 7.5 mm long and 0.6 mm wide, and is spaced 0.6 mm from its neighboring electrode.

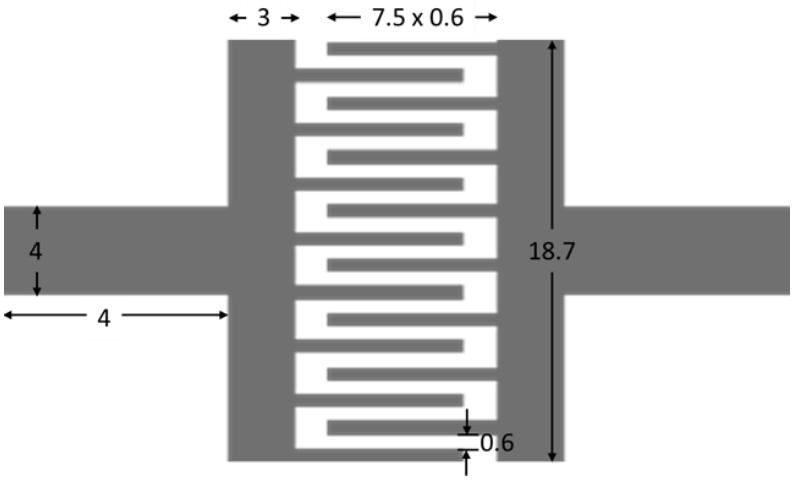

Fig. 4.3: IDE dimension and layout. All measurements are in mm

After the IDEs were cooled down, a 1" plastic tube section was affixed around the IDE with silicon resin and left to dry for 48 hours. This step was necessary to constrain the PBS and DDS on top of the IDE. After 48 hours, wires were attached to the IDE terminals using copper tape (Fig. 4.4).

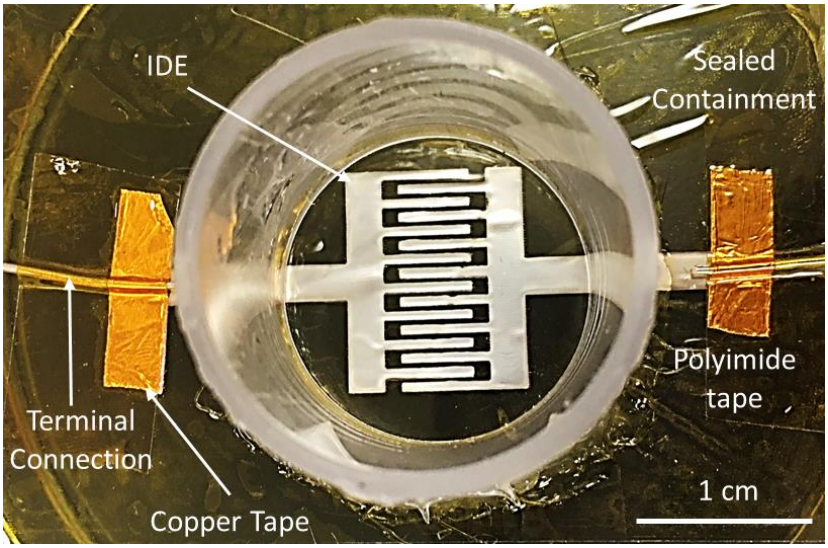

Fig. 4.4: IDE setup on Polyimide substrate

The IDE are now ready to be used for stimulation. A 1Ω resistor was connected in series with the IDE to aid in current measurement. The whole setup was connected to a signal generator (DG4062, Rigol, USA). An oscilloscope (Tektronix TDS1001B, USA) was used to record all requisite waveforms. The setup schematic is drawn in Fig. 4.5 and a photograph in presented in Fig. 4.6.

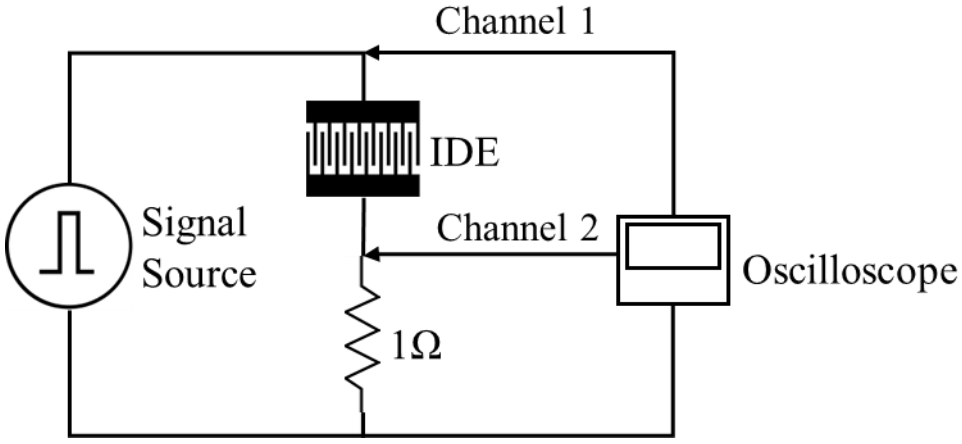

Fig. 4.5: Schematic diagram for stimulating IDE

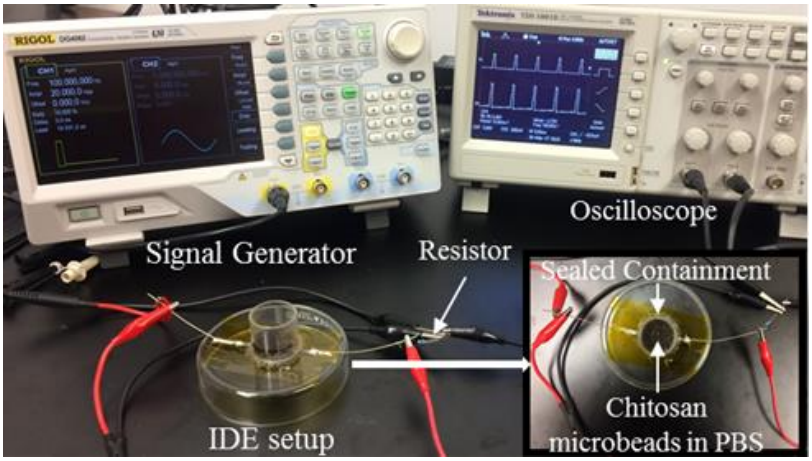

Fig. 4.6: The complete setup connected according to the schematic in Fig. 4.5

4.2(d) Drug Delivery results using printed IDEs to apply stimulation:

In initial results to study if drug release is possible with this setup, a simple 4 min timeline was used, as shown in Fig. 4.7. Both stimuli were 100 Hz bipolar rectangular current pulses of 250 mA for 10% duty cycle and -25 mA for 90% duty cycle, applied for 30 s to the test groups. The control samples did not receive any stimulation. Both control and test groups had 5 samples, each sample containing 100 mg of DDS in 5 ml PBS.

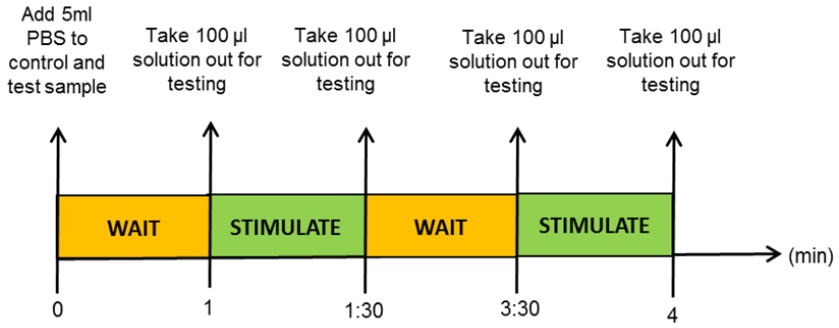

Fig. 4.7: Short term timeline (4 mins) used to stimulate the DDS with printed IDEs

Following this study, we wanted to extend the timeline to span a longer duration with electric pulses provided at a later time-point to simulate more practical in vivo scenarios The DDS were divided into 10 samples, each weighing 100 mg. The samples were divided into two groups of 5 samples each. One group was labeled as “test groups” which received the

stimulation and the other group was labelled as “control groups” and did not receive any excitation. The test timeline is showed in Fig. 4.8.

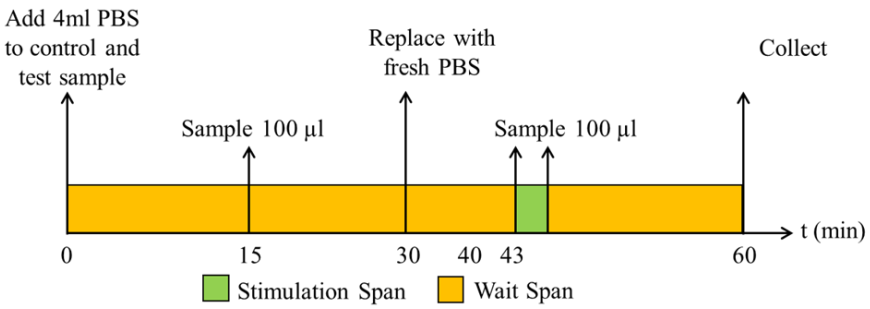

Fig. 4.8: Extended timeline with stimulation at a later timepoint

The electric stimulus given to the test groups was a bipolar rectangular current waveform of 100 Hz, with 40 mA applied for 10% duty cycle and -25 mA applied on the remaining 90%.

4.2(e) Scanning Electron Microscope Images (SEM):

The microbeads and IDEs before and after stimulation were imaged with an SEM (Nova NanoSEM) to study the effects of stimulation on both.

4.3 RESULTS

4.3(a) Chitosan Microbead Characterization:

The XRD of MNP and chitosan microbeads are shown in Figs. 4.9 and 4.10. The crystallographic peaks in MNP match those expected for Fe_3O_4 MNP and the XRD of the chitosan confirms the integrity of MNP, vancomycin and chitosan in the final product. The FTIR of the microbeads is shown in Fig. 4.10 along with the labelled peaks which also correspond to those expected of chitosan [16]. The MNP had an average size of 10±2.67 nm.

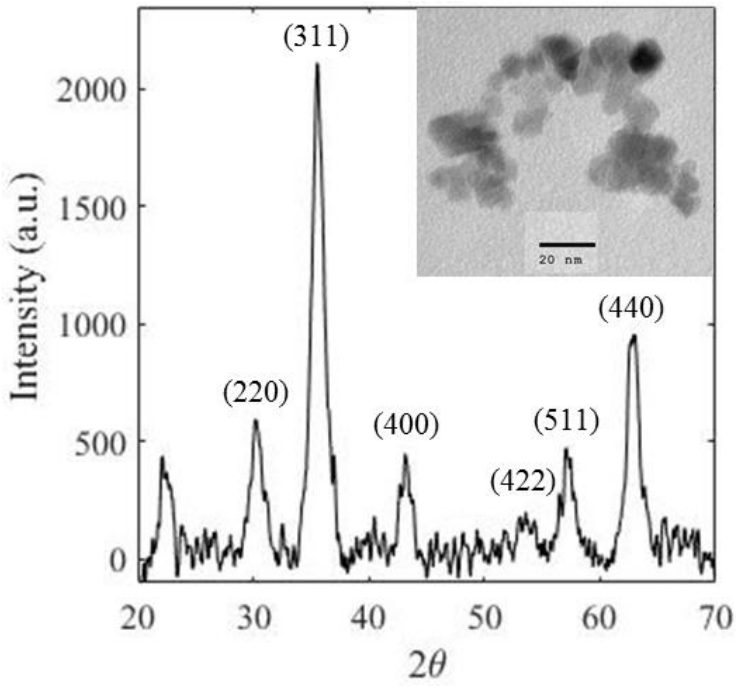

Fig. 4.9: XRD of MNP with labelled diffraction peaks (inset) Transmission Electron Microscope image of MNP

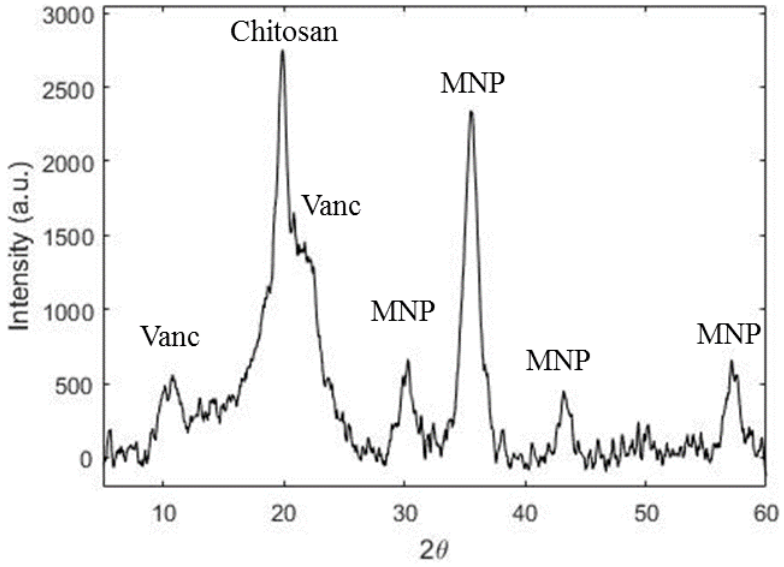

Fig. 4.10: XRD of chitosan DDS with labelled peaks of chitosan, MNP and vancomycin (vanc)

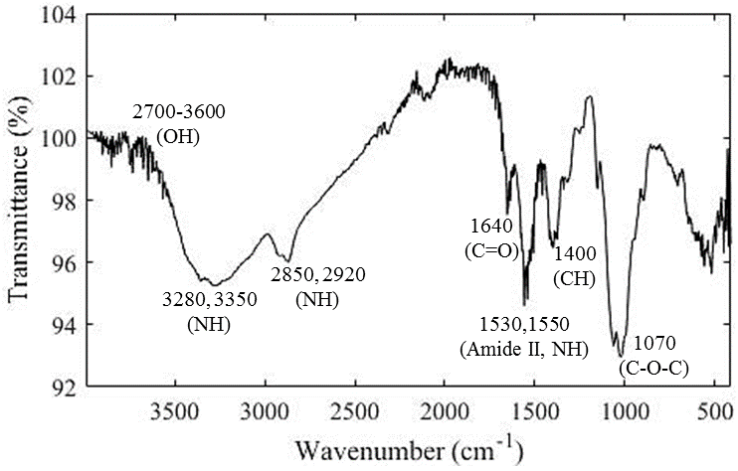

Fig. 4.11: FTIR spectra for chitosan microbeads with vancomycin, MNP and PEGDMA crosslinker

4.3(b) Preliminary Drug Delivery results using SAW resonators to apply stimulation:

The absorbance measured was analyzed with a one-tailed t test. At 5% significance level, only the bipolar rectangular pulses released a significantly higher amount of alizarin in comparison to control. Lower frequencies were also concluded to be more efficient in inducing elution from the substrate (Fig. 4.12).

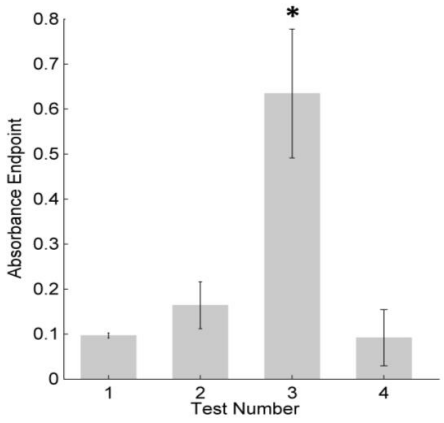

Fig. 4.12: Absorbance endpoint measured at 350 nm for (1) control (2) 20 Vpp, 1 KHz, bipolar rectangular (3) 20 Vpp, 500 Hz, bipolar rectangular and (4) 20 Vpp, 1 kHz, sinusoidal

The tests were also repeated on plain chitosan microbeads to ascertain the necessity of MNP in the drug release mechanism. The absorbance measured at 350 nm (Fig. 4.13) did not show

significant elution differences in alizarin between both groups, indicating that MNP are required to aid drug release.

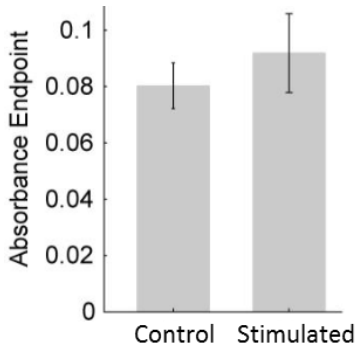

Fig. 4.13: Absorbance of alizarin measured between stimulated

4.3(c) Drug Delivery results using printed IDEs to apply stimulation:

For the 4 minutes stimulation timeline (Fig. 4.11), the test groups were found to elute a statically significantly ($p<0.05$) higher amount of vancomycin in both stimulation spans (Fig. 4.14).

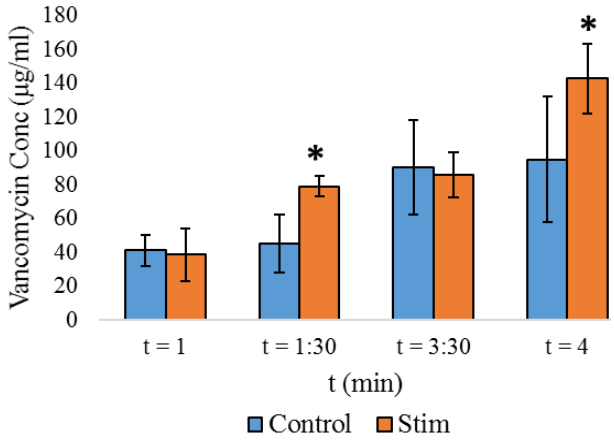

Fig. 4.14: Concentration of vancomycin released from DDS with (Stim) and without (Control) stimulation. These samples followed the timeline depicted in Fig. 4.7

The microbeads that followed the extended timeline in Fig. 4.8 showed vancomycin discharge increased by ~800% in the stimulation span (t = 40 min to t = 43min), as compared to non-stimulated groups (Fig. 4.15).

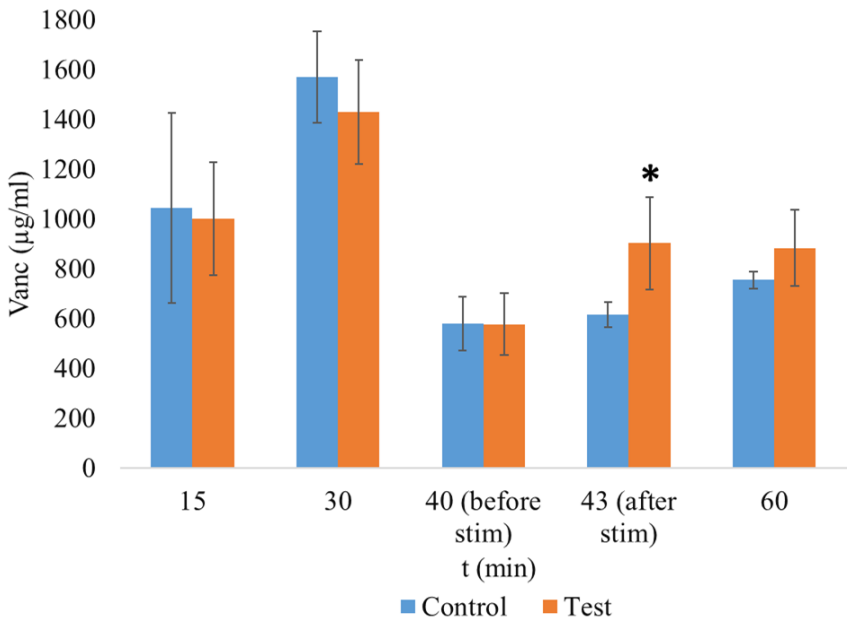

Fig. 4.15: Concentration of vancomycin released from DDS with (Stim) and without (Control) stimulation. These samples followed the timeline depicted in Fig. 4.8.

The waveforms recorded during the excitation in timeline depicted in Figs. 4.8 are plotted in Figs 4.16 and 4.17. Energy dissipated in the stimulation span for a single pulse of 10 ms was calculated as 0.5 mJ, and 9.14 J for the total stimulation of 3 mins.

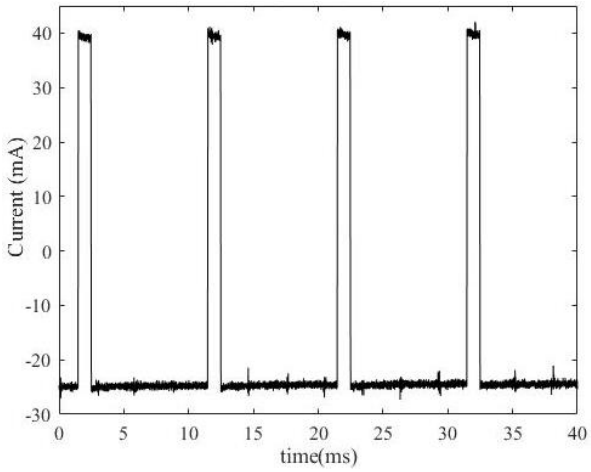

Fig. 4.16: Plot of current through setup

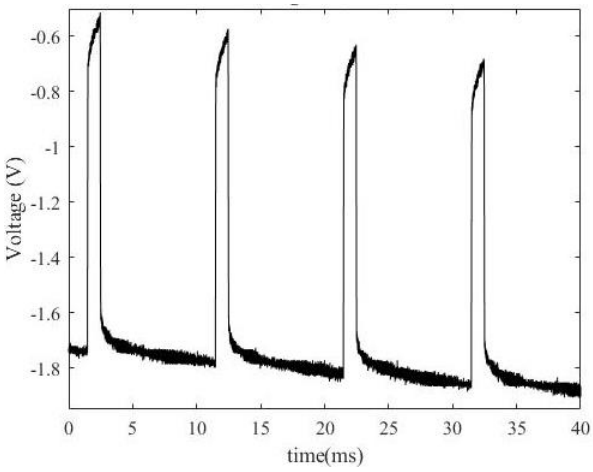

Fig. 4.17: Plot of Voltage drop across setup

4.3(d) SEM Images:

The images taken for microbeads from test and control groups did not show any noticeable surface damage, indicating that the electric stimulus is not physically damaging the beads or causing structural disintegration (Figs. 4.18, 4.19). The average size of the microbeads was measure at 288.4±62.2 µm.

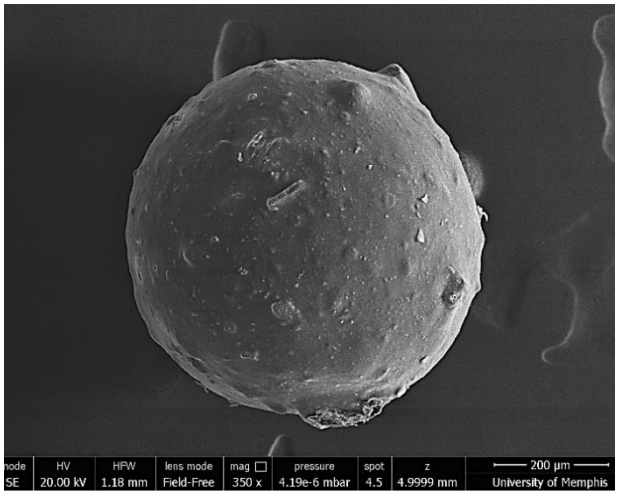

Fig. 4.18: SEM image (350x) of Chitosan DDS before electric stimulation

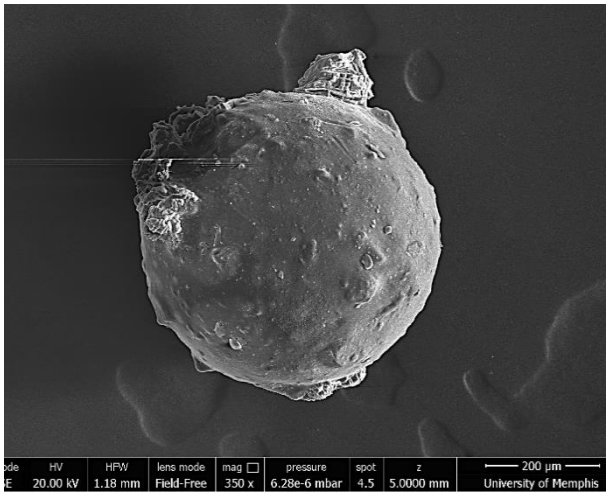

Fig. 4.19: SEM image (350x) of Chitosan DDS after electric stimulation

The control IDEs appeared smooth and undamaged after the tests. It was also noticed that although the design width of an IDE finger was 600 µm, the silver ink tends to spread on PI tape Fig. 4.20) and the actual printed IDEs had an average width of 783.68±52.6µm. The stimulated IDE showed significant damage and peeling from the substrate (Fig. 4.21), owing to the electrochemical reactions occurring between the PBS and IDE.

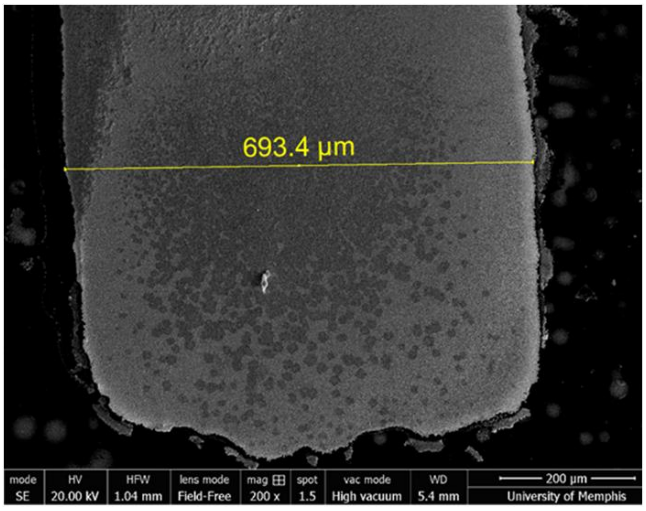

Fig. 4.20: SEM image of IDE that did not receive stimulation

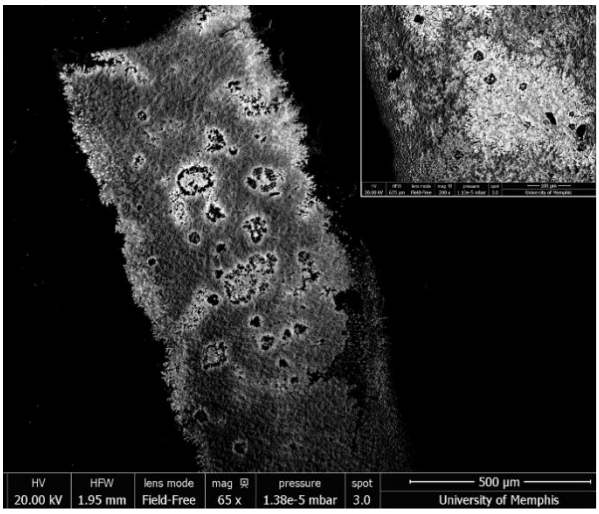

Fig. 4.21: SEM image of IDE after stimulation, showing widespread IDE damage at anode, with a zoomed in section (inset)

4.4 DISCUSSION

A cross-section of the IDE on PI and glass substrates (Fig. 4.22) was considered for simulation in COMSOL to understand the system better and attempt to explain mechanisms that cause drug transport. Current density and expected ion migration to the electrodes were also studied.

The migration of a charged ion in an electric field is given by the following Nernst Planck transport equation (1):

$$\frac{dc}{dt} + \nabla(-D\nabla c - zKFc\nabla V + c\vec{u}) = R \quad (1)$$

Where

c = Concentration, D = Diffusion coefficient, z = Charge of ion, K = Ion mobility,

R = Rate of chemical reaction of z, F = Faraday constant, V = Electric potential, u = Velocity field

A normalized dc voltage of 1V was applied to the positive terminal A and 0V to B (Fig. 4.22). A chitosan microbead of radius 200 µm was also placed between the IDE fingers. The

conductivity and dielectric permittivity of chitosan were approximated from [17]. The PBS was assumed as 1M uniform mixture of only two charged ions (+1 and -1 charge) for simplicity. A time dependent study was run for 0.1 s.

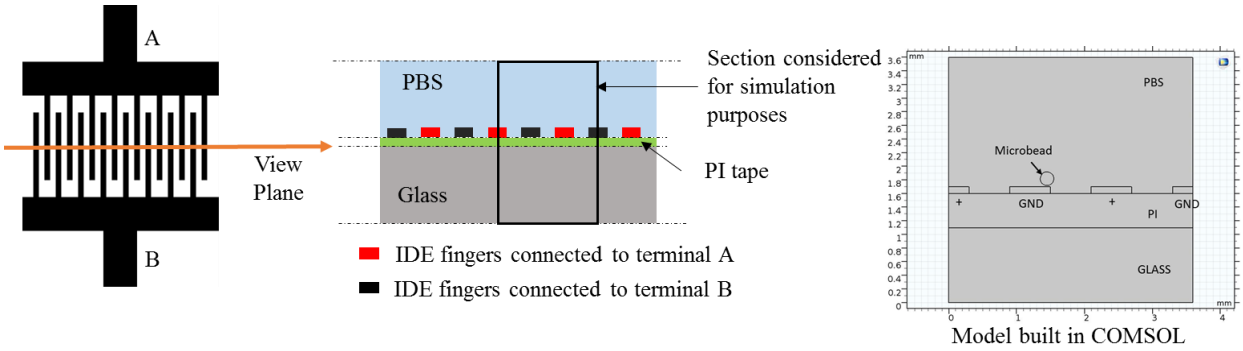

Fig. 4.22: Description of the layout built in COMSOL to study electric potential distribution, current density and ion migration

The electric potential surface distribution is shown in Fig. 4.23. An examination of the electric field plot in Fig. 4.24 distinctly shows the distortion of the field lines around the chitosan microbead. The net electric force acting on the bead could also be causing poration in the microbead's polymeric network, further encouraging the elution of vancomycin when electric current pulses are applied.

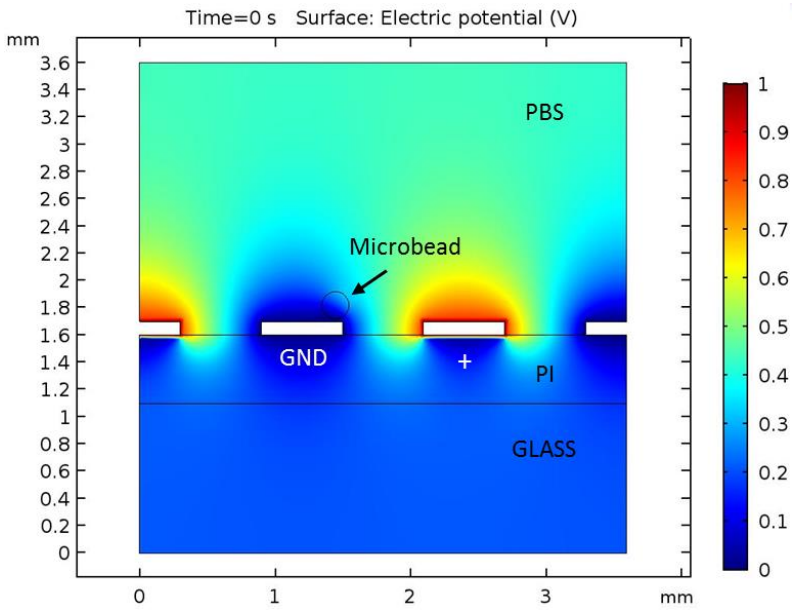

Fig. 4.23: Electric Potential distribution

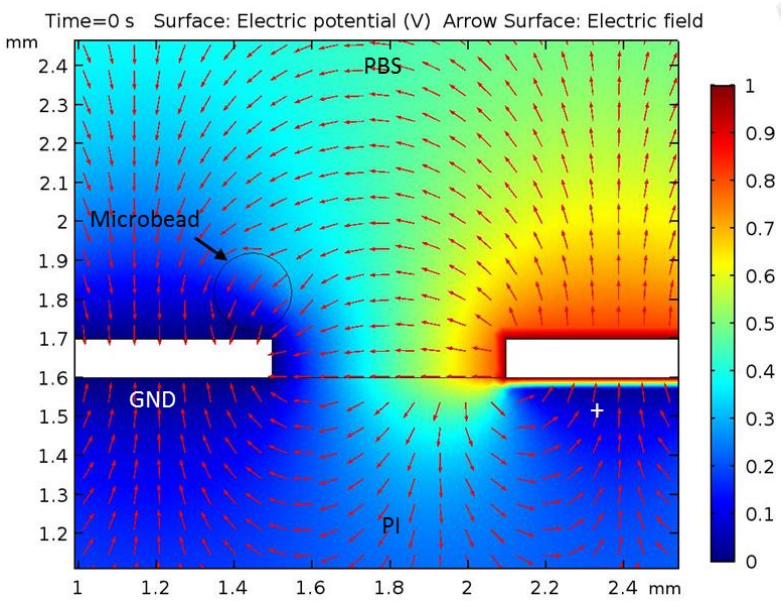

Fig. 4.24: Electric field arrows clearly show distortion caused by the chitosan microbead

The expected current density through the setup is plotted in Fig. 4.25. At beginning of simulation both types of ions were uniformly distributed throughout the PBS. However at the end of simulation at t = 0.1 s, a larger concentration of ions with charge +1 had migrated to negative electrode while those with -1 were more concentrated at the positive electrode (Figs. 4.26, 4.27).

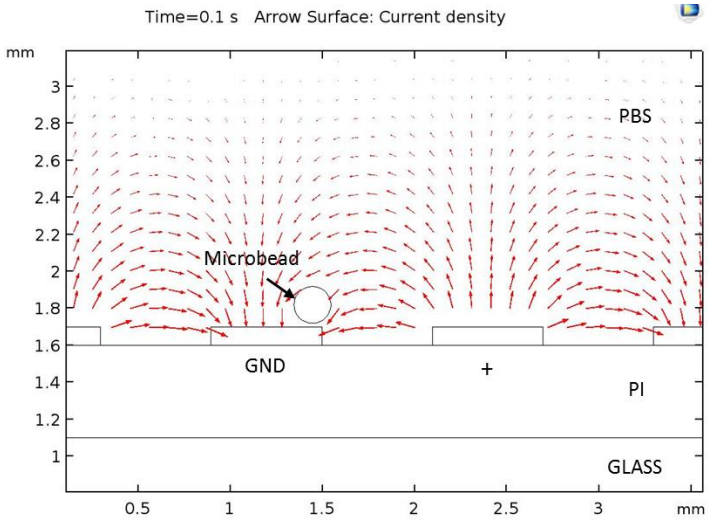

Fig. 4.25: Surface plot of current density through the setup

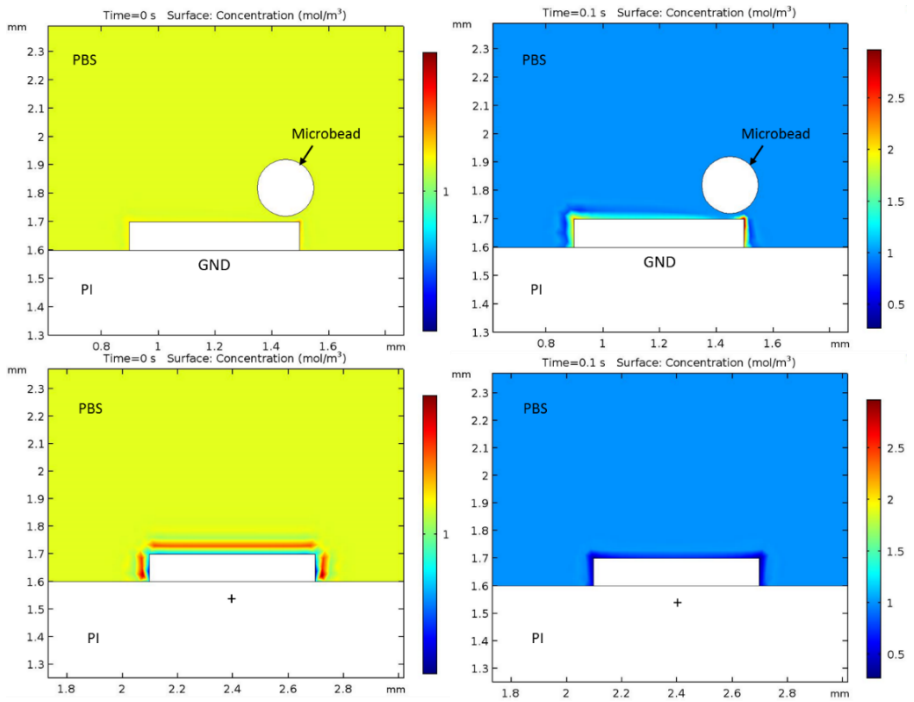

Fig. 4.26: Concentration of positive ions at the electrodes at beginning (t = 0s) and end (t = 0.1s) of simulation

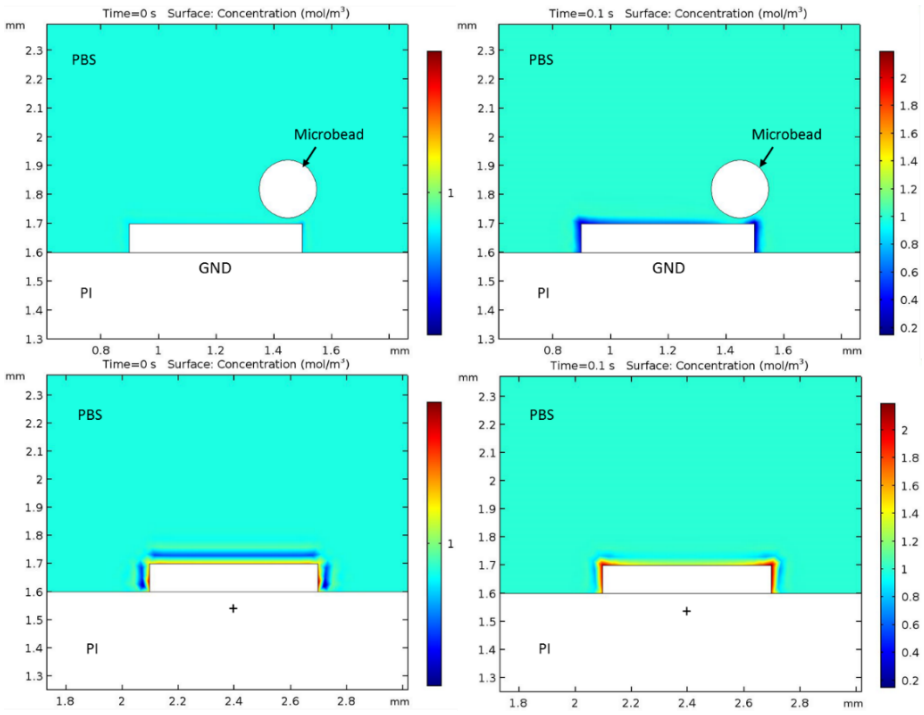

Fig. 4.27: Concentration of negative ions at the electrodes at beginning (t = 0s) and end (t = 0.1s) of simulation

The major electrochemical reactions between the silver electrodes and PBS are:

$$NaCl \rightarrow Na^{+} + Cl^{-} \quad (2)$$

$$Ag(s) + Cl^{-} \rightarrow AgCl(s) + e^{-} \quad (3)$$

$$H_2O \rightarrow H^{+} + OH^{-} \quad (4)$$

Reaction at Anode: $Ag \rightarrow Ag^{+} + e^{-}$ (5)

Reaction at cathode: $2H^{+} + 2e^{-} \rightarrow H_2$ (6)

These reactions are the primary cause of electrode degradation and formation of bubbles as seen in Fig. 4.28.

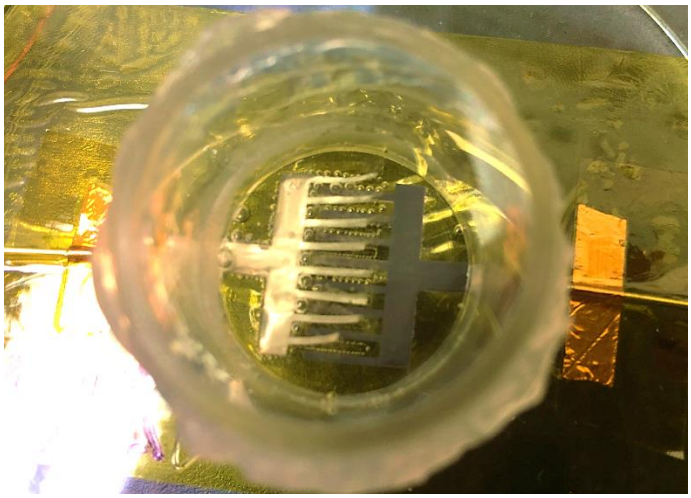

Fig. 4.28: IDEs after stimulation showing degraded fingers and hydrogen bubbles

A plausible explanation of drug release could be that chitosan, being a cationic molecule due to the acidic condition during preparation is neutralizing as the pH increases. The localized high pH is being generated at the cathode surface by the reaction in Eqn 4, which leads to the acid-base reaction of chitosan:

$$Chit - NH_3^{+} + OH^{-} \rightarrow Chit - NH_2 + H_2O \quad (7)$$

This de-protonation reaction of the chitosan amine group in Eq 7 is likely changing the polymer chain interaction and the microstructure of polymer network inside the particle, accelerating the

diffusion of vancomycin. Temperature change caused by the flow of current could also be promoting hydrolysis of the chemically conjugated vancomycin from the PEG crosslinker [13].

4.5 CONCLUSION

This paper has laid the groundwork for using Inkjet printing technology to design inexpensive, flexible, thin and implantable substrates for providing electric pulses to a DDS and causing a higher release of drug as a response. The amount of vancomycin eluted from DDS was significantly ($p < 0.05$) boosted by excitation. A future challenge is to fabricate inert electrodes that do not degrade and are capable of providing sustainable and repeatable stimulation separated by hours, or even days.

4.6 REFERENCES:

[1] A. Mohapatra, B. I. Morshed, W. O. Haggard, R. A. Smith, "Stealth Engineering for in vivo Drug Delivery Systems", Crit. Rev. Biomed. Eng., vol. 43, pp. 347-69, 2016.

[2] C. Ding, L. Tong, J. Feng, J. Fu, "Recent Advances in Stimuli-Responsive Release Function Drug Delivery Systems for Tumor Treatment", Molecules, vol. 21, 2016.

[3] M. S. Shim, Y. J. Kwon, "Stimuli-responsive polymers and nanomaterials for gene delivery and imaging applications", Adv. Drug Deliv. Rev., vol. 64, pp. 1046-1059, 2012.

[4] M. N. Yasin, D. Svirskis, A. Seyfoddin, I. D. Rupenthal, "Implants for drug delivery to the posterior segment of the eye: A focus on stimuli-responsive and tunable release systems", J. Control Rel., vol. 196, pp. 208-221, 2014.

[5] B. Zinger, L. L. Miller, "Timed release of chemicals from polypyrrole films", J. Am. Chem. Soc., vol. 106(22), pp. 6861-6863, 1984.

[6] C. L. Weaver, J. M. LaRosa, X. Luo, X. T. Cui. "Electrically Controlled Drug Delivery from Graphene Oxide Nanocomposite Films", ACS Nano, vol. 8(2), pp. 834-1843, 2014.

[7] J. M. Maloney, S. A. Uhland, B. F. Polito, N. F. Sheppard Jr, C. M. Pelta, J. T. Santini Jr. "Electrochemically activated microchips for implantable drug sensing and biosensing", J. Control. Rel., vol. 109, pp. 244-255, 2005.

[8] Y. T. Yi, J. Y. Sun, Y. W. Lu, Y. C. Liao, "Programmable and on-demand drug release using electrical stimulation", Biomicrofluidics, vol. 9, pp. 022401-1:022401-10, 2015.

[9] A. J. Chung, Y. S. Huh, D. Erickson, “A robust, electrochemically driven microwell drug delivery system for controlled vasopressin release”, vol. 11(4), pp. 861-867, 2009.

[10] S. Ramanathan, L. H. Block. “The use of chitosan gels as matrices for electrically modulated drug delivery”. J. Control. Rel., vol. 70, pp. 109-123, 2001.

[11] B. Sheen, R. C. Guzman. “Electroresponsive PEG-chitosan matrix for anion release”, Biomater. Tissue Technol., vol. 1(2), pp. 1-5, 2017.

[12] A. Mohapatra, B. I. Morshed, S. Shamsir, S. K. Islam. “Inkjet Printed Thin Film Electronic Traces on Paper for Low-Cost Body-Worn Electronic Patch Sensors”, IEEE Body Sensor Networks, Las Vegas (Nevada, USA) 2018, accepted.

[13] A. Mohapatra, M. A. Harris, D. LeVine, M Ghimire, J A Jennings, B I Morshed, W O Haggard, J D Bumgardner, S R Mishra, T Fujiwara. “Magnetic stimulus responsive vancomycin drug delivery system based on chitosan microbeads embedded with magnetic nanoparticles”, J. Biomed. Mater. Res. B Appl. Biomater., 2017.

[14] S. K. Jain, N. K. Jain, Y. Gupta, A. Jain, D. Jain, M. Chaurasia. “Mucoadhesive chitosan microspheres for non-invasive and improved nasal delivery of insulin”, Ind. J. Pharm. Sci., vol. 69, pp. 498-504, 2007.

[15] A. Mohapatra, G. McGraw, B. I. Morshed, J. A. Jennings, W. O. Haggard, J. D. Bumgardner, S. R. Mishra. “Electric Stimulus Response of Chitosan Microbeads Embedded with Magnetic Nanoparticles for Controlled Drug Delivery”, IEEE Healthcare Innovation Conference, Seattle (WA) 8-10 Oct 2014.

[16] J. Xu, B. Xu, D. Shou, X. Xia, Y. Hu. “Preparation and Evaluation of Vancomycin-Loaded N-trimethyl Chitosan Nanoparticles”, Polymers, vol. 7, pp. 1850-1870, 2015.

[17] C. G. A. Lima, R. S. Oliviera, S. D. Figueiro, C. F. Wehmann, J. C. Goes, A. S. B. Sombra, “DC conductivity and dielectric permittivity of collagen-chitosan films”, vol. 99, pp. 284-288, 2006.

Chapter 5

CONCLUSIONS AND FUTURE DIRECTIONS

5.1 KEY RESULTS

The outcomes of this research can be summarized as follows:

1. We were able to design a drug delivery system (DDS) that is sensitive to both electric and magnetic fields. The DDS displays a burst release when excited, but follows a profile similar to the non-stimulated groups otherwise. For magnetic stimulation, we applied 25 mT, 100 Hz to the samples for at least 30 mins, but not greater than 60 mins. A bipolar rectangular pulse waveform of electric current at 100 Hz and several milli-amperes was applied for 30 – 180 sec to the DDS for electric stimulation. A healthcare provider could choose either of these stimuli as deemed necessary, or even use them in conjunction to maximize release.
2. In the studies involving magnetic hyperthermia, the DDS was stimulated multiple times over a period of several hours or several days. The drug release observed from test groups was incremented by as much as 200% in the stimulation period. The magnetic field was also able to boost drug release above Minimum Inhibitory Concentration even 16 days after regular elution from the DDS, proving that this substrate is also functional over longer intervals that are more clinically relevant. Electric stimulation was capable of triggering a higher drug discharge by ~800% above the normal amount discharged without any excitation.
3. We also described a novel approach of applying electric pulses to the IDE by printed silver inter-digitated electrodes on polyimide tape. This substrate is flexible, thin (< 2μm), inexpensive and does not require complicated fabrication processes like etching or

photolithography. The overall ease of designing IDE permits the flexibility to of quick re-designing according to the desired implant site type.

5.2 FUTURE RESEARCH DIRECTIONS

1. Although our preliminary in vivo studies (appendix) indicated the DDS is biocompatible, the impact of magnetic stimulation on drug release could not be determined to be as pronounced as *in vitro*. A future direction of this research would be to do more detailed studies and characterize the DDS performance in vivo.
2. The IDE setup used for electric stimulation can be extended to be wirelessly powered, making it a fully implantable device. As described in Chapter 4, the IDEs tend to degrade after stimulation due to electrochemical corrosion occurring at the silver anode. Formulating Gold or Platinum nanoparticle inks can be explored for printing instead.

APPENDIX

A.1: Flowchart for Chitosan/MNP/vancomycin preparation

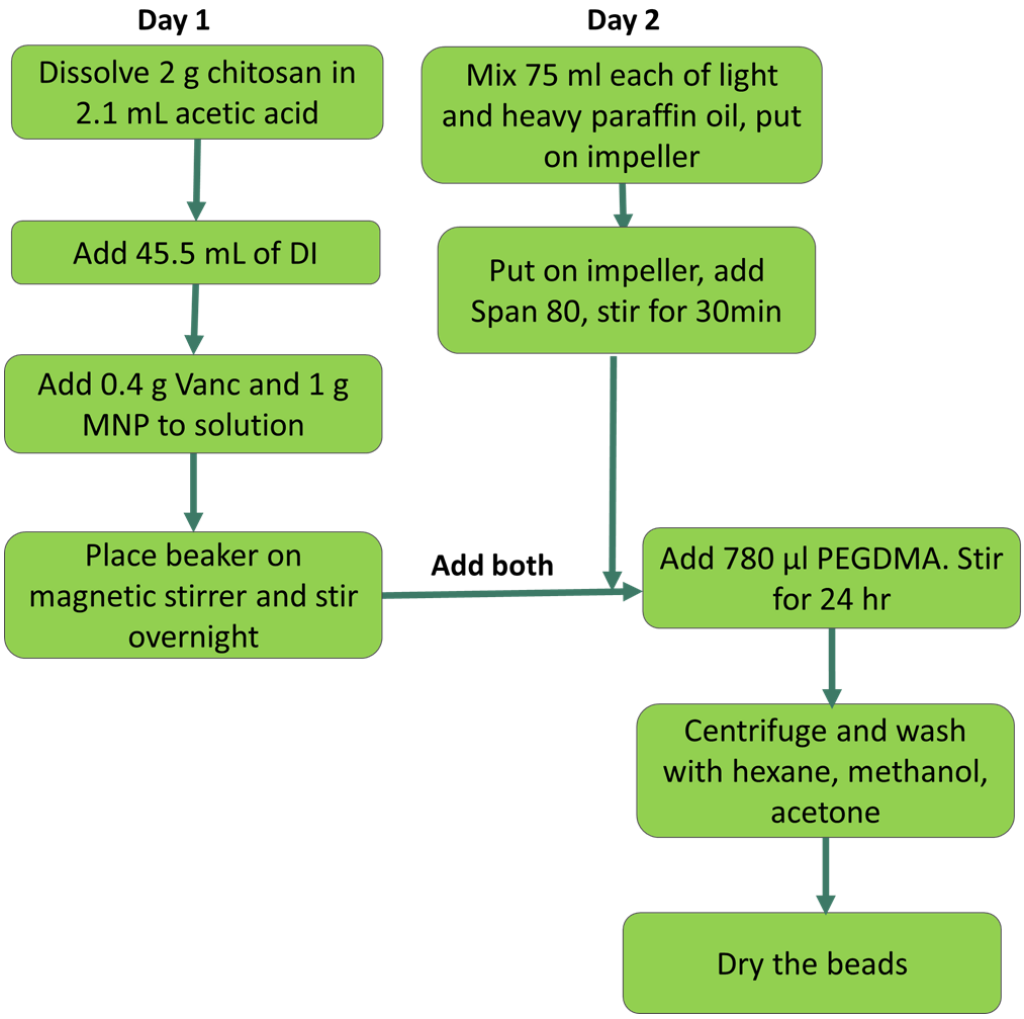

A.2: Flowchart for stimulation tests

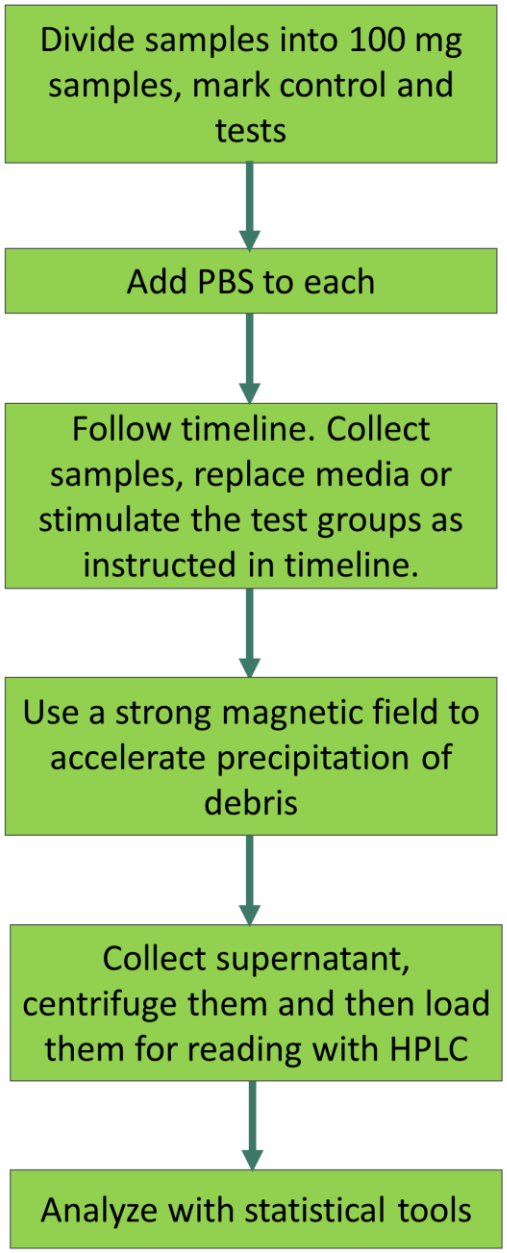

A.3: Flowchart showing procedure to print IDEs on PI tape

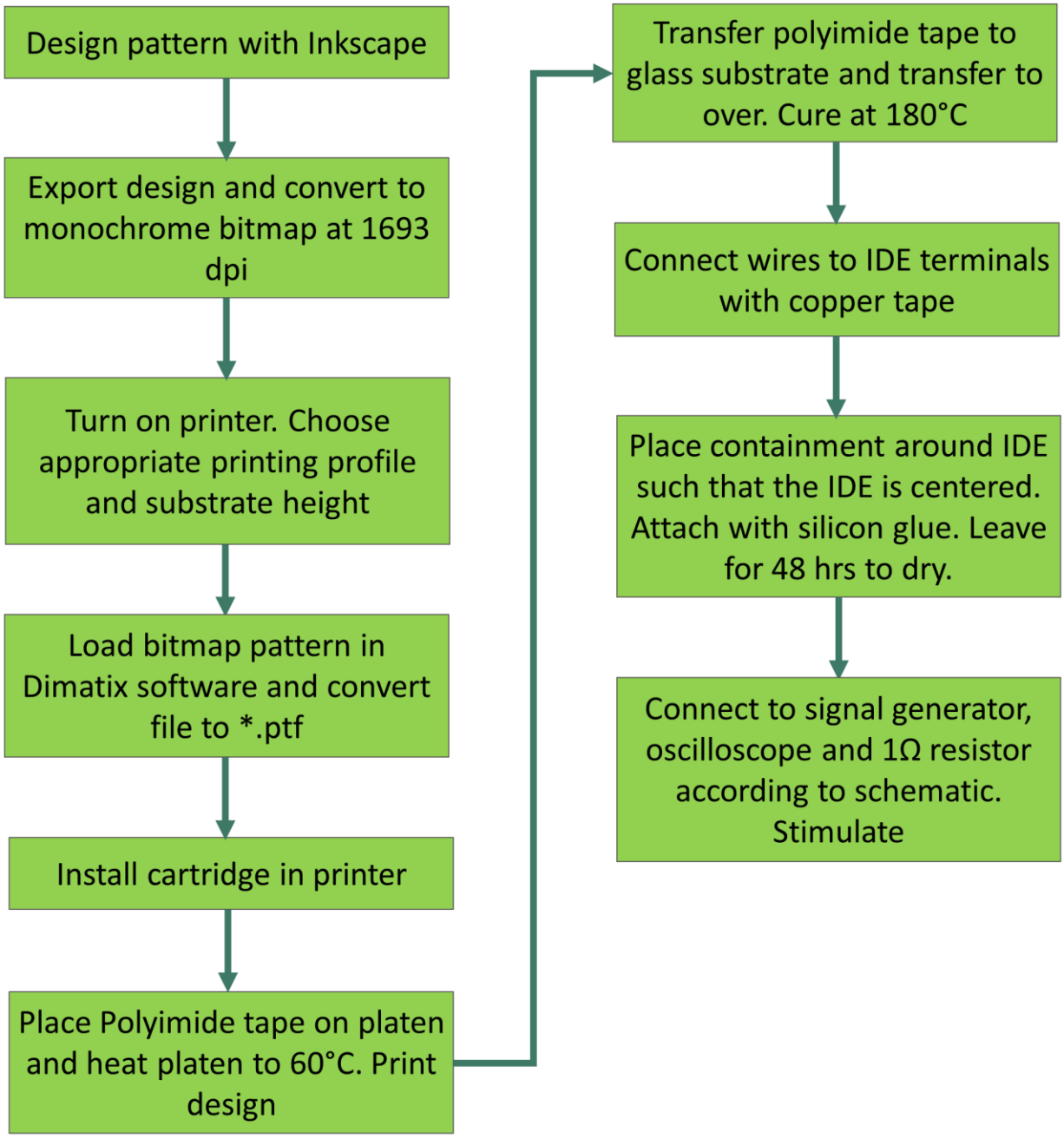

A.4: MATLAB® code to analyze voltage and current waveforms

```
%% READ DATA FROM EXCEL SHEET
dt = xlsread('C:\Users\mhapatra\Dropbox\Work\2018\March 2018\IEEE J\Waveforms\Waveform2\T0000.csv');

x = dt(:,1)*1000;   % convert x axis to ms scale
ch1 = dt(:,2);      % read voltage data

ch2 = dt(:,4)*1000; % read current, convert to mA

%% VOLTAGE
figure(1)
plot(x,ch1)
title('Voltage before filter')

figure(2)
windowWidth = 5;    % to decrease harmonics
polynomialOrder = 3;
smoothY_V = sgolayfilt(ch1, polynomialOrder, windowWidth);
plot(x,smoothY_V+.1)
xlabel('time(ms)')
ylabel('Voltage')
title('Voltage after filter')

%% CURRENT
figure(3)
plot(x,ch2)
title('Current before filter')

figure(4)
windowWidth =39;
polynomialOrder = 3;
smoothY_I = sgolayfilt(ch2, polynomialOrder, windowWidth);
plot(x,smoothY_I)
xlabel('time(ms)')
ylabel('Current')
title('Current after filter')

pw= 0;

for i = 1:size(ch1)
   pw = ch1(i)*smoothY_I(i);
end

mj = pw*0.04;      % Calculate total energy in observed waveform (4 pulses)

mj_single_pulse = mj/4; % energy in single pulse

no_of_pulse = 3*60/0.01; % calculate number of pulses in 3 min
                    % (total stimulation duration)

mJ-stim = no_of_pulse*mj_single_pulse % total energy spent in stimulation
```

A.5: Sample code of Wilcox's test in R for comparing vancomycin elution®

```
Control_1 ← c(307.78,362.22,119.20,126.21,141.53,186.36,268.49,604.48)

Stim_1 ← c(139.78,221.31,193.90,183.66,173.38,133.62,99.04,237.97)

wilcox.test(Control_1, Stim_1)
```

A.6: Model Parameters used for simulation in COMSOL®

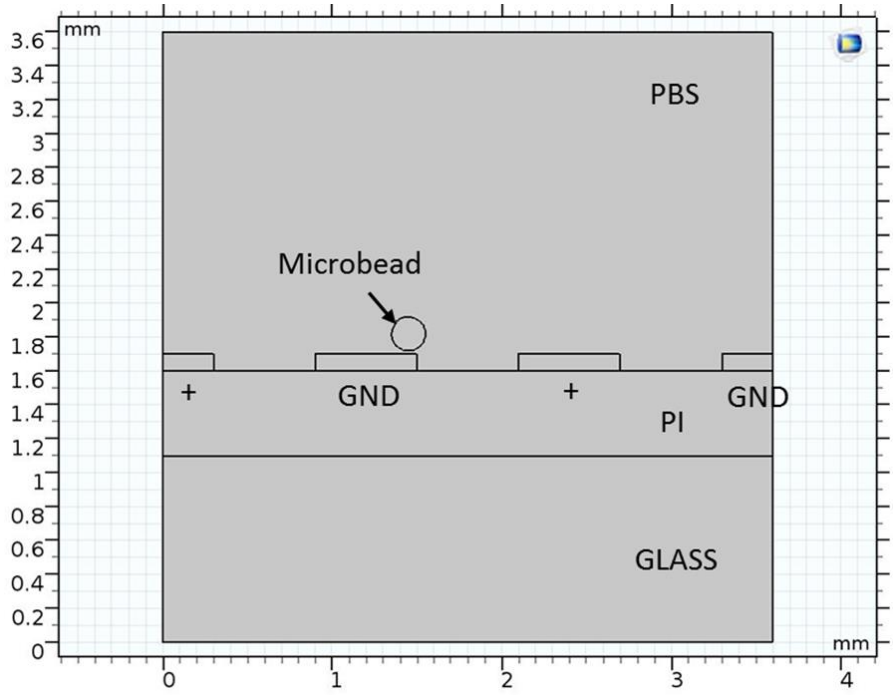

Fig. A.6.1: 2D model drawn for simulation

Table A.6.1: Dimensions of the various components in the model in Fig. A.6.1

Glass	3.6mm x 1.1mm
Polyimide tape (PI)	3.6mm x 0.5 mm
Phosphate Buffered Solution (PBS)	3.6mm x 2mm
Chitosan microbead	0.1 mm radius

Table A.6.2: Material properties used for simulation

	Relative permittivity	Electrical Conductivity	Source
PBS (Phosphate Buffered Solution)	88	0.01	[1]
Polyimide	3.4	6.7e-14	COMSOL® Inbuilt material
Glass	4.7	1e-13	COMSOL® Inbuilt material
Chitosan	3.94	3.4e-17	[2]

[1] Supplementary Information for Lab on a Chip, 2013

[2] C.G.A. Lima et al., “DC conductivity and dielectric permittivity of collagen–chitosan films”, Materials Chemistry and Physics, vol. 99, pp. 284-288, 2006